Terms and Conditions of Use of Digitised Theses from Trinity College Library Dublin

Copyright statement

All material supplied by Trinity College Library is protected by copyright (under the Copyright and Related Rights Act, 2000 as amended) and other relevant Intellectual Property Rights. By accessing and using a Digitised Thesis from Trinity College Library you acknowledge that all Intellectual Property Rights in any Works supplied are the sole and exclusive property of the copyright and/or other IPR holder. Specific copyright holders may not be explicitly identified. Use of materials from other sources within a thesis should not be construed as a claim over them.

A non-exclusive, non-transferable licence is hereby granted to those using or reproducing, in whole or in part, the material for valid purposes, providing the copyright owners are acknowledged using the normal conventions. Where specific permission to use material is required, this is identified and such permission must be sought from the copyright holder or agency cited.

Liability statement

By using a Digitised Thesis, I accept that Trinity College Dublin bears no legal responsibility for the accuracy, legality or comprehensiveness of materials contained within the thesis, and that Trinity College Dublin accepts no liability for indirect, consequential, or incidental, damages or losses arising from use of the thesis for whatever reason. Information located in a thesis may be subject to specific use constraints, details of which may not be explicitly described. It is the responsibility of potential and actual users to be aware of such constraints and to abide by them. By making use of material from a digitised thesis, you accept these copyright and disclaimer provisions. Where it is brought to the attention of Trinity College Library that there may be a breach of copyright or other restraint, it is the policy to withdraw or take down access to a thesis while the issue is being resolved.

Access Agreement

By using a Digitised Thesis from Trinity College Library you are bound by the following Terms & Conditions. Please read them carefully.

I have read and I understand the following statement: All material supplied via a Digitised Thesis from Trinity College Library is protected by copyright and other intellectual property rights, and duplication or sale of all or part of any of a thesis is not permitted, except that material may be duplicated by you for your research use or for educational purposes in electronic or print form providing the copyright owners are acknowledged using the normal conventions. You must obtain permission for any other use. Electronic or print copies may not be offered, whether for sale or otherwise to anyone. This copy has been supplied on the understanding that it is copyright material and that no quotation from the thesis may be published without proper acknowledgement.

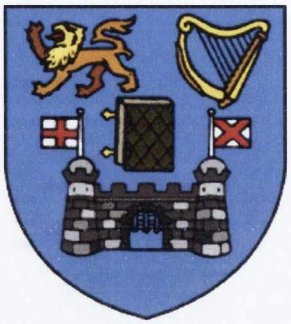

Dye Laser Micro-Fluidic Amplifiers

By

Paula Russell-Hill

A thesis submitted for the degree of
Doctor of Philosophy
in the
University of Dublin.

School of Physics
Trinity College Dublin

2011

Dedicated to

my parents, Derek and Teresa

my brother, Owen

and to Cian

Declaration

I declare that the work in this thesis has not been previously submitted as an exercise for a degree to this or any other university.

The work described herein is entirely my own, except for the assistance mentioned in the acknowledgements and the collaborative work mentioned in the list of publications.

I agree that Trinity College Library may lend or copy this thesis on request.

Acknowledgements

Firstly, I would like to thank my supervisor, Prof. Werner Blau, for the opportunity to do a postgraduate degree with the department, and for all of the support over the years. I would also like to acknowledge the help of Dr. Takeyuki Kobayashi in the first two years of my project.

I would like to sincerely thank Dr. Jun Wang for all of his help over the last few years. I am forever grateful for all of the advice you have provided – I would have been lost without it.

To all the members of group BU, including the CoCo Pops and MI, both past and present: I can honestly say that my time in Trinity would not have been nearly as much fun without you. Whenever a tough day comes about, there is always someone there for reassurance and a cup of coffee! Darren and Niall – who have not only had to put up with me through our time in the group, but also throughout our undergraduate days – it has been great to have such good company along the way. To Shane you have always been there to help, from day one, and I am forever grateful (oh, and don't worry, we forgive you…)! To those that always see us as the 'newbies'; Yenny, Fiona, Helen, Denis, David B, Emer, Adam, James, Rory, Valeria, Sharon, Eimhin, Chris. Thanks to Martin; as the only other laser-operator in a sea of carbon nanotubes, you were always a great help to me. Anna; thank you for everything over the years, the place would be a much less safe place without you! Eddie, Trevor, Zhenyu, Umar, Les, Ronan H, Denise, Evelyn, Phil, David R, Karen, Marguerite, Mustafa, Brian, Arlene, Paul, Sophie, Ronan S, Peter, and all the new newbies.

A special word has to be said for everyone in 22 Westland Row, in particular to those who I have had the joy of sharing an office with over the years (in the B.R.O.H.). I hope it always remains dictatorship-free…

I would like to say thank you to everyone in the School of physics, in particular Jeanette, John, Jemer, Robbie, Joe, Gillian and Pat, everyone in the workshop and school office. I would also like to thank Dr. Clare Higgins and Dr. Bradley for their help with the fluorescence excitation lifetime measurements.

I would like to acknowledge everyone who helped with this thesis. In particular; Neal in CMA (and Darren) for their help with the optical microscope; Niall for providing the micro-spheres and Jun for the Mathematica help. I would also, most sincerely, like to thank those that took the time (and effort) to help proof read this thesis.

I would also like to acknowledge my friends outside of college who always been there to lend an ear, and, even now, still try to understand what it is that we do everyday in the basement labs.

Finally, to my Mum and Dad, Derek and Teresa, and my brother, Owen. I do not think I have the words express how thankful I am for all of the endless support, help and guidance you have given me over the years. You have always supported me in whatever venture I set out in. I just hope I have done you proud. The very last word has to go to Cian, who has always been there - through the tears, tantrums and triumphs – not many people could put up with the seemingly-endless years spent as a student. Thank you all, from the very bottom of my heart.

Abstract

Dye lasers, based on micro-fluidic systems, have been the focus of increasing attention in recent years. Whereas micro-fluidics networks, such as a 'lab-on-a-chip', involve expensive and complicated fabrication processes, the use of micro-capillaries as cavities for dye solutions provides a low cost option. Employing the well-known organic laser dye, Rhodamine 590, as the active material, a series of micro-amplifiers are developed by incorporating the dye solutions into various micro-cavities, namely, capillary tubes and photonic crystal fibres (PCFs), via capillarity.

Photophysical properties, such as absorption, emission and fluorescence lifetime, were studied for the dye solutions with and without the addition of micro-scatterers. The absorption and emission spectroscopies revealed the characteristically strong absorption and emission performances of the dye molecules in the visible region in the micro-cavities. Upon pulsed nanosecond photoexcitation by the second harmonic of an Nd:YAG laser at 532 nm, strong amplified spontaneous emission (ASE) was observed for even the narrowest of device diameters, down to 6 μm.

Gain characteristics were investigated by measuring the gain coefficient of the micro-amplifiers. The variable stripe length (VSL) method was employed to determine the amplification properties of the dye-doped micro-capillaries. At low pump powers, in the region of 6 mW, gain was measured up to 5.3 cm^{-1} for the 25 μm device. The one-dimensional amplifier model was applied to fit the VSL data, resulting in the unsaturated and saturated gain coefficients of the micro-devices.

To modify the emission properties of the dye-doped micro-capillaries, micro-scatterers, including the polymer PVP and polystyrene micro-spheres, were incorporated into the devices. Whereas the scatterer-involved micro-amplifiers exhibited similar amplification performances with the dye-doped micro-capillaries, the scatterers significantly improved the photoluminescence efficiency of the dye solutions, implying a better emission property of the devices.

The structure of the device was then changed by replacing the capillary tube with a hollow-core photonic crystal fibre (PCF). The periodic array of nano-sized capillaries

surrounding the hollow-core had an effect on the observed emission properties. The combination of micro-spheres and PVP in particular, generated a strong shift of 20 nm in the peak emission wavelength. In comparison to the 25 μm devices the PCFs exhibited higher gain values for the equivalent solutions. It is thought that, due to the greater degree of confinement within the 6 μm hollow-core PCF, the increase in the refractive index has a greater effect on the emission properties. The interference caused by the periodic structure causes the higher level of amplification efficiency.

The polarised emission of the laser beam is important in fundamental science and real-life applications. In this work, the polarised stimulated emission was generated by adjusting the polarisation state of the pump beam. The polarisation direction within the pump beam profile was orientated by way of a waveplate, whereby the direction of the oscillating electric field is altered. A strong dependence of the intensity of the light emitted from the filled micro-capillaries on the polarisation conditions was observed, primarily for s-polarised and positively circular-polarised pumping. The effect of these changes in the polarisation condition on the optical gain is also measured, and hence the optimum settings for strong emission can be achieved.

This study shows how dye-doped micro-capillaries and PCFs exhibited strong emission properties in order to enable them to be incorporated into devices for amplification purposes. A high level of tunability is achieved by simply changing the dye used, the structure of the device and the polarisation state of the exciting beam. Hence, such devices show promise for a range of applications. The feasibility of using such cavities as micro-dye laser amplifiers is demonstrated. It is expected that these capillary based micro-amplifiers could be easily integrated into optofluidic networks as versatile light sources for lab-on-a-chip systems.

Table of Contents

Chapter 1

Introduction

1.1 Motivation

A laser consists of a material capable of amplifying light (the gain medium) in a cavity (or resonator) which applies an optical feedback [1]. The amplification occurs by the process of stimulated emission whereby an incident photon stimulates a transition from the excited state to ground state of the medium, generating further photons. When a photon is incident on a material, it can cause an electron to be excited from a lower to a higher energy level, a process known as absorption. Similarly, when a photon is incident on a material which has already been excited, it can cause an electron to fall from a higher to a lower energy level and the emission of another photon, a process known as stimulated emission. This was first proved by Einstein based on thermodynamic considerations [2, 3] and shall be discussed in further detail in Chapter 2.

In 1954 Townes and co-workers realised the first maser (microwave amplification by stimulated emission of radiation). They designed a microwave oscillator based on stimulated emission by molecules (NH_3) in an excited state [4, 5]. In 1960, Schawlow and Townes extended the concept of the maser to higher frequencies of the electromagnetic spectrum. They proposed Infrared and Optical Masers, based on the use of a plane and parallel Fabry-Perot interferometer as an optical resonator to provide a strong coupling between light and the amplifying laser materials [6]. This laid the groundwork for the development of the laser. Maiman realised the first laser using the fluorescence of a ruby crystal pumped by a xenon discharge lamp [7, 8]. Shortly thereafter followed the operation of the first gas (Helium-Neon) laser by Javan [9], and the following year Hall et al. described the first semiconductor laser [10]. In contrast to a usual thermal light source such as an incandescent (tungsten) lamp, a laser source produces coherent light amplified by stimulated emission in an active medium inside an optical resonator, whose spectrum is exceptionally narrow and highly directional.

1.1.1 Optical Amplifier

A laser amplifier is a device whereby the input signal directly amplifies or increases the power of the output signal, through the process of stimulated emission. There are many different types of laser amplifiers available, such as laser crystal [11] or glass which are doped with active ions, waveguide structures i.e. optical fibres [12], etc. Common doping materials are rare earth elements, such as erbium or ytterbium, or transition metal elements, such as titanium or chromium, are also used. Semiconducting optical amplifiers use a semiconductor, such as gallium arsenide or indium phosphide, or alloys thereof, to act as the gain medium [13, 14]. Both types can be either optically or electrically pumped. By combining these materials with mirrors or an additional series of amplifiers, stronger amplification can be observed. Optical amplifiers can also be based on the non-linear response parameters of a material, as opposed to stimulated emission. For example in a Raman amplifier, the amplification is achieved through the non-linear scattering interaction between the signal and the pump beam [15]. Today, commercially available amplifiers tend to be based on semiconductor amplifiers and rare-earth doped optical fibres, primarily in the IR region.

As will be discussed later in further detail, lasers dyes are materials which have very broad and strong emission bands, over the ultra-violet, visible and near infra-red spectral range. In 1966, Sorokin and Lankard published the first report of laser emission from a phthalocyanine-based laser dye [16]. The importance of this observation was that these laser dyes could provide simple, tunable and high power light sources. Dye lasers consist of dye molecules mixed with a solvent and circulated through the system. A high energy pump, such as a flashlamp or external laser is used to excite the dye molecules. Typically, mirrors are used within the optical cavity to provide a feedback mechanism for the amplification of the signal. Each laser dye emits at a characteristic wavelength, depending on its molecular structure. The dyes can be easily interchanged in order to tune the laser to the spectral range required. Adjusting the concentration, solvent used, temperature, etc. can also alter the emitted wavelength. A wavelength-dispersive optical element such as a diffraction grating or prism can be introduced in order to perform selective tuning [17]. Dye laser amplifiers have been used to boost the power of weak laser oscillators and improve spectral brightness and spatial radiance of laser outputs [18].

1.1.2 Micro-fluidics

The next generation of emerging technologies in optical devices is *micro-fluidics*, whereby the tunability and versatility of fluids is incorporated into the devices. The field of micro-fluidics study was originally motivated by the need for small-volume biological assays and experiments [19, 20]. The utilisation of microscopic volumes of fluids to perform tasks *in situ*, such as modifying optical properties of an air void, and thus the optical response of a micro-structured device. For example, the modification of an optical device by a fluid in a known way can be used as environmental or analysis sensors [21].

The field of micro-fluidics is rapidly growing, and one of the main challenges is to integrate multifunctionalities onto a chip for a wide variety of applications, such as bioanalytical studies [22], analysis sensors, etc. Among many others, integration of planar optical components is of great importance for the development of on-chip detection [23-25]. It has previously been shown that a laser micro-cavity can be integrated into a micro-fluidic system that can be used to produce desired laser emission peaks [26-30]. However, the techniques described, more often than not, require the dye flow through the cell. Such devices can be used as light-based sensors on-chip [23], which otherwise requires cumbersome optical alignment of light source and chip at every use. In particular single-mode laser devices are important for interference-based sensors [31, 32].

One of the main reasons behind the development of lasing micro-amplifier is the potential ability to incorporate these micro-scale devices into 'lab-on-a-chip' systems [33, 34]. In much of the literature, the fabrication of the reported micro-cavity amplifiers requires expensive and complex state-of-the-art crystal growth and micro-fabrication facilities [26, 30, 35]. In this work, we propose a straightforward (to manufacture) and inexpensive alternative. By keeping the gain medium in the liquid phase, it allows control which is not achievable in solid-state devices.

Micro-cavity lasers have already been fabricated [26], however they require metallic mirrors or semiconducting Bragg reflectors and complicated fabrication processes, and pumping of the dye solution through the channels of the device. For example, Cao et al. developed a cluster of ZnO micro-particles, which exhibit laser-like behaviour in the UV region [36]. Vasdekis et al. [37] have also demonstrated the possibility of compact fluidic fibre lasers (2 μm), based on capillary tubes. An et al. have reported the observation of laser oscillation from a single atom in an optical resonator [38]. Frolov et al. developed

polymer-based micro-ring and micro-disk devices which showed narrow line laser emission [39, 40]. These 'micro-lasers' usually require complex experimental techniques, the use of optical tweezers, high fabrication temperatures, etc. The key issue for a micro-laser is to confine light in a small volume with dimensions in the order of the optical wavelength [41].

Many of these devices can be integrated with other micro-fluidic systems without adding further process steps. The functionality of micro-systems can be significantly enhanced by the integration of lasers and other active optical components. Conjugated organic molecules, dye molecules, can be used as active medium, either dissolved in a liquid solution or cast into a solid polymer matrix [42]. Capillaries have been integrated into micro-chips by Yokoyama et al., whereby a Fabry-Perot micro-cavity of two glass wafers with dielectric multi-layer mirrors was assembled [43]. They observed spontaneous and stimulated emission from their 300 μm long devices when excited to a maximum of 5 mW pump power from a continuous-wave Argon laser. Li et al. used a dye-based distributed feedback structure as the optical cavity of an optofluidic dye laser system, whereby the flow of dye solution through the structure acted as a Bragg grating in order to guide the emission output [44].

The integration of micro-fluidics into devices and the miniaturising of liquid dye lasers on a micro-fluidic device have many advantages. Undesirable features of conventional bulk dye lasers can be eliminated. The size and complexity of both the optical and liquid-handling systems can be dramatically reduced. The extremely small consumption of dye solutions reduces the cost, and (if sealed) the safety and ease of use. They can also offer unique optical performances, i.e. the lasing wavelength can be easily changed by mixing or switching the solvents (to modify refractive index or concentration), the choice of dye molecule, etc.

The aim of this work is to develop a series of capillary based micro dye amplifiers as the potential light sources for the micro-fluidic devices. Through the control and enhancement of the optical gain in organic media, an experimental examination of various methods is presented in this thesis. The organic laser dye, Rhodamine 590, is used as the gain medium as it is a well established and characterised model substance. The strong amplification, ease of fabrication and versatility in changing the organic dye in question are strong driving points. Due to the off chip optical pumping required the dye-doped

micro-amplifiers discussed in this work are not stand alone systems. In this thesis it is proposed that such devices have strongly advantageous properties that will be useful as tunable, effective and inexpensive micro-amplifiers than many of the devices available today. The fibres presented in this research are easily fabricated and tuned, to the desired wavelength region. They have the ability to be integrated with other optical and micro-fluidic functions to build complete 'lab-on-a-chip' systems.

1.2 Outline

The thesis will be outline as follows:

Chapter 2 – Theory and Background. An introduction into the theory behind the basic concepts of the dye-doped micro-capillaries is presented. An overview of the fundamental mechanisms and properties of the organic lasers dyes, which act as the gain medium, are described.

Chapter 3 – Materials and Basic Spectroscopic Characterisations. This chapter outlines the materials used in this study, namely the organic dye, Rhodamine 590. The basic spectroscopic properties are presented, such as absorption and emission spectra and fluorescence lifetime measurements. The effect of organic dye concentration on the absorption and emission properties is also investigated. Much of this basic information is used in the following chapters.

Chapter 4 – Optical Gain Characterisation. The fabrication and measurement of the amplification of these dye-doped capillaries is presented. The amplification of the micro-capillaries is determined by measuring the optical gain, via the variable stripe length method. The theories behind the methods used and the experimental setup are also discussed. The optical gain coefficients for a range of capillary diameters are measured.

Chapter 5 – Polarised Dye Micro-Amplifiers. The effect of changing the polarisation properties of the pump beam is investigated. The variation of the emission characteristics from the micro-amplifiers is determined as the pump conditions are changed. It is important to ascertain these effects as the optical gain of many laser systems depends strongly on the state of polarisation of the pump beam. This gain-polarisation dependency is verified in this chapter.

Chapter 6 – Dye Micro-Amplifiers Incorporating Micro-Scatterers. This chapter investigates how micro-scatterers, when added to the dye-doped capillaries, can change the properties observed. Ordinarily, in laser systems scattering is thought to be detrimental to the emission. However, it has been theorised and experimentally proven that scattering centres can enhance the amplification of such optical devices by increasing the path length, and hence cause further stimulated emission. The concept of such 'random lasing' systems is investigated. The emission and amplification dependence on the polarisation state of the exciting pump beam is determined.

Chapter 7 – Photonic Crystal Fibre Amplifiers. The standard capillary tube used thus far is replaced with the periodic array of a photonic crystal fibre. Along with the addition of the micro-scatterers, and the polarisation condition of the pump beam, the amplification features of these dye-doped periodic fibres are investigated. The combination of such fibres with the refractive-index changing polymer and the micro-scatters induces a shift in the characteristic emission wavelength of the laser dye, Rhodamine 590.

Chapter 8 – Conclusions and Future Work. Finally, brief synopses of the findings of this thesis are given. Potential suggestions for the future work with these micro-scale amplifiers are also included in the discussion.

References

1. Samuel, I.D.W. and G.A. Turnbull, *Chemical Reviews*, 2007. **107**(4): p. 1272-1295.
2. Siegman, A.E., *Lasers*. 1986: University Sceince.
3. Svelto, O., *Principles of Lasers*. 1998, New York London: Springer.
4. Gordon, J.P., H.J. Zeiger, and C.H. Townes, *Physical Review*, 1954. **95**(1): p. 282-284.
5. Gordon, J.P., H.J. Zeiger, and C.H. Townes, *Physical Review*, 1955. **99**(4): p. 1264-1274.
6. Schawlow, A.L. and C.H. Townes, *Physical Review*, 1958. **112**(6): p. 1940-1949.
7. Maiman, T.H., *Nature*, 1960. **187**(4736): p. 493-494.
8. Maiman, T.H., *Journal of the Optical Society of America*, 1960. **50**(11): p. 1134-1134.
9. Javan, A., D.R. Herriott, and W.R. Bennett, *Physical Review Letters*, 1961. **6**(1): p. 106-110.
10. Hall, R.N., R.O. Carlson, T.J. Soltys, G.E. Fenner, and J.D. Kingsley, *Physical Review Letters*, 1962. **9**(9): p. 366-&.
11. Kaminskii, A.A., *Laser & Photon. Rev.*, 2007. **1**(2): p. 93–177.
12. Koester, C.J. and E. Snitzer, *Applied Optics*, 1964. **3**(10): p. 1182-1186.
13. Connelly, M.J., *Semiconductor optical amplifiers*. 2002: Springer.
14. Eisenstein, G., *Ieee Circuits and Devices Magazine*, 1989. **5**(4): p. 25-30.
15. López-Higuera, J.M., *Handbook of optical fibre sensing technology*. 2002: Wiley.
16. Sorokin, P.P. and J.R. Lankard, *Ibm Journal of Research and Development*, 1966. **10**(2): p. 162-163.
17. Capelle, G. and D. Phillips, *Applied Optics*, 1970. **9**(12): p. 2742-2745.
18. Schäfer, F.P. and K.H. Drexhage, *Dye lasers*. 2nd rev. ed. ed. Topics in applied physics ; vol.1. 1977, Berlin ; New York: Springer.
19. Cao, X.D., B.C. Barnett, K.H. Ahn, Y. Liang, G.R. Williams, M. Vaziri, and M.N. Islam, *Optics Letters*, 1996. **21**(16): p. 1211-1213.
20. Tang, Z.L., S.B. Hong, D. Djukic, V. Modi, A.C. West, J. Yardley, and R.M. Osgood, *Journal of Micromechanics and Microengineering*, 2002. **12**(6): p. 870-877.
21. Domachuk, P., H.C. Nguyen, B.J. Eggleton, M. Straub, and M. Gu, *Applied Physics Letters*, 2004. **84**(11): p. 1838-1840.
22. Manz, A. and H. Becker, *Microsystem Technology in Chemical and Life Sciences*. 1999, Berlin: Springer.
23. Verpoorte, E., *Lab on a Chip*, 2003. **3**(3): p. 42-52.
24. Roulet, J.C., R. Volkel, H.P. Herzig, E. Verpoorte, N.F. de Rooij, and R. Dandliker, *Journal of Microelectromechanical Systems*, 2001. **10**(4): p. 482-491.
25. Vezenov, D.V., B.T. Mayers, D.B. Wolfe, and G.M. Whitesides, *Applied Physics Letters*, 2005. **86**(4).
26. Helbo, B., A. Kristensen, and A. Menon, *Journal of Micromechanics and Microengineering*, 2003. **13**(2): p. 307-311.
27. Wendt, J.R., M.E. Warren, W.C. Sweatt, C.G. Bailey, C.M. Matzke, D.W. Arnold, A.A. Allerman, T.R. Carter, R.E. Asbill, and S. Samora, *Journal of Vacuum Science & Technology B*, 1999. **17**(6): p. 3252-3255.
28. Gersborg-Hansen, M., S. Balslev, N.A. Mortensen, and A. Kristensen, *Microelectronic Engineering*, 2005. **78-79**: p. 185-189.
29. Kytina, I.G., V.G. Kytin, and K. Lips, *Applied Physics Letters*, 2004. **84**(24): p. 4902-4904.

30. Cheng, Y., K. Sugioka, and K. Midorikawa, *Optics Letters*, 2004. **29**(17): p. 2007-2009.
31. Brecht, A. and G. Gauglitz, *Biosensors & Bioelectronics*, 1995. **10**(9-10): p. 923-936.
32. Balslev, S. and A. Kristensen, *Optics Express*, 2005. **13**(1): p. 344-351.
33. Li, Z.Y. and D. Psaltis, *Microfluidics and Nanofluidics*, 2008. **4**(1-2): p. 145-158.
34. Psaltis, D., S.R. Quake, and C.H. Yang, *Nature*, 2006. **442**(7101): p. 381-386.
35. Galas, J.C., J. Torres, M. Belotti, Q. Kou, and Y. Chen, *Applied Physics Letters*, 2005. **86**(26).
36. Cao, H., J.Y. Xu, E.W. Seelig, and R.P.H. Chang, *Applied Physics Letters*, 2000. **76**(21): p. 2997-2999.
37. Vasdekis, A.E., G.E. Town, G.A. Turnbull, and I.D.W. Samuel, *Optics Express*, 2007. **15**(7): p. 3962-3967.
38. An, K., J.J. Childs, R.R. Dasari, and M.S. Feld, *Physical Review Letters*, 1994. **73**(25): p. 3375-3378.
39. Frolov, S.V., A. Fujii, D. Chinn, M. Hirohata, R. Hidayat, M. Taraguchi, T. Masuda, K. Yoshino, and Z.V. Vardeny, *Advanced Materials*, 1998. **10**(11): p. 869-872.
40. Frolov, S.V., Z.V. Vardeny, and K. Yoshino, *Applied Physics Letters*, 1998. **72**(15): p. 1802-1804.
41. Cao, H., *Waves in Random Media*, 2003. **13**(3): p. R1-R39.
42. Barroso, J., A. Costela, I. Garcia-Moreno, and R. Sastre, *Chemical Physics*, 1998. **238**(2): p. 257-272.
43. Yokoyama, H., M. Suzuki, and Y. Nambu, *Applied Physics Letters*, 1991. **58**(23): p. 2598-2600.
44. Li, Z.Y., Z.Y. Zhang, T. Emery, A. Scherer, and D. Psaltis, *Optics Express*, 2006. **14**(2): p. 696-701.

Chapter 2

Theory and Background

2.1 Basic Properties of Organic Compounds

2.1.1 Organic Compounds

Organic materials are those whose structure is based on carbon. Organic compounds and their derivatives can be subdivided into saturated and unsaturated compounds, whereby the former contains single bonds and the latter at least one double or triple bond. These multiple bonds have a strong effect on the chemical reactivity and influence the spectroscopic properties [1]. One of the most important properties, for this work, is that the presence of the double or triple bonds strongly influences the wavelength at which absorption occurs.

Atomic carbon is unique as it is able to form a wide variety of different structures. It is unusual because it has the ability to form strong, stable bonds with the majority of elements in the periodic table. The nature of the bonds between the carbon atoms underlies the varied chemical and physical properties of the carbon allotropes. Its electronic configuration is $1s^2 2s^2 2p^2$.

-C=C-C=C-C=C-

Figure 2.1 Alternating bonds in a conjugated molecule

Conjugated molecules consist of both alternating single and double bonds. The electronic structure of these compounds is such that the level separation is significantly less than the dissociation energy, so photochemical decomposition is less likely to occur. Compounds without double or triple bonds usually have higher photon energies, increasing the likelihood of photochemical decomposition; hence such compounds are not suitable as the active medium in lasers. Single bonds form σ bonds by the end-on overlap of two molecular orbitals. The probability of finding an electron is highest along the axis joining the nuclei of the bonded atoms, and has a rotational symmetry along this axis. The σ electrons are tightly bound to the nuclei and high energies are required to promote them to

higher molecular orbitals. The double bonds in a conjugated molecule are made of both σ and π bonds. A π bond is constructed from the side-on overlap of two p orbitals (providing more electron delocalisation, lower electron energy and greater stability). In this position, the π bond gives the conjugated molecule a planar structure, with high rigidity, as the bond energy is highest and the molecule most stable when they symmetry axes of the p_z lobes, as seen in Fig. 2.2 (b), are parallel. The probability of finding an electron is largest above and below the axis joining the two atoms and the rotational symmetry is along the line through the nucleus and perpendicular to the σ bond. An electron is more weakly bound to a π bond than it is to a σ bond. Therefore, the σ molecular orbital has to be filled first in order to stabilise the molecule. The basic mechanism responsible for light absorption by compounds containing conjugated double bonds is the same in whatever part of the spectrum these compounds have their longest wavelength absorption band.

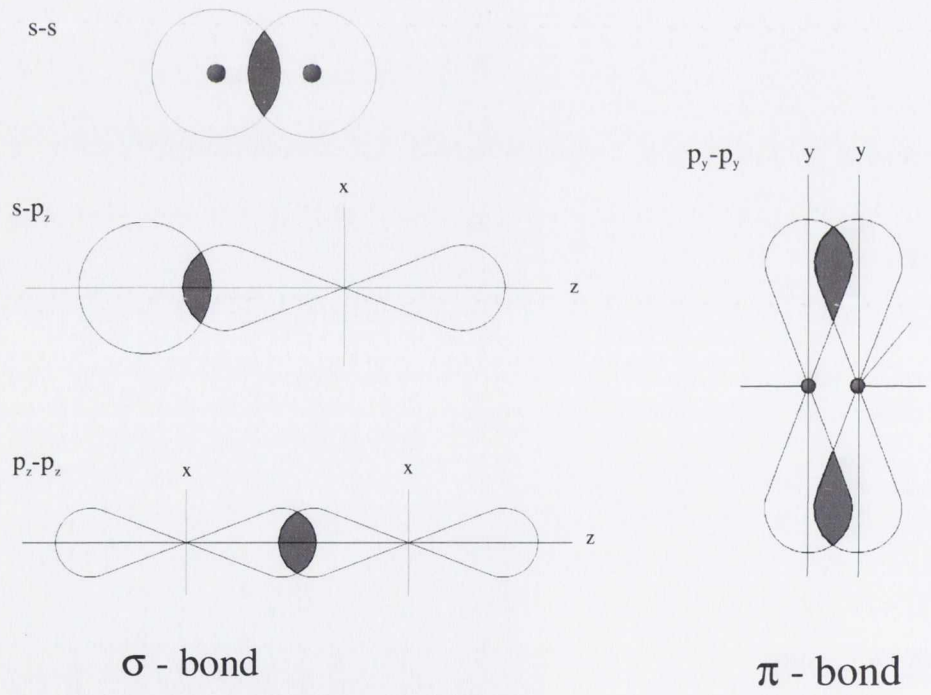

Figure 2.2 Schematic of the formation of (a) σ-bond and (b) π-bond by the overlap of molecular orbitals

2.1.2 Properties of Organic Dyes

The term 'dye' encompasses all substances containing conjugated double bonds. Organic dyes are a class of coloured compounds which have strong and wide absorption and

emission bandwidths ranging from the ultraviolet to the near infrared. Such properties are only found in organic compounds which contain an extended system of conjugated bonds, i.e. alternating single and double bonds. This makes them particularly suitable for use in tunable and pulsed lasers. Moreover, in many systems the dye can be easily replaced by another type in order to generate different wavelengths within the same device. The large number of available dyes and the wide range of applications provide proof of their flexibility and versatility. They have applications in many fields such as industrial, medical, military, studies of fundamental physics, spectroscopy, light detection, etc.

The first report of dye laser action was that of Sorokin and Lankard in 1966 who observed laser emission form a solution of chloroaluminium pthalocyanine [2]. Independently, Schäfer, Schmidt and Volze (1966) obtained laser action in the infrared from a number of cyanin-type dyes [3]. These contributions were significant as they were the first reports of laser action from broad, diffuse energy bands rather than a set of discrete energy levels, typical of gas and rare earth lasers.

Photophysical properties such as absorption, emission (fluorescence) yield, Stokes shift, and triplet formation influence the threshold and peak power lasing characteristics of the dyes. Laser dyes typically show large absorption bands, as measured by their molar extinction coefficients, ε. This feature is responsible for the high optical densities associated with moderate concentrations of dye and results from the high degree of delocalisation and polarisability of π electrons in dye structures. The degree to which electron density in a dye molecule is 'rearranged' or polarised, as the result of absorption of photons, is related to the transition dipole moment for the electronic transition [1]. The photophysical properties of laser dyes were found to be highly sensitive to the nature of solvents and to environment [4-7]. The polarity of solvents, their viscosity and dielectric constants are found to be critical in the photochemical behaviour of laser dyes.

There are several classes of dyes including; oxazoles, conjugated hyrdrocarbons, coumarins, xanthenes and cyanines. All of these classes of structures share the property of conjugation of π bonds to carbon. The group of Xanthene dyes, of which Rhodamine 590 is one, have a xanthene ring as the chromophore. Rhodamine 590 has been a standard for evaluating other dyes ever since the early days of dye laser operation [4, 5]. It has a very high lasing efficiency and good chemical stability.

The material parameters crucial for the design of efficient light amplification and lasing devices can be fine-tuned by varying the chemical structure. These parameters include emission colour, photoluminescence quantum yield, bandwidth, Stokes shift and compatibility with host materials [6]. Homogeneous broadening of laser dyes is the physical mechanism which allows optical power to be efficiently channelled into a small oscillating bandwidth (for a dye laser). Normally, a dye molecule is excited at some wavelength corresponding to the optical pump energy, and spontaneous and stimulated emission occurs at a range of longer wavelengths according to the Franck-Condon principle [7]. Dye lasers have been demonstrated to be useful and versatile sources of tunable coherent radiation with wide applicability in many different fields [8].

Organic laser dyes are known to exhibit optical gain upon optical excitation in solution or when dispersed in an inert polymer matrix. The advantage of combining dyes and conjugated polymers are that they can have high photoluminescence quantum yields even as neat films, thereby enabling very high optical gain in solid state; their capacity for simple fabrication of waveguides; and the future prospect of electrical pumping, etc [9-11]. Amplified spontaneous emission (ASE) and lasing action from photopumped polymers have been demonstrated with a variety of device configurations such as waveguide structures [12, 13], the Fabry-Perot micro-cavity [14], the photonic band gap [15], two-mirror resonators [16] and glass-clad polymer fibres [17, 18]. The exponential increase of the output intensity as a function of the excited stripe length clearly shows the existence of optical gain occurring by ASE [18]. Laser dyes have been used for amplification of light pulses for many years [19-21]. The main limitation is that the dye concentration should be kept low to avoid concentration quenching due to aggregation of dye molecules [22].

The current surge for the development of organic lasers has been driven by several advantages of organic materials over their inorganic counterparts [6]. Organic materials allow for a great degree of flexibility in molecular design and chemical synthesis. Organic materials also enable low temperature fabrication processes (typically less than 100°C), whereas inorganic materials need high-temperature processing. The broad spectral features of organic systems give rise to colour tunability and provide favourable implications for generation and amplification of ultrashort optical pulses. The potential very low cost makes organic materials competitive for industrial applications.

However, it should be noted that organic dyes also have some disadvantages. For example, dye aggregation can occur, usually for higher concentrations. This effect is connected with the reduced lifetime of the dye molecule (for Rhodamine study [23]). Photodegredation is also a factor, especially when dealing with high excitation powers and frequencies.

2.1.3 Absorption of Light

The π-bonds are much weaker than the σ-bonds; therefore they have much lower energy and are more readily excited, which extends their absorption wavelength further into the longer wavelength region of the spectrum. The delocalisation of π-electrons is an important aspect to understanding the interaction of visible and near UV light with organic molecules. Molecules with extensively delocalised π-electron systems can have the maximum of their absorption band extend far into the visible part of the spectrum. The long wavelength limit to absorption is related to the thermal stability of the dye.

Considering the energy levels of a system, whereby S_0 is the ground state and S_1 the excited state. The optical excitation of dyes corresponds to transitions of molecules in the singlet state, with the absorption $S_0 \rightarrow S_1$ being the strongest and is specific for each dye molecule. Most dyes have additional absorption bands in the UV, from which fast internal relaxation processes lead to the upper laser level (S_1) with high quantum efficiency. This is the reason why most dyes can be pumped by a single UV laser.

The light absorption of dyes can be understood by taking a simplified quantum-mechanical model, such as the free-electron gas model [1]. This model is based on the fact that dye molecules are essentially planar, with all atoms of the conjugated chain lying in a common plane and linked by σ bonds. The electrostatic potential for any single π electron moving in the field of the rest of the molecule may be considered constant, provided all bond lengths and atoms are the same. It is assumed that the conjugated chain has length L, so then the energy E_n of the nth eigenstate of this electron is given by $E_n=h^2n^2/8mL^2$, where h is Planck's constant, m is the mass of the electron and n is the quantum number giving the number of antinodes of the eigenfunction along the chain. According to the Pauli principle, each state can be occupied by two electrons. Therefore, if there are N electrons, the lower $1/2N$ states are filled with two electrons each, while all higher states are empty (provided N is an even number, which is usually the case in stable

molecules as only highly reactive radicals possess an unpaired electron). The absorption of one photon of energy $\Delta E=hc_0/\lambda$ (where λ is the wavelength of the absorbed radiation and c_0 is the velocity of light) raises one electron from an occupied to an empty state. The longest wavelength absorption band then corresponds to a transition from the highest occupied to the lowest empty state with

$$\Delta E_{\min} = \frac{h^2}{8mL^2}(N+1)$$

$$\text{or } \lambda_{\max} = \frac{2mc_0}{h}\frac{L^2}{N+1} \qquad (2.1)$$

This indicates that, to first approximation, the position of the absorption band is determined only by the chain length and by the number of π electrons, N.

The ground state absorption cross-section is determined directly from the absorption spectrum and is given by $\sigma_{abs}(\lambda) = \alpha/c$ (where c is the concentration and α is the absorption coefficient) and $\alpha = ln(1/T(\lambda))/l$ (where l is the thickness of the cuvette and T is the measured transmittance of the samples). Amplification is obtained by stimulated emission. In laser dyes the relevant transition is from the first excited state back down to the ground state. It is stimulated by an incident photon; as a result, another photon is emitted of the same frequency and direction as the stimulating photon. The presence of ASE indicates that the gain is greater than α.

2.2 Organic Dyes: A Four-Level Laser System

The most important electronic energy levels for organic dyes in fluidic media are the ground state (S_0) and the first excited state (S_1). The absorption of light which raises molecules to the upper level is associated with promotion of an electron in a bonding orbital to an antibonding orbital of the molecule. This electronic rearrangement is accompanied by a displacement of the equilibrium nuclear coordinates of the molecule; the vibrational energy states associated with these nuclear coordinate changes are depicted by the subspacings (Fig. 2.3). In other words, each electronic level is a band composed of a continuum of vibrational and rotational levels. Thus, the dye laser may be viewed as a 'four-level' system in that the most probable excitations proceed to populate upper vibrational levels in S_1, a vibrational relaxation to the 'zeroth' level in S_1 then

follows, and emission occurs to repopulate an upper vibrational level of the ground state (S_0), as seen in Fig. 2.3.

When the dye is pumped with an intense light source such as a laser or flashlamp, the molecules are excited typically to some higher electronic state. The lowest energy absorption is due to absorption from the electronic singlet ground state S_0 to the first excited singlet state S_1. This strong absorption, usually in the visible region of the spectrum, is responsible for the useful property of the dyes that they colour other substances such as cloth, food, plastics, etc. Rhodamine 590, for example, has an absorption spectrum which is about 50 nm wide and it has a strong fluorescence emission in the 555 to 585 nm region.

Once the dye molecules absorb the pump light, the energy is then released. Some of the energy is lost due to thermal effects and the rest is radiated in the form of light. Spontaneous emission, or fluorescence, occurs when the excited dye molecule lowers its energy by spontaneously emitting a photon i.e. the process whereby the electron relaxes from the excited state, S_1, to the ground state, S_0. Due to the large transition moment the rate of spontaneous emission is relatively high (the radiative lifetime is in the order of nanoseconds) and the gain of a dye laser may exceed that of sold-state lasers by several orders of magnitude.

For optimal lasing efficiency it is desirable for the dye molecules to remain in the excited energy level for long enough in order to be involved in stimulated emission. Stimulated emission occurs when photons further interact with the dye molecule within an excited state. It is this process that increases or amplifies the optical energy of the system coherently. Stimulated emission or laser action can occur over the fluorescence band, with typical lifetimes of 1 to 5 ns.

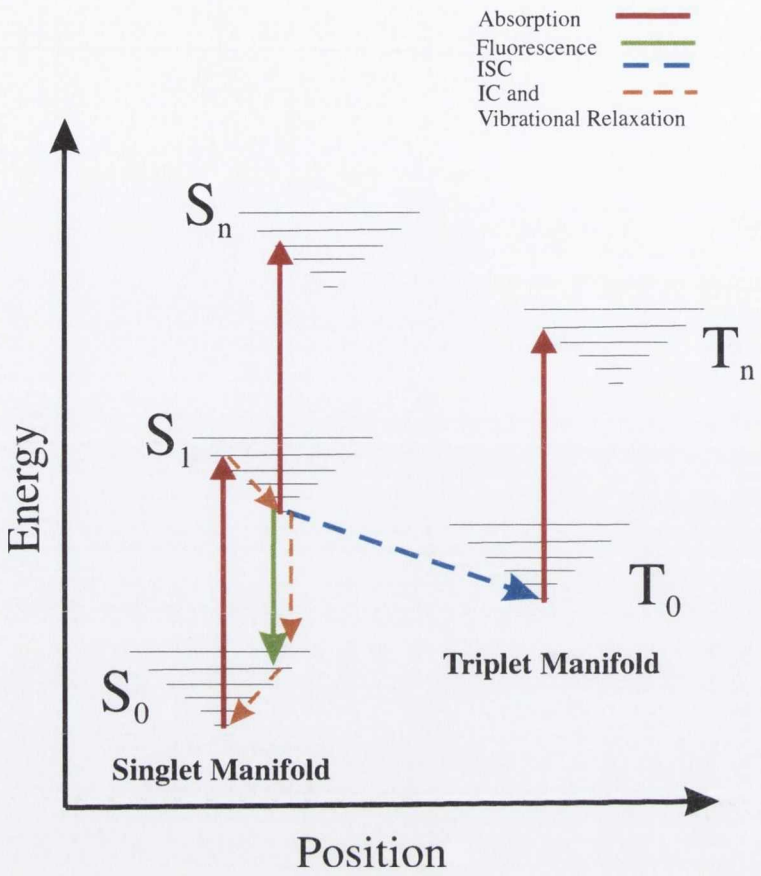

Figure 2.3 Jablonski diagram for a four-level laser system

However, there are many non-radiative processes that can compete effectively with the light emission and thus reduce the fluorescence. These non-radiative processes can be divided into those that cause a direct relaxation to the ground state (internal conversion (IC)) and those that are responsible for intersystem crossing (ISC) to the triplet manifold. For organic dye molecules, the interaction of electron spin and orbital motion is developed to such a degree that spin-prohibited processes are probable, involving transitions to other excited states (principally, the lowest triplet state). Intersystem crossing is such a forbidden process, and is comparatively slow considering the small energy gap between S_1 and T_1. This is due to the relatively long lifetime of the triplet molecules (in the order of microseconds) that the dye accumulates during the pumping process in the triple state T_1, which often has considerable absorption for the laser light.

2.2.2 Einstein's Coefficients

To summarise, when an atom in its lowest energy level, or ground state configuration, is excited by a photon of adequate energy, it causes the electrons in the atom to be excited into a higher energy state. As it reverts back to its lower energy level, it emits a photon in a process known as spontaneous emission. It is also possible for the photon to interact with an excited atom while it is in an excited state, this atom in turn can emit a photon – a process known as stimulated emission. For absorption, the rate of change of the number of atoms in an initial state, as they leave to a higher state, must depend of the strength of the photon incident on those atoms, i.e. the energy density, specifically the energy density driving the transition.

The Einstein coefficients, A and B, describe the transitions of the atoms between the energy levels, 1 and 2. The coefficients B_{12} and A_{21} describe the absorption and spontaneous emission transitions respectively, at equilibrium [24]. Through these coefficients, Einstein introduced the concept of stimulated emission, B_{21}, which created the theoretical foundation for the laser. The rates of such transitions can be described as follows:

(a) for absorption

$$\left(\frac{dN_1}{dt}\right)_{ab} = -B_{12}N_1\rho(\nu) \qquad (2.2)$$

where $\rho(\nu)$ is the spectral energy density, B_{12} is a constant of proportionality, where the negative arises because the population density of the first energy level, N_1, is decreasing

(b) for stimulated emission

$$\left(\frac{dN_2}{dt}\right)_{st} = -B_{21}N_2\rho(\nu) \qquad (2.3)$$

(c) for spontaneous emission

$$\left(\frac{dN_2}{dt}\right)_{sp} = -A_{21}N_2 \qquad (2.4)$$

Therefore, the process is independent of the field environment.

The transition rate, the number of atoms making transitions per second divided by the number of atoms present, is the probability of a transition occurring per second. Consequently, A_{21} is the probability per second of spontaneous emission. From the rate equations, it can be assumed that the thermodynamic equilibrium exists between the radiation field and the atoms at any temperature; that the energy density has the characteristics of a blackbody at any temperature; and that the number of densities of the two states is in accordance with the Maxwell-Boltzmann distribution. Planck's' blackbody radiation law states that

$$I(\lambda) = \frac{2\pi\ hc^2}{\lambda^2 (e^{hc/\lambda kT}) - 1} \qquad (2.5)$$

where I is the intensity, h is Planck's constant, c is the speed of light, k is the Boltzmann constant, T is absolute temperature and λ is the wavelength. The Maxwell-Boltzmann distribution shows that the probability distribution function equates to

$$f(\upsilon) = 4\pi \left(\frac{m}{2\pi\ kT} \right)^{3/2} \upsilon^2 e^{-m\upsilon^2/2kT} \qquad (2.6)$$

where υ is the molecular velocity and $\varepsilon = 1/2 m\upsilon^2$.

Considering an ideal material with two non-degenerate energy levels, *1* and *2*, which have populations of N_1 and N_2, respectively. The total number of atoms in these two levels is assumed to be constant

$$N = N_1 + N_2 \qquad (2.7)$$

Radiative transfer between the two energy levels is dominated by the three processes; absorption, spontaneous emission and stimulated emission. If an electromagnetic wave, of frequency ν, passes though a material, with an energy gap $h\nu$, the change in the upper and lower level populations in the two-level model can be described as

$$-\frac{dN_1}{dt} = \frac{dN_2}{dt} = -A_{21}N_2 - B_{21}\rho(\nu)N_2 + B_{12}\rho(\nu)N_1 \qquad (2.8)$$

At equilibrium, the number of transitions per unit time from E_1 to E_2 must equal the number of transitions from E_2 to E_1, hence

$$-\frac{dN_1}{dt} = \frac{dN_2}{dt} = 0 \qquad (2.9)$$

Therefore,

$$A_{21}N_2 + B_{21}\rho(\nu)N_2 = B_{12}\rho(\nu)N_1 \qquad (2.10)$$

Dividing this equation by N_1 yields

$$\frac{N_2}{N_1} = \frac{B_{12}\rho(\upsilon)}{A_{21} + B_{21}\rho(\upsilon)} \qquad (2.11)$$

Using the Boltzmann equation for this ratio of N_2/N_1, the equation can be rewritten in the form

$$\rho(\nu) = \frac{A_{21}}{\frac{g_1}{g_2}\exp\left(\frac{h\nu}{k_B T}\right)B_{12} - B_{21}} \qquad (2.12)$$

where g_1 and g_2 are the degeneracy states of the two levels. When this expression is compared to the law of black body radiation, is obtained by rearranging Eq. 2.5

$$\rho(\nu)d\nu = \frac{8\pi\, n^3 h\nu^3}{c^3}\frac{d\nu}{\exp\left(\frac{h\nu}{k_B T}\right)-1} \qquad (2.13)$$

The expressions can then be rearranged to get

$$\frac{A_{21}}{B_{21}} = \frac{8\pi\, n^3 h\nu^3}{c^3} \qquad (2.14)$$

and subsequently

$$B_{21} = \frac{g_1}{g_2}B_{12} \qquad (2.15)$$

The above equation states that the probability for stimulated absorption and emission factors are equal, apart from the degeneracy states. The relations between A and B are known as Einstein's relations. The relationship between the Einstein coefficients shows the high probability of absorption and emission transitions, for both the spontaneous and stimulated processes.

2.3 References

1. Schäfer, F.P. and K.H. Drexhage, *Dye lasers*. 2nd rev. ed. ed. Topics in applied physics ; vol.1. 1977, Berlin ; New York: Springer.
2. Sorokin, P.P. and J.R. Lankard, *Ibm Journal of Research and Development*, 1966. **10**(2): p. 162-163.
3. Schäfer, F.P., W. Schmidt, and J. Volze, *Applied Physics Letters*, 1966. **9**(8): p. 306-&.
4. Geetha, K., M. Rajesh, V.P.N. Nampoori, C.P.G. Vallabhan, and P. Radhakrishnan, *Journal of Optics a-Pure and Applied Optics*, 2006. **8**(2): p. 189-193.
5. Barroso, J., A. Costela, I. Garcia-Moreno, and R. Sastre, *Chemical Physics*, 1998. **238**(2): p. 257-272.
6. Kobayashi, T., W.J. Blau, H. Tillmann, and H.H. Horhold, *IEEE Journal of Quantum Electronics*, 2003. **39**(5): p. 664-672.
7. Shank, C.V., *Reviews of Modern Physics*, 1975. **47**(3): p. 649-657.
8. Duarte, F.J. and L.W. Hillman, *Dye laser principles : with applications*. Quantum electronics. principles and applications. 1990, Boston ; London Academic Press.
9. Scherf, U., S. Riechel, U. Lemmer, and R.F. Mahrt, *Current Opinion in Solid State & Materials Science*, 2001. **5**(2-3): p. 143-154.
10. Samuel, I.D.W. and G.A. Turnbull, *Chemical Reviews*, 2007. **107**(4): p. 1272-1295.
11. Yap, B.K., R.D. Xia, M. Campoy-Quiles, P.N. Stavrinou, and D.D.C. Bradley, *Nature Materials*, 2008. **7**(5): p. 376-380.
12. Hide, F., M.A. DiazGarcia, B.J. Schwartz, M.R. Andersson, Q.B. Pei, and A.J. Heeger, *Science*, 1996. **273**(5283): p. 1833-1836.
13. Berggren, M., A. Dodabalapur, R.E. Slusher, and Z. Bao, *Nature*, 1997. **389**(6650): p. 466-469.
14. Becker, H., R.H. Friend, and T.D. Wilkinson, *Applied Physics Letters*, 1998. **72**(11): p. 1266-1268.
15. Dodabalapur, A., M. Berggren, R.E. Slusher, Z. Bao, A. Timko, P. Schiortino, E. Laskowski, H.E. Katz, and O. Nalamasu, *Ieee Journal of Selected Topics in Quantum Electronics*, 1998. **4**(1): p. 67-74.
16. Holzer, W., A. Penzkofer, S.H. Gong, A.P. Davey, and W.J. Blau, *Optical and Quantum Electronics*, 1997. **29**(7): p. 713-724.
17. Kobayashi, T., W.J. Blau, H. Tillmann, and H.H. Horhold, *Journal of Optics a-Pure and Applied Optics*, 2002. **4**(3): p. L1-L3.
18. McGehee, M.D., R. Gupta, S. Veenstra, E.K. Miller, M.A. Diaz-Garcia, and A.J. Heeger, *Physical Review B*, 1998. **58**(11): p. 7035-7039.
19. Koch, T.L., L.C. Chiu, and A. Yariv, *Journal of Applied Physics*, 1982. **53**(9): p. 6047-6059.
20. Huth, B.G., *Applied Physics Letters*, 1970. **16**(4): p. 185-&.
21. Flamant, P. and Y.H. Meyer, *Applied Physics Letters*, 1971. **19**(11): p. 491-&.
22. McGehee, M.D. and A.J. Heeger, *Advanced Materials*, 2000. **12**(22): p. 1655-1668.
23. Ojeda, P.R., I.A.K. Amashta, J.R. Ochoa, and I.L. Arbeloa, *Journal of the Chemical Society-Faraday Transactions Ii*, 1988. **84**: p. 1-8.
24. Fox, M., *Optical Properties of Solids*. 2001, Oxford: Oxford University Press.

Chapter 3

Materials and Basic Spectroscopic Characterisations

3.1 Introduction

In this chapter, the materials investigated as being suitable for optical amplification devices in the visible region are introduced. The basic spectroscopic and optical properties are presented. The strong absorption and emission properties of the organic dye, Rhodamine 590, are verified.

3.1.1 Rhodamine Dye

As described in Chapter 2, laser action was first reported in organic chromophores by Sorokin and Lankard in 1966 [1]. In this thesis the organic laser dye, Rhodamine 590, was chosen as it is one of the most widely known of all the laser dyes. 2-[6-(ethylamino)-3-(ethylimino)-2,7-dimethyl-3H-xanthen-9-yl]-benzoic chloride is also known as Rhodamine 6G, but herein shall be referred to as Rhodamine 590.

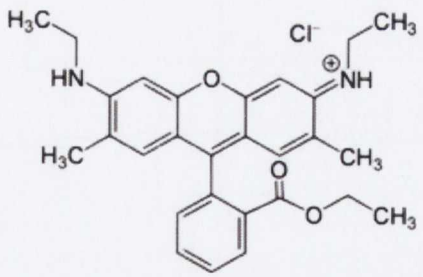

Figure 3.1 *Structure of the Rhodamine 590 molecule*

Rhodamine 590 is a red crystalline solid, purchased commercially from Exciton Inc. and has a molecular weight is 479.01 g. As with the majority of laser dyes, Rhodamine 590 has a broad absorption and emission peak, high photostability and high quantum yield [2], low cost, and its lasing range is in close proximity to its absorption maximum (which is approximately 530 nm). The lasing range of the dye is from 555 to 585 nm. For Rhodamine 590, the absorption cross section at the peak wavelength of 530 nm is approximately 3.8×10^{-16} cm^2 and the emission cross section is 1.2×10^{-16} cm^2 at the lasing wavelength of 580 nm [3].

Due to its central molecular structure (primarily, the aromatic C_6H_4 group) as seen in Fig. 3.1, Rhodamine 590 is from the class of laser dyes known as the Xanthene dyes, which cover the wavelength range from 500 to 700 nm. Their fluorescence spectra is known to closely resemble the mirror image of their absorption band [4].

The first measurement of flashlamp-pumped Rhodamine 590 dye laser was reported by Huth et al. in 1970, yielding a gain coefficient of 95 dB/m [5]. Since then Rhodamine 590 has been one of the most commonly used of all the organic laser dyes as it is often used as a standard to judge the properties of other materials by and is seen as a benchmark for efficiency and photostability studies [6-8]. In addition to being used as dye-based optical amplifiers, in dye lasers and in sensors [9], Rhodamine 590 has also been shown to be useful in the study of photo-biological processes, or to asses the importance of nonlinear absorption processes, due to the effectiveness of its photochemical reactions. It has also been used as a tracer in a fluid to monitor the rate and direction of flow and transport of the liquid [10].

3.1.2 Solvents

Rhodamine 590 dissolves most readily in ethanol, due to the fact that both molecules are polar. The emission from laser dyes is strongly dependent on many factors, including; temperature, concentration and solvent choice, among others.

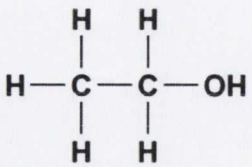

Figure 3.2 *Structure of the Ethanol molecule*

Also known as ethyl alcohol or pure alcohol, ethanol has a molar mass of 46.07 g mol^{-1}, a refractive index of 1.36 (at room temperature) and a molecular formula of C_2H_6O. It is a colourless liquid and is highly polar so its applications are restricted to polar dyes, such as the Rhodamine dyes.

Rhodamine 590 also dissolves easily in methanol. However, upon experimental observation, the solutions were found to be less efficient than their ethanol-based counterparts.

The importance of the solvent selection can affect the performance of laser dyes in terms of altering the fluorescence yield and lifetime as well as emission wavelength. This phenomenon is related to the observation that dyes often perform better when rigidly fixed in planar geometries [11]. This restriction of allowed nuclear motion results from the structural constraints imposed by the assembly of the dye substituent in rings. These findings can be understood in terms of a combination of effects associated with the creation of dye dipoles, the mobility of substituent groups and solvent stabilisation of charged species [3].

3.1.3 Capillary Tubes

Capillaries are an easy way to handle the laser dyes in liquid form as, once filled, they can easily be moved and adjusted in a variety of experimental setups. They were investigated as a candidate for optical telecommunications in the 1960's, before the development of modern silica fibre technology [12]. Thin capillaries have also been used by coating their inner surface to increase their reflectance and improve their waveguiding efficiency [13, 14].

In our work, the capillaries used were purchased from Polymicro Technologies, the structure of which is illustrated in Fig. 3.3. They are flexible fused silica capillary tubing which have a standard polyimide coating. The coating was removed by boiling the cleaved capillary tubes in sulphuric acid for two hours. The tubing used in this work had inner diameters of 530, 320, 100, 50 and 25 μm diameters. Each tube was cleaved, using a razor blade, into sections of approximately 25 mm in length.

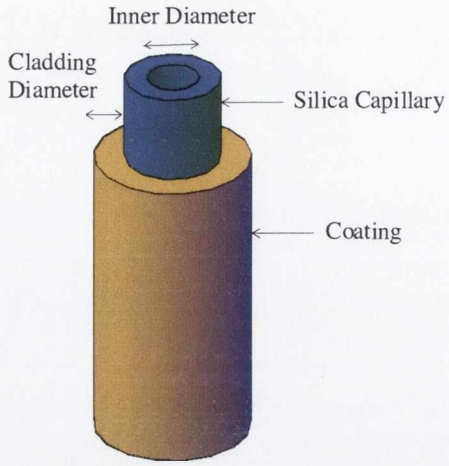

Figure 3.3 *Diagram of the capillary tube*

The micro-scale tubes are filled by capillary action, i.e. the tendency of fluids to rise up capillary tubes, which is a result of surface tension. When a capillary tube is placed in the fluid, a concave meniscus forms and the surface tension pulls the column of liquid up the tube, until a sufficient amount of liquid causes the gravitational forces to overcome the intermolecular forces.

The amount of liquid which can fill each tube through capillary action depends on several factors, including the pressure, surface tension, contact angle and tube diameter. For example, the pressure exerted by a column of liquid of density ρ and height h is

$$p = \rho g h \tag{3.1}$$

The pressure of the fluid (hydrostatic) itself is approximately $2\gamma/r$, where γ is the surface tension and r is the radium of the tube. They can be considered equal at equilibrium, and can hence be rearranged to get the height

$$h = \frac{2\gamma}{\rho g r} \tag{3.2}$$

The contact length (around the edge) between the top of the liquid column and the tube is proportional to the diameter of the tube, while the weight of the liquid column is proportional to the square of the tubes diameter, so a narrow tube will draw a liquid column higher than a wide tube. Taking this into account, the above equation can be rearranged to give

$$h = \frac{2\gamma \, Cos\theta}{\rho g r} \tag{3.3}$$

In our case, the capillary tubes were cut to approximately 2 cm in length, so the contact angle really only becomes an issue for the smallest of capillary diameters.

3.1.4 Micro-fluidics

Micro-cavity fluidic dye lasers have already been fabricated [15], however most require metallic mirrors, complicated fabrication processes and the pumping of the dye solution through the channels of the device. These devices can be integrated with other micro-fluidic systems without adding further process steps. The functionality of micro-systems, such as a 'lab-on-a-chip', can be significantly enhanced by the integration of lasers and other active optical components. Capillaries have been integrated into micro-chips by Yokoyama et al., whereby a Fabry-Perot micro-cavity of two glass wafers with dielectric multi-layer mirrors was assembled [16].

The field of micro-fluidics is rapidly growing, and one of the main challenges is to integrate a multitude of functionalities onto a chip in order to enable a wider variety of applications, such as bioanalytical studies [17], sensors, etc. They can be used as light-based sensors on-chip [18], which otherwise requires cumbersome optical alignment of light source and chip at every use. Among many others, integration of planar optical components is of great importance for the development of on-chip detection [18-20]. It has previously been shown that laser micro-cavities can be integrated into a micro-fluidic system that can be used to produce desired laser emission peaks [15, 21-24].

3.1.5 Liquid Phase versus Solid Phase

The use of dye-doped optical fibres has already been proven to be useful, usually when incorporated into the solid state with a polymer [25-28], and as fibre lasers and amplifiers. In these solid state devices the polymer host acts to disperse the active molecules in order to avoid aggregation of the molecules which quenches the emission. There are many advantages in developing solid state devices such as ease of handling and hence their incorporation into certain devices, etc. However, these advantages are outweighed by those of the liquid state.

There is less of an issue with molecular aggregation and therefore emission quenching is no longer a serious concern when in solution. Photodegradation, caused by the exciting

laser beam, also does not occur as easily due to the continuous movement of the particles in solution (Brownian motion). Hence, in the liquid state, devices can operate at high average powers, as the process of heat removal is facilitated. This is due to the fact that the dye solutions can be easily circulated, and hence the operation lifetime is improved. However, there are also disadvantages; issues such as toxicity [29] of the laser dyes and solvents in the liquid phase can pose a potential risk and limit the applications.

To date, highly efficient emission properties have been observed in Rhodamine 590 based systems, although these have primarily been found in solid state devices [30, 31]. However, by keeping the gain medium in solution, it allows a greater amount of control, they can be used at higher pump energies and hence provide a broader scope for potential applications.

3.2 Absorption Spectroscopy

3.2.1 Absorption Cross-section

The intensity of a beam of light $I(d)$ that travels a distance d though a sample is expressed by the Beer-Lambert law as

$$I(d) = I_0 e^{-N\sigma d} \tag{3.4}$$

where N is the concentration or number density of active (absorbing) molecules and I_0 is the intensity of the light beam before entering the sample. The absorption cross-section of the material, σ, is an indication of the strength of the absorption transition. This equation can be rearranged, by taking the logarithm, to get

$$\log\left(\frac{I(d)}{I_0}\right) = \log\left(e^{-N\sigma d}\right) \tag{3.5}$$

This equation can then be arranged in terms of the absorbance, A, to obtain the optical density

$$A = -\log\left(\frac{I(d)}{I_0}\right) = -\log(T) \tag{3.6}$$

where T is the transmission of the beam of light. These two equations can be rearranged to get

$$A = \frac{\sigma N d}{\ln(10)} \quad \text{or} \quad \sigma(\lambda) = \frac{-\ln T(\lambda)}{Nd} \tag{3.7}$$

The number density, N, can be calculated as follows

$$N = \frac{\rho N_A}{M} \tag{3.8}$$

where ρ is the density, N_A is Avogadro's constant and M is the molecular weight. From this equation, the absorbance coefficient is calculated due to the fact that

$$\alpha = N\sigma \tag{3.9}$$

3.2.2 UV-Vis Absorbance Spectroscopy

Absorbance measurements were taken using a Cary Varian 6000i ultraviolet-visible-near infrared (UV-Vis-NIR) spectrophotometer. A diagram outlining the various components of the absorbance spectrometer is shown in Fig. 3.4. As the beam of light from a broad spectrum source (Xeon lamp) passes through a monochromator, it is separated into its component wavelengths. When the polychromatic beam reaches the grating, the resulting diffraction occurs so that the angle at which each spectral component is reflected depends on its particular wavelength. Each monochromatic beam, in turn, is split into two equal intensity beams by a beam splitter. One beam is passed through a reference cell filled with the solvent to be used whilst the other is passed through the sample. The amount of light absorbed at a particular wavelength is deduced from the Beer-Lambert law as described previously in section 3.2.1. The monochromator scans through a range of wavelengths (from ultra violet to near infrared) allowing the absorbance of the sample to be monitored as a function of wavelength.

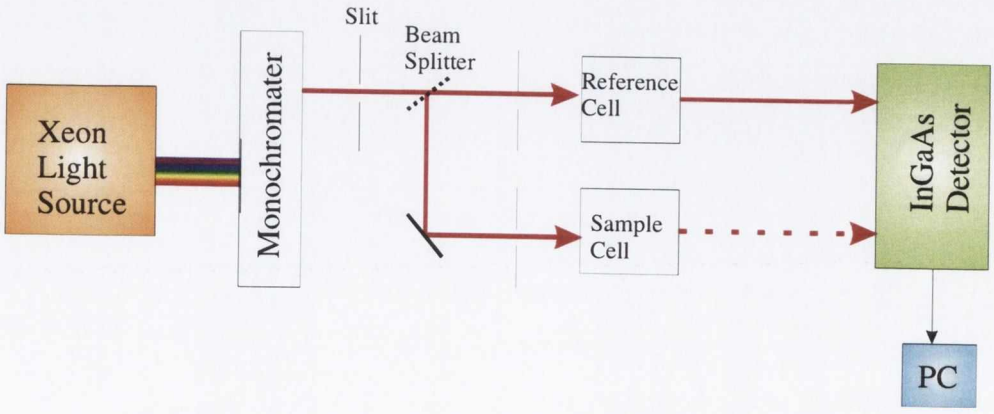

Figure 3.4 *Basic outline of the UV-Vis-NIR absorbance spectrometer*

Measurements were taken in a 1 mm glass cuvette. The concentrations of the Rhodamine 590 in ethanol were looked at. Solutions of concentrations from 1 x 10^{-2} to 10^{-4} M were made up in ethanol, as can be seen in Fig. 3.5.

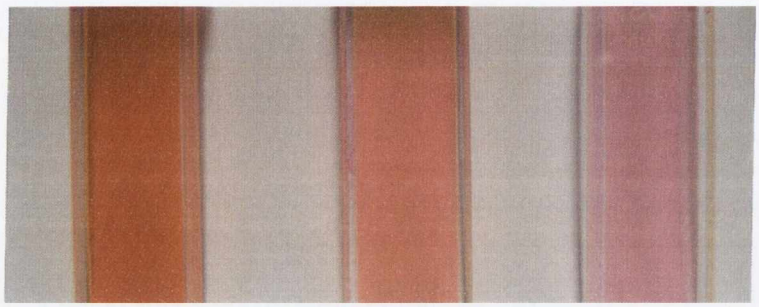

Figure 3.5 *The three concentrations of Rhodamine 590 in ethanol investigated: 1x10^{-2}; 1x10^{-3}; 1x10^{-4} M (left to right)*

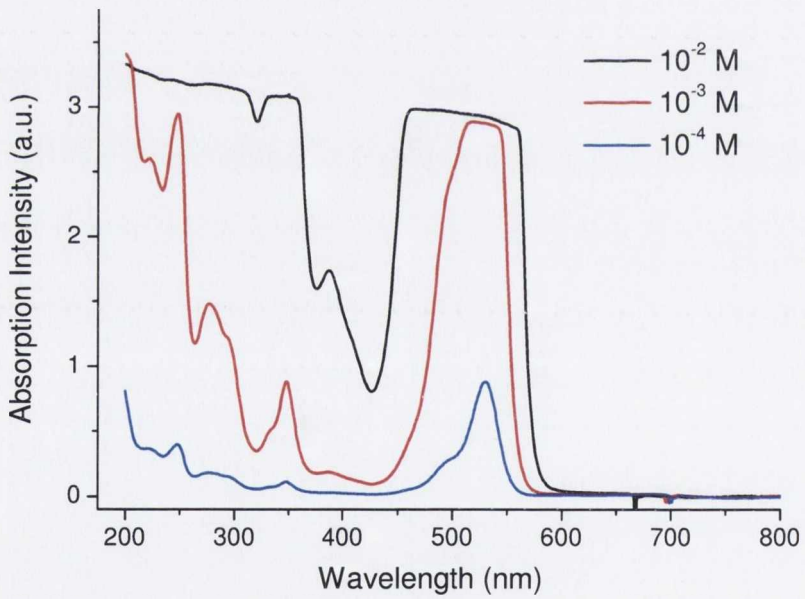

Figure 3.6 *UV-Vis absorption spectra of the three Rhodamine 590 concentrations*

The graph of the absorption spectra for the three different concentrations of Rhodamine 590 dye in solution shows a broad absorption spectrum in the 500 to 550 nm region, in particular for the two higher concentrations of laser dye. The absorption band indicates that the pump laser, at 532 nm, is very suitable for pumping the Rhodamine 590 dye. At first glance, the two larger concentrations appear to have reached the sensitivity limit of the photodetector within the UV-Vis spectrometer. The incoming light beam from

the UV-Vis is not completely transmitted through the solutions, due to the high concentrations of the dye molecules. From the simplified version of the Beer-Lambert Law, the absorbance A can be written as

$$A = \varepsilon c l \qquad (3.10)$$

As ε, the molar absorption coefficient, is a fixed constant for the material. The observed effect on the absorbance intensity limitations can be lessened by either lowering the concentration, c, of active molecules, as seen with the 1 x 10^{-4} M solution, or by decreasing the path length, l; hence a better picture of the absorbance can be ascertained. In these measurements a 1 mm cuvette was used, which was the smallest available. However, it is still possible to reasonably determine the regions in which the two solutions of higher concentration absorb strongly.

3.3 Emission Spectroscopy

3.3.1 Photoluminescence Spectroscopy

Photoluminescence (PL) measurements were carried out on a Perkin Elmer Luminescence Spectrometer. The spectrometer operates as follows: a broad spectrum of light from the excitation source passes through a monochromator that selects a specific excitation wavelength and bandwidth. This is then directed through a beam splitter where a small amount of light is reflected onto a reference detector. The beam continues through a slit and the incident excitation beam is focused on the sample. A portion of any emitted light from the sample is collected at 90° to the incident light, passed through another slit, and is focused on the emission monochromator. The emission monochromator selects a wavelength and spectral bandwidth of this emission and finally the beam passes onto a detector.

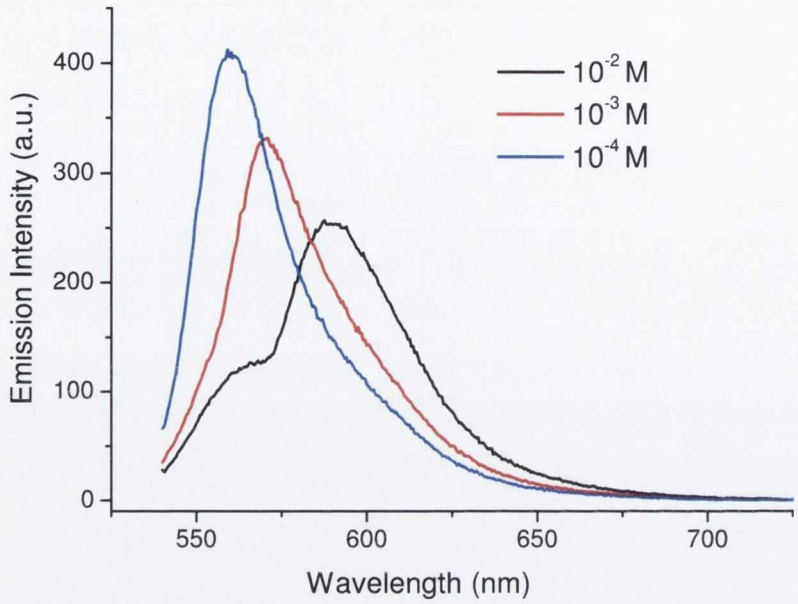

Figure 3.7 *PL emission spectra for the three concentrations of Rhodamine 590 in ethanol in 1 mm cuvette*

The PL spectra were taken when the excitation wavelength was set to 532 nm and the resulting emission peaks are measured, in a 1 mm cuvette. A 10 % transmission neutral density glass filter (NG) was put in place in order to stop the intensity emitted from the Rhodamine samples from saturating the spectrometer. Figure 3.7 shows that the emission intensity for the 1 x 10^{-4} M solution in ethanol showed the highest peak intensity at 570 nm. The intensity of the PL peaks decreases with increasing dye concentration. The redshift of the emission peak is observed as the dye concentration is increased. Schäfer et al. describes how this redshift is due to the reabsorption of the Rhodamine 590 dye caused by the overlap of the absorption spectra with the PL spectra over a certain wavelength region [4].

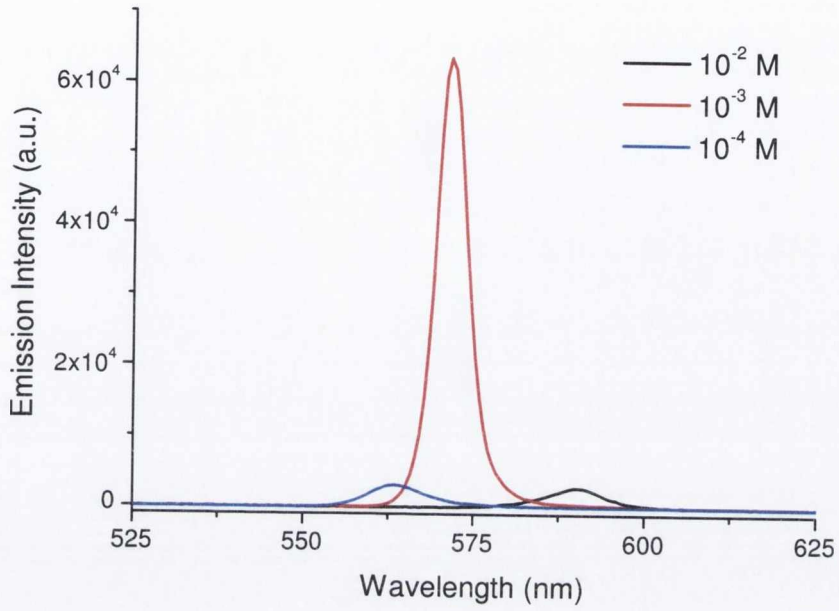

Figure 3.8 *532 nm photoexcited emission spectra in 530 μm capillary tube*

When each concentration was photoexcited with the Nd:YAG laser in a 530 μm capillary tube at 14 mW pump power, the 1 x 10^{-3} M solution had, by far, the highest pump efficiency. Figure 3.8 shows the difference between the three concentrations when excited with the high pump powers of the Nd:YAG laser. It is likely that at higher dye concentrations within the capillary tubes, such as the 1 x 10^{-2} M concentration, the occurrence of aggregation of the dye molecules increases, which leads to quenching of the emission intensity. Out of the three concentrations, the 1 x 10^{-3} M solution has, by far, the highest emission intensity, at 570 nm. The two other concentrations have emission intensities which are several orders of magnitude lower. This concentration is therefore chosen for further investigation.

The reason why such a large difference in the emission properties are seen in Fig. 3.7 and 3.10 is that the PL measures the amount of fluorescence of the sample, when excited at a particular wavelength. However, when the material is photoexcited above a certain 'threshold' power the fluorescence becomes overshadowed by the onset of amplified spontaneous emission (ASE) from the material.

3.3.2 Stokes Shift

A Stokes shift is defined as the difference between the peak position of the absorption and emission spectra. A large Stokes shift implies a low reabsorption rate of the fluorescence in an amplifier or laser device [32]. This facilitates population inversion and hence efficient light amplification, or in other words, low ASE or laser threshold. For comparative purposes, an estimate of the Stokes shift for all three concentrations is included in Table 3.1. A Stokes shift of approximately 45 nm is observed for the 1×10^{-3} M concentration, more clearly presented in Fig. 3.10, which is considered to be relatively large [33].

Dye Concentration	λ_{abs} (nm)	λ_{PL} (nm)	Stokes shift (nm)
1×10^{-2} M	460-560	559	49
1×10^{-3} M	505-545	571	46
1×10^{-4} M	530	591	30

Table 3.1 Concentration dependent properties of Rhodamine 590 in ethanol

Note that the 1×10^{-4} M solution has a much smaller Stokes shift. The two more concentrated samples have relatively similar values. We can therefore conclude that this relatively large Stokes shift will cause the reabsorption effects to be reduced [34].

3.3.3 Full-Width-Half-Maximum

From the PL emission spectra alone in Fig. 3.7, the 1×10^{-4} M solution would appear to be a good concentration choice, as it has the highest emission intensity. However, when the solutions were looked at further, in the experimental setup described in Chapter 4, it was the 1×10^{-3} M concentration that gave the greatest efficiency, from Fig. 3.8. When the 530 μm capillary tubes were filled with each solution concentration, the full-width half-maximum (FWHM) of the emission spectra was measured as the laser pump power was increased.

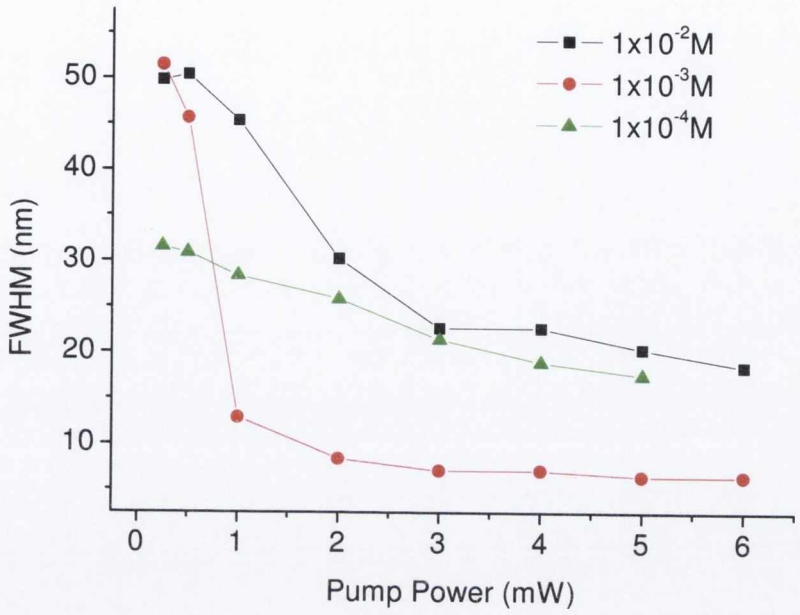

Figure 3.9 *FWHM against pump power for the three concentrations of Rhodamine 590 in a 530 μm capillary*

As the pump power is increased, the FWHM for each concentration decreases, the most dramatic of which is for the $1x10^{-3}$ M solution. This narrowing of the line-width as the pump power is increased signifies the transition into the lasing regime. This dramatic narrowing of the emission peaks is a strong indication of the occurrence of amplified spontaneous emission (ASE). ASE is the process whereby the spontaneous emission of the photons (luminescence) is optically amplified through stimulated emission in the gain medium [3]. Its bandwidth is narrower than that of spontaneous emission, has directionality and tends to have intense emission [35]. Its characteristics are a superlinear increase in emission intensity with excitation length and a narrowing of the emission spectrum with increasing intensity. It is usually considered as the first test for a laser medium [36]. This phenomenon will be further investigated in the following chapters.

3.3.4 Chosen Concentration

Due to the higher emission intensity values, large Stokes shift and strong line-narrowing, the 1 x 10^{-3} M Rhodamine 590 ethanol solution was chosen for further investigation.

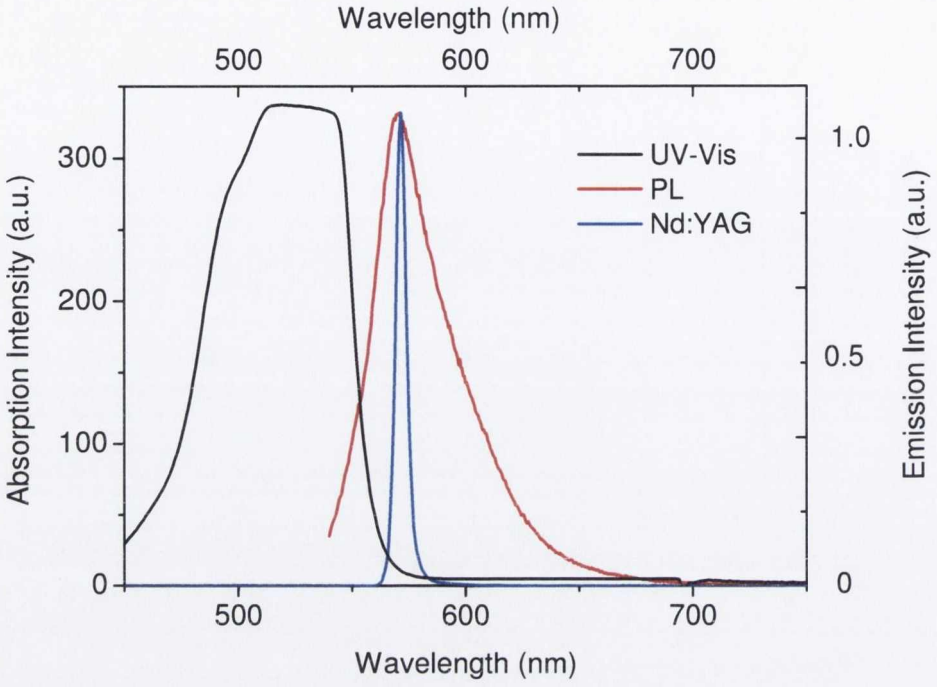

Figure 3.10 *UV-Vis absorption and PL and photoexcited emission spectra for 1 x 10^{-3} M solution in 1 mm cuvette(UV-Vis and PL) and 530 μm capillary tube (Nd:YAG), respectively*

To compare the absorption and emission spectra, they are plotted together in Fig. 3.10. The results have been normalised in order to emphasise the spectral differences between the fluorescence and the ASE. The PL spectrum shows a broad emission peak and when the solution is photoexcited by the SHG of the Nd:YAG laser, the emission peak is dramatically narrower. This substantial difference in the photoexcited emission intensities is evidence that the 1 x 10^{-3} M solution exhibits ASE and hence possesses the best amplification performance from the dye concentrations measured.

The overlap between the UV-Vis and PL peaks for the 1 x 10^{-3} M solution occurs at 553 nm. The slight redshift between the PL and photoexcited emission peaks can be attributed to the overlap of the absorbance and emission peaks, as discussed previously [4].

3.4 Fluorescence Lifetime Measurement

Fluorescence lifetime is a measurement of the average length of time that a molecule stays in its excited state before it emits a photon. A long 'upper-state' or fluorescence

lifetime in a gain medium means that a significant population inversion can be maintained with a relatively low pump power.

Time-resolved fluorescence decay lifetime measurements were taken using a PicoQuant Microtime 200 time-resolved confocal microscope system with 150 ps resolution and a 5 MHz repetition rate. An Argon laser was used to excite the solution containing 1×10^{-3} M Rhodamine 590 in ethanol, at 480 nm. Although this is not the wavelength at which we will be working at, it is still within the absorbance band of the dye, and will give a good indication of the lifetime value.

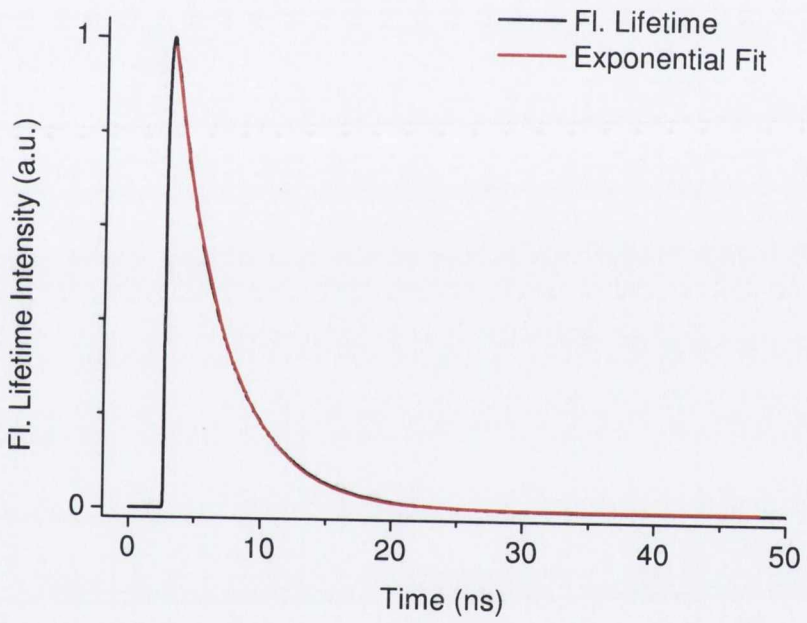

Figure 3.11 *Fit of fluorescence lifetime measurement for Rhodamine 590 in ethanol*

The measured intensity $I(t)$ from the sample as a function of the elapsed time t is given by the following exponential decay expression

$$I(t) = Ae^{-t/\tau} \qquad (3.11)$$

where A is a constant and τ is the fluorescence lifetime. The fluorescence lifetime was measured to be 4.01 ± 0.001 ns by fitting the exponential decay in Fig. 3.11. This value is comparable with that found in literature for this particular Rhodamine dye in ethanol [37].

3.5 Summary

In summary, the materials under investigation were introduced in this chapter, as were their basic spectroscopic properties. This information will be used in subsequent chapters. The effect of Rhodamine 590 dye concentration in ethanol on the absorbance and emission properties was investigated and the solution of 1 x 10^{-3} M concentration was chosen for further examination. The strong absorption and emission characteristics of this dye were confirmed, as well as the distinctive fluorescence lifetime of the laser dye.

3.6 References

1. Sorokin, P.P. and J.R. Lankard, *Ibm Journal of Research and Development*, 1966. **10**(2): p. 162-163.
2. Kubin, R.F. and A.N. Fletcher, *Journal of Luminescence*, 1982. **27**(4): p. 455-462.
3. Duarte, F.J. and L.W. Hillman, *Dye laser principles : with applications*. Quantum electronics. principles and applications. 1990, Boston ; London Academic Press.
4. Schäfer, F.P. and K.H. Drexhage, *Dye lasers*. 2nd rev. ed. ed. Topics in applied physics ; vol.1. 1977, Berlin ; New York: Springer.
5. Huth, B.G., *Applied Physics Letters*, 1970. **16**(4): p. 185-188.
6. Barroso, J., A. Costela, I. Garcia-Moreno, and R. Sastre, *Chemical Physics*, 1998. **238**(2): p. 257-272.
7. Peterson, O.G., J.P. Webb, W.C. Mccolgin, and J.H. Eberly, *Journal of Applied Physics*, 1971. **42**(5): p. 1917-1928.
8. Maeda, M., *Laser Dyes: Properties of Organic Compounds for Dye Lasers*. 1984, Tokyo Osaka Kyoto: Academic Press.
9. Shi, L.F., V. De Paoli, N. Rosenzweig, and Z. Rosenzweig, *Journal of the American Chemical Society*, 2006. **128**(32): p. 10378-10379.
10. Arcoumanis, C., J.J. Mcguirk, and J.M.L.M. Palma, *Experiments in Fluids*, 1990. **10**(2-3): p. 177-180.
11. Reynolds, G.A. and K.H. Drexhage, *Optics Communications*, 1975. **13**(3): p. 222-225.
12. Marcatili, E.A.J. and R.A. Schmeltzer, *Bell System Technical Journal*, 1964. **43**(4p2): p. 1783-1809.
13. Knight, J.C., J. Broeng, T.A. Birks, and P.S.J. Russel, *Science*, 1998. **282**(5393): p. 1476-1478.
14. Cregan, R.F., B.J. Mangan, J.C. Knight, T.A. Birks, P.S. Russell, P.J. Roberts, and D.C. Allan, *Science*, 1999. **285**(5433): p. 1537-1539.
15. Helbo, B., A. Kristensen, and A. Menon, *Journal of Micromechanics and Microengineering*, 2003. **13**(2): p. 307-311.
16. Yokoyama, H., M. Suzuki, and Y. Nambu, *Applied Physics Letters*, 1991. **58**(23): p. 2598-2600.
17. Manz, A. and H. Becker, *Microsystem Technology in Chemical and Life Sciences*. 1999, Berlin: Springer.
18. Verpoorte, E., *Lab on a Chip*, 2003. **3**(3): p. 42-52.
19. Roulet, J.C., R. Volkel, H.P. Herzig, E. Verpoorte, N.F. de Rooij, and R. Dandliker, *Journal of Microelectromechanical Systems*, 2001. **10**(4): p. 482-491.
20. Vezenov, D.V., B.T. Mayers, D.B. Wolfe, and G.M. Whitesides, *Applied Physics Letters*, 2005. **86**(4).
21. Wendt, J.R., M.E. Warren, W.C. Sweatt, C.G. Bailey, C.M. Matzke, D.W. Arnold, A.A. Allerman, T.R. Carter, R.E. Asbill, and S. Samora, *Journal of Vacuum Science & Technology B*, 1999. **17**(6): p. 3252-3255.
22. Gersborg-Hansen, M., S. Balslev, N.A. Mortensen, and A. Kristensen, *Microelectronic Engineering*, 2005. **78-79**: p. 185-189.
23. Kytina, I.G., V.G. Kytin, and K. Lips, *Applied Physics Letters*, 2004. **84**(24): p. 4902-4904.
24. Cheng, Y., K. Sugioka, and K. Midorikawa, *Optics Letters*, 2004. **29**(17): p. 2007-2009.
25. Peng, G.D., P.L. Chu, Z.J. Xiong, T.W. Whitbread, and R.P. Chaplin, *Journal of Lightwave Technology*, 1996. **14**(10): p. 2215-2223.

26. Kuriki, K., T. Kobayashi, N. Imai, T. Tamura, Y. Koike, and Y. Okamoto, *Polymers for Advanced Technologies*, 2000. **11**(8-12): p. 612-616.
27. Kuriki, K., T. Kobayashi, N. Imai, T. Tamura, S. Nishihara, Y. Nishizawa, A. Tagaya, Y. Koike, and Y. Okamoto, *Applied Physics Letters*, 2000. **77**(3): p. 331-333.
28. Liang, H., Z.Q. Zheng, Z.C. Li, J. Xu, B. Chen, H. Zhao, Q.J. Zhang, and H. Ming, *Journal of Applied Polymer Science*, 2004. **93**(2): p. 681-685.
29. Beckering, G., S.J. Zilker, and D. Haarer, *Optics Letters*, 1997. **22**(18): p. 1427-1429.
30. Costela, A., F. Florido, I. Garciamoreno, R. Duchowicz, F. Amatguerri, J.M. Figuera, and R. Sastre, *Applied Physics B-Lasers and Optics*, 1995. **60**(4): p. 383-389.
31. Duarte, F.J., T.S. Taylor, A. Costela, I. Garcia-Moreno, and R. Sastre, *Applied Optics*, 1998. **37**(18): p. 3987-3989.
32. Yang, C.Y., F. Hide, M.A. Diaz-Garcia, A.J. Heeger, and Y. Cao, *Polymer*, 1998. **39**(11): p. 2299-2304.
33. Kobayashi, T., W.J. Blau, H. Tillmann, and H.H. Horhold, *IEEE Journal of Quantum Electronics*, 2003. **39**(5): p. 664-672.
34. Arbeloa, F.L., T.L. Arbeloa, I.L. Arbeloa, A. Costela, I. GarciaMoreno, J.M. Figuera, F. AmatGuerri, and R. Sastre, *Applied Physics B-Lasers and Optics*, 1997. **64**(6): p. 651-657.
35. Svelto, O., *Principles of Lasers*. 1998, New York London: Springer.
36. Lahoz, F., C.J. Oton, N. Capuj, M. Ferrer-Gonzalez, S. Cheylan, and D. Navarro-Urrios, *Optics Express*, 2009. **17**(19): p. 16766-16775.
37. Magde, D., R. Wong, and P.G. Seybold, *Photochemistry and Photobiology*, 2002. **75**(4): p. 327-334.

Chapter 4

Optical Gain Characterisation

4.1 Introduction

This chapter describes the amplification performance of Rhodamine 590 based micro-amplifiers. Capillary tubes of varying diameters were filled with the laser dye, and the emission properties were measured. Amplified spontaneous emission was observed. Using the variable stripe length method, the amplification properties of the dye filled micro-capillaries were measured. The unsaturated and saturated models were fitted to measure the values of the gain coefficient for each capillary tube diameter.

4.1.1 One-Dimensional Amplifier Theory

The *Variable Stripe Length* method (VSL) was first developed by Shaklee and Leheny as a method of measuring the gain induced by active molecules [1]. Since then it has been widely used as one of the most common methods of measuring the strength of amplification, i.e. gain, from both organic [2, 3] and inorganic materials [2].

The basis for the VSL method is the one-dimensional amplifier approximation. It is assumed here that the spontaneous and stimulated emissions are independent of each other in such an amplifier. The light intensity I coming from the waveguide pumped at power P_0 is given by the following equation, from the Beer-Lambert law

$$\frac{dI}{dz} = \gamma + gI \qquad (4.1)$$

where g is the net small-signal gain, γ is equated to AP_0 i.e. the fraction of spontaneous emission that travels along the amplifier axis, which is proportional to the pump intensity, and gI is the stimulated emission term. The solution may be obtained by rewriting the equation as

$$\frac{dI}{\gamma + gI} = dz \qquad (4.2)$$

By integrating both sides, the following equation is obtained

$$\frac{1}{g}\ln(\gamma + gI) = z + c \tag{4.3}$$

where c is the integration constant. Now, when the previous equation is rearranged, and an exponential is taken of both sides

$$\gamma + gI = e^{g(z+c)} = Ce^{gz} \tag{4.4}$$

where $C = e^{gc}$. The boundary condition I(0)=0, leads to

$$I_{ASE} = \frac{\gamma}{g}(e^{gL} - 1) \tag{4.5}$$

where L is the maximum length of the excitation stripe. From this equation, it can be seen that the output intensity, i.e. the ASE intensity from the sample, will vary with the length of the excitation stripe. Hence it is possible to fit the data and obtain a value for the net gain. This is for the unsaturated gain model. It can also be rewritten as

$$L = \frac{1}{g}\ln(\frac{gI_{ASE} + \gamma}{\gamma}) \tag{4.6}$$

As the stripe length is increased, the light travelling along the sample can become so strongly amplified that a substantial fraction of the excited energy level becomes depleted. This is known as gain saturation, as the value for the gain coefficient is reduced because the light is no longer exponentially amplified with increasing stripe length [3]. In the case of the saturated model, a saturation parameter s is introduced to take into account this phenomenon

$$s = \frac{1}{I_{sat}} = \frac{\sigma\tau}{hv} \tag{4.7}$$

where σ is the emission cross-section, τ is the fluorescence lifetime, h is Planck's constant and v is the frequency of the ASE emission. When this parameter is substituted into Eq. (4.1), the equation becomes

$$\frac{dI}{dz} = \gamma + \frac{gI}{1 + sI} \tag{4.8}$$

And when this equation is reorganised,

$$\frac{dI}{dz} = \frac{(g + \gamma s)I + \gamma}{1 + sI} \tag{4.9}$$

Equation 4.9 can then be solved analytically, resulting in

$$L = \frac{sI_{ASE}}{g + s\gamma} + \frac{g}{(g + s\gamma)^2} \ln[\frac{(g + s\gamma)I_{ASE} + \gamma}{\gamma}] \quad (4.10)$$

Note that if s = 0, the above equation reduces back to the unsaturated form in Eq. 4.6.

4.2 Experimental Procedure

4.2.1 Sample Preparation

Rhodamine 590 dissolves readily in ethanol up to very high concentrations. As discussed in Chapter 3, a concentration of 1 x 10^{-3} M Rhodamine 590 in ethanol was used. The different diameters of capillary tubing were cut into 25 mm lengths and their polyimide coating was removed by boiling in sulphuric acid. Once they were thoroughly cleaned with deionised water, they were filled with the Rhodamine 590 and ethanol solution by capillary action, as described in Chapter 3. Once filled, one end of the tubing was sealed, so the tube could be easily repositioned.

4.2.2 Pumping alignment

There are several different pumping alignment possibilities when dealing with capillary tubing. When choosing the alignment, one must be careful to avoid considerable energy loss, or poor emission quality, while ensuring the detector remains undamaged [4].

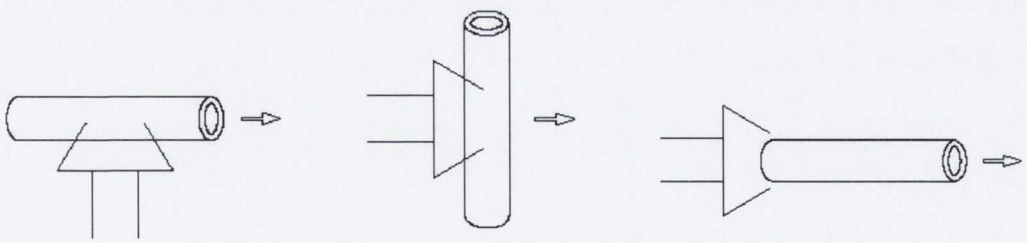

Figure 4.1 Three possible orientations of the input laser beam (large arrow) on the capillary tube and the resulting emission (small arrow).

Several different orientations of the capillary with respect to the input laser beam are possible. In the above Fig. 4.1: (a) transverse pumping entails a horizontal capillary position, whereby the pump beam is a narrow slit along the capillary profile and the

output emission is from the tube end; (b) side pumping means that the capillary is orientated vertically, and the beam excites a band along the surface of the tube and; (c) longitudinal pumping is the end-on approach, whereby the solution within the capillary is excited at one end, and the input and output beams are in the same direction along the tube length. From this, it was deduced:

(c) has a large inherent risk of damaging the CCD spectrometer due to the high pump powers incident directly onto the detector slit.

(b) has large losses as the emission is non-directional and widely scattered.

(a) is the alignment chosen as the output has good directionality and will enable the VSL method to be easily implemented.

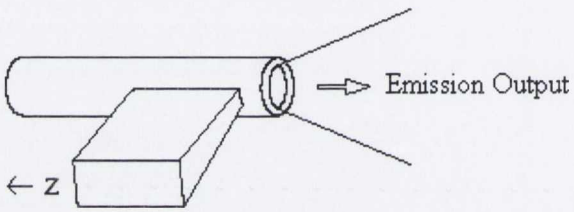

Figure 4.2 Preferred horizontal capillary alignment

As the laser beam is passed through the two cylindrical lenses, it forms a narrow stripe along the surface of the capillary tube. The input laser beam (wedge) is increased along the z-direction, along the length of the capillary tube, as shown in Fig. 4.2. This is known as the VSL method as described above.

4.2.3 Experimental Procedure

Optical gain is a measure of the light amplification of a material. The measurement of optical gain presented involves the measurement of fluorescent emission, amplified via stimulated emission, as it passes through the excited volume of a sample. This technique has previously been reported by Shaklee & Sorek [1, 5]. *Amplified Spontaneous Emission* (ASE) is a random process which relies on chance interactions of spontaneously emitted (fluorescent) photons, with excited states lying along the optical path. By measuring the change in the intensity of the fluorescent emission as the pump conditions are changed, it can be established if stimulated emission occurs. Similar work has been shown by Urbach et al. and Zakowicz et al. [6, 7]. In order to implement the VSL method, the material must

be shown to behave in such a manner that it exhibits ASE. One general indicator that the light emitted from the capillary tubes exhibits ASE is when the emission peak narrows considerably, as the intensity of the pump energy is increased [5, 6]. As the name suggests, the VSL method consists of the stripe length along the sample surface being slowly increased in precise increments and the resulting emission output is measured. Important information can be determined about the amplifying abilities of the material by monitoring the intensity of the ASE from the sample.

4.2.4 Experimental Setup

In this work a series of micro-amplifiers were developed by filling capillary tubing with dye solutions. Five different diameters of tubing, ranging from 530 to 25 μm diameters, were purchased from Polymicro Ltd. Capillary forces were used to pull the 1×10^{-3} M solution of the laser dye, Rhodamine 590, in ethanol into the micro-cavity of the tubing. The filled capillary tubes were placed in a horizontal direction (Fig. 4.1 (a)), relative to the pump beam in the experimental setup, as seen in Fig. 4.3.

From Chapter 3, it is known that the 1×10^{-3} M solutions of Rhodamine 590 absorb strongly in the 500 to 550 nm region. Hence, this indicates that this concentration can be excited with the second harmonic of a Continuum Minilite Neodymium Yttrium Aluminium Garnet laser (Nd:YAG). The PL emission spectra indicate that, when excited at 532 nm, the solution will strongly emit in the 570 nm region.

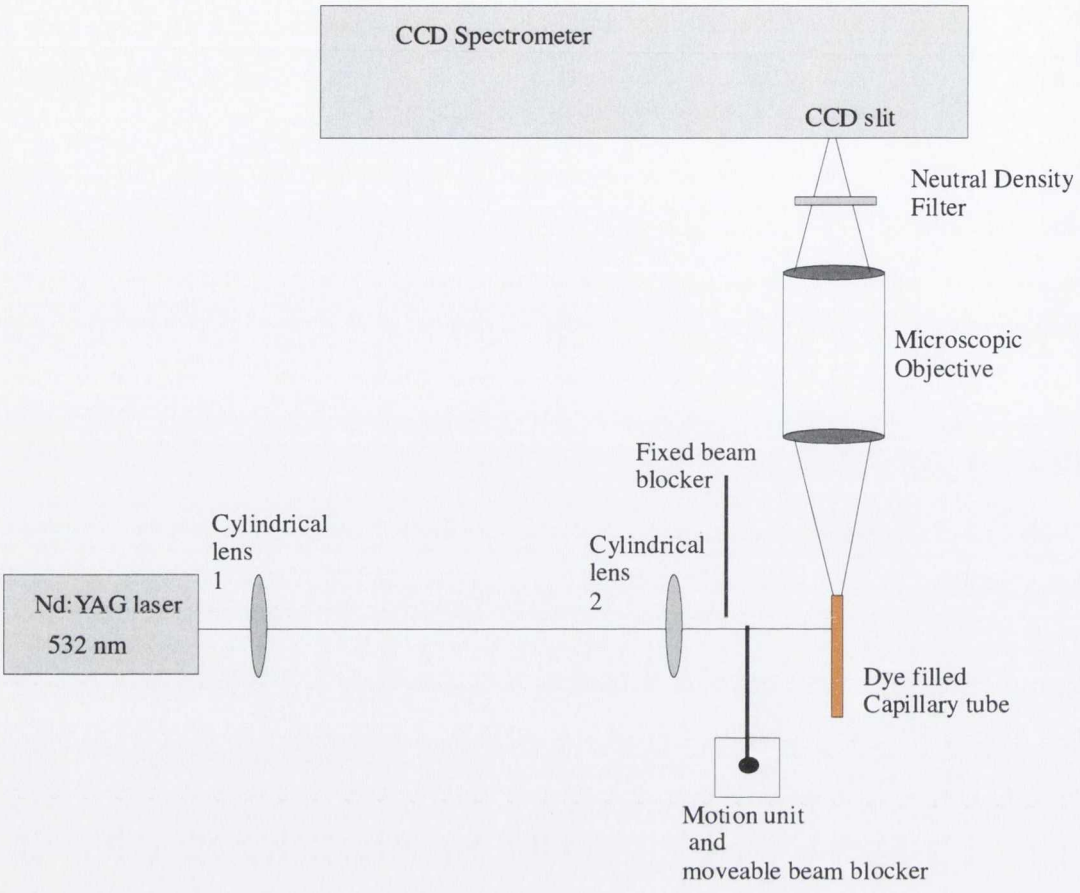

Figure 4.3 Experimental setup using the VSL method

Upon pulsed nanosecond photoexcitation of an Nd:YAG laser at 532 nm with a 10 Hz repetition rate, the beam was passed through two cylindrical lenses to produce a narrow horizontal stripe along the horizontal capillary tube surface. The focal length of the two lenses is 20 and 5 cm, respectively. Light emitted from the end of the capillary tube was collected through a microscope objective and subsequently analysed with a spectrograph attached to a charged coupled device camera (CCD). The optical gain of these micro-amplifiers was measured using the VSL method. The stripe length was increased by means of two straight-edged beam blockers; one of which was fixed and the other mounted on a computationally controlled translational stage.

4.3 Results – Dye Based Micro-capillary Amplifier

4.3.1 Emission Properties

In order to compare the different diameters of capillary tubing directly, a neutral density filter was implemented in order to stop the emission from the larger diameter tubing saturating the CCD spectrometer. The filter, labelled as an NG 4 filter, allows approximately 27 % transmission in the 550 to 600 nm region. However, this means that the intensity from the smaller capillaries is much noisier, as without a filter, they would not saturate the CCD.

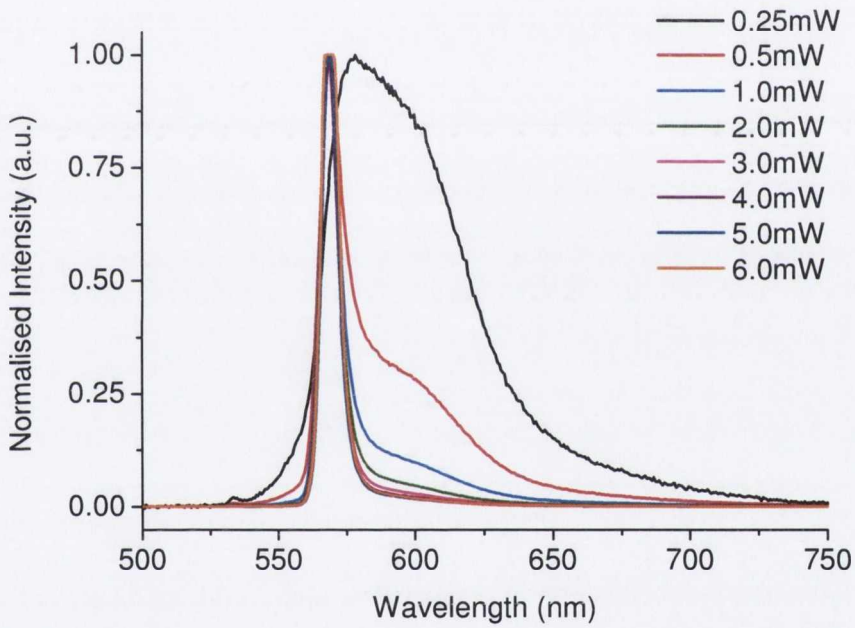

Figure 4.4 Emission intensity against wavelength for different pump powers in 530 μm capillary tube

An example of the emission properties for the 530 μm capillary tube in Fig. 4.4 shows the emission peaks from the Rhodamine 590 solution at a concentration of 1 x 10^{-3} M as the pump power is increased from 0.25 to 6 mW. The capillaries exhibit strong line-narrowing of the emission peak as the power of the pump beam was increased. This is a strong indication that ASE has been observed. Similar narrowing was measured for each of the capillary diameters; Fig. 4.4 is merely shown as an example. The pump power values given represent the average power of the beam, measured with a power meter. The broad fluorescence peak narrows (and shifts) to become the ASE peak. At lower pump

powers, the fluorescence band dominates. However, as the power increases, the emission of photons occurs due to their being excited by the increased stimulated emission.

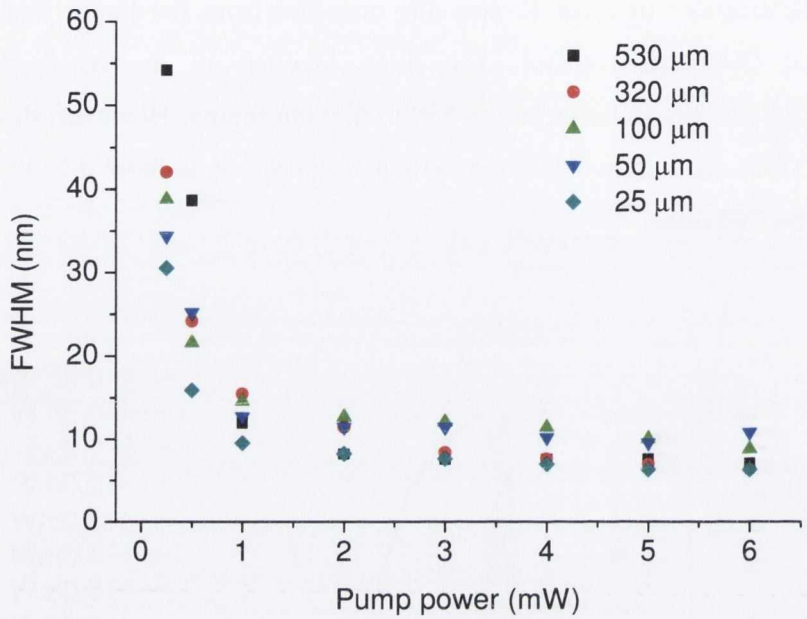

Figure 4.5 FWHM data for each of the five different diameters of filled capillary tubing

Figure 4.5 shows the ASE, or the narrowing of the emission peaks, observed in each of the five different diameters of capillary tubing. As the pump beam intensity is increased, the corresponding full-width-half-maximum (FWHM) of the emission peak decreases. In a similar manner, the output intensity of the capillary emission increases significantly with increasing pump intensity. This is most noticeably observed with the larger of the capillaries, due to the fact that a greater volume of dye molecules are being excited by the laser and that the capillary diameter is comparable with the width of the excitation stripe. In other words, for the smaller capillary tubes, where the pump beam stripe width is larger than that of the capillary, a smaller area is being excited and hence the amount of energy exciting the active dye molecules directly is reduced.

A decrease in the initial value for the FWHM at 0.25 mW pump power is observed as the diameter of the capillary is decreased, i.e. the 530 μm capillary has a value of 52 nm for the FHWM, the 100 μm is 38 nm and the 25 μm is 33 nm. As is expected when observing ASE, the values for the FWHM reduce dramatically as the pump power is increased. At

approximately 1 mW, all of the capillary tubes show a FWHM value of less than 10 nm. These narrowest FWHM values measured are likely to be at the maximum spectral resolution of the spectrometer grating. Although these values are sufficient for the present study, by substituting a finer grating into the instrument, a more in-depth and precise picture can be obtained of exactly how the line-width narrows with increasing pump power as it is possible that lasing modes could be observed.

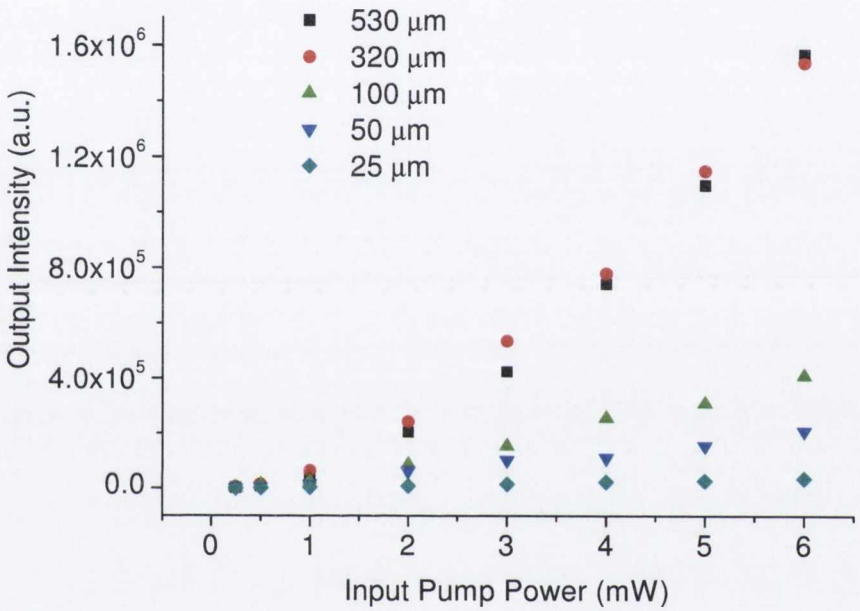

Figure 4.6 Input–output emission for the five different diameters of filled capillary tubing

The input pump beam power is plotted against the output emission intensity in Fig. 4.6. The emission characteristics for the two larger capillary tube diameters, 530 and 320 μm, are very similar and indicate a strong exponential increase in the output intensity as the pump power is increased. The similar slope efficiency of the 530 and 320 μm tubes is probably due to the limited width of the pumping strip, which is typically less than 300 μm. That is to say, the excited volume of the dye solutions is almost even for the two larger tubes, resulting in the similar slope. To a lesser extent, a linear increase is also observed for the three smaller capillary diameters.

As would be expected, the largest capillary diameter gave the highest emission peak intensity. This could be due to the fact that it contains the largest volume of dye

molecules. The volume within a 25 mm length of capillary tubing with diameter of 530 μm is approximately 5.5 x 10^{-3} cm^3. Hence, when this volume of tubing contains a concentration of 1 x 10^{-3} M, the number of active molecules present in the capillary is approximately 1.6 x 10^{21} dye molecules. The length of 100 μm capillary tubing has in the region of 5.7 x 10^{19} dye molecules and the 25 μm capillary has 3.5 x 10^{18} molecules. As one would expect, as the capillary diameter decreases, so does the number of active molecules present. Since the total number of active molecules decreases as the capillary diameter is made smaller, the slope of the intensity output is lowered and the resulting input-output emission efficiency is expected to decrease.

It is important to take into account the effect of the overlap of the beam stripe on the dye doped capillary tube. The width of the stripe is approximately 300 μm. Therefore, for the two larger capillary inner diameters (530 and 320 μm), the entire pump energy within the area of the excitation stripe is incident on the sample. However, when the capillary diameter decreases further, not all of the energy within the area of the pump beam stripe excites the solution. For example, for the 100 μm capillary tube, only one third of the stripe width impacts the capillary tube, therefore only approximately one third of the energy is directly excites the dye doped capillary. When this factor is taken into account, for the five capillary diameters, the results are plotted below in Fig. 4.7.

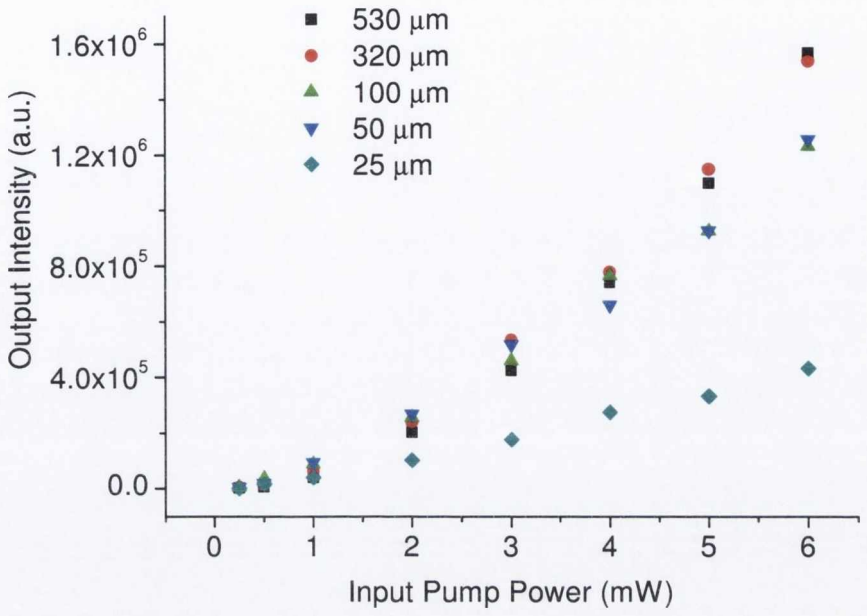

Figure 4.7 Input–output emission normalised with respect to the overlap of the beam on the capillary tube

The normalised emission characteristics, with respect to the overlap of the pump beam on the capillary diameter, in Fig. 4.7 indicate that the values of emission intensity are dependent on the amount of exciting laser energy incident on the sample itself. The narrowest diameter, 25 μm, does not appear to follow this trend. However, the inherent losses caused by the increased dispersion from the sample edge as the capillary diameter decreases, could account for this deviation from the trend. Therefore, it can be concluded that the decreased number of molecules in the smaller tube diameters does not have a strong influential effect on the emission output properties.

4.3.2 Threshold

The conventional measurement of the lasing threshold is not possible in this case. It is traditionally measured from the input-output emission graph, where an obvious point can be seen as the pump intensity dramatically increases at the onset of lasing. However, as can be see in Fig. 4.6, in the case of these capillary tubes the graph does not display a distinct lasing threshold, but it can be estimated to be at approximately 1 mW. As this is only an estimate, instead, the ASE pump power threshold can be more accurately measured. The ASE pump power threshold is usually defined as the power at which the

FWHM of the emission band is reduced to half [12]. From the FWHM graph in Fig. 4.5, the threshold values can be calculated.

Capillary Diameter (μm)	ASE Pump Power Threshold (mW)	ASE Pump Energy Threshold (mJ/cm^2)
530	0.84	0.42
320	0.79	0.40
100	0.71	0.36
50	0.67	0.34
25	0.44	0.22

Table 4.1 Summary of the ASE pump power threshold values for the capillary tube diameters

As can be seen from the summary in Table 4.1, the trend indicates that there is a dependence of the ASE pump power threshold on the capillary diameter. As the capillary diameter decreases, so does the ASE power threshold. Although this decrease is minimal, from 0.84 mW for the largest capillary diameter to 0.44 mW for the smallest diameter, it is noteworthy as less power is needed with smaller volumes to reach the power threshold for ASE. This is primarily due to the fact that the smaller tubes are excited more completely by the pump beam stripe than the larger tubes, resulting in an easier generation of ASE. On the other hand, in the smaller diameter capillary tubes, confinement of the emission is increased, which in turn means that there is a higher electric field within the capillary and therefore, it would be expected to have a lower threshold. When there are fewer molecules present, the threshold is smaller as the confinement becomes greater than the inherent loss. The results in Table 4.1 are presented graphically below in Fig. 4.8.

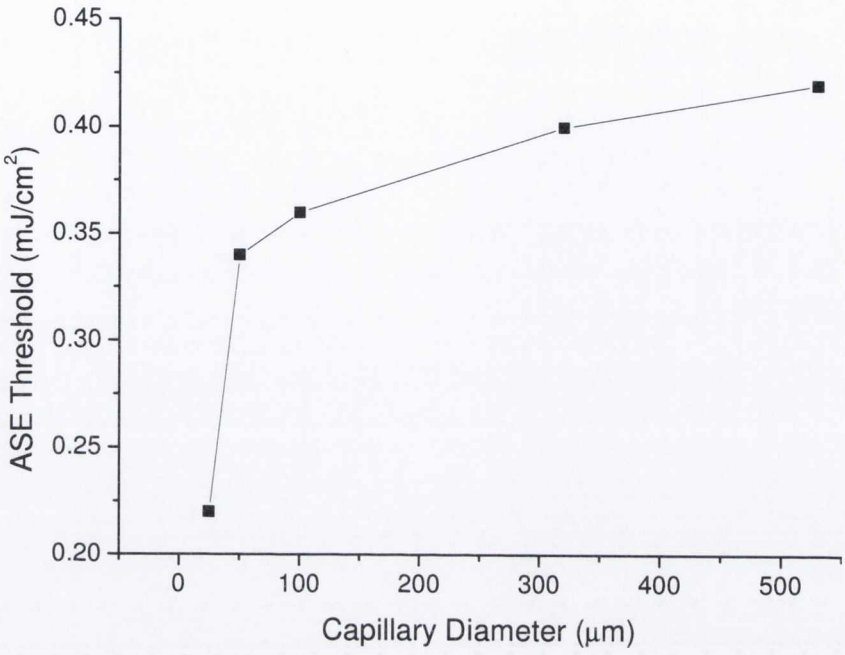

Figure 4.8 Increase in the ASE threshold with capillary diameter

The ASE behaves as theory predicts. Below the threshold, the emission is dominated by spontaneous decay. Above the threshold, when the excitation stripe length is long enough to produce non-negligible amplification, stimulated emission becomes higher than spontaneous emission and the spectrum becomes narrower due to the exponential dependence of the output on the excitation length. The ASE peak wavelength also redshifts as the illumination length increases. As the fluorescence light is guided through the dye-doped fibre, the effective path length is increased [7]. The farther the point of illumination is from the observation end, the larger the effective path length. This results in increased interaction between the dye molecules and the beam propagating through the fibre, causing enhanced fluorescence emission. This in turn leads to an increase in the self-absorption of the fluorescence from the dye molecules and thereby shifts the emitted fluorescence peak towards the longer wavelength region. This mechanism is similar to the concentration-dependent redshift that is observed in dye solution, and has been observed from dye doped fibres [8, 9].

Author	Material	Dimensions	Threshold Value	Ref.
Lahoz et al.	porous silicon organic-inorganic waveguides	130-170 nm thick film	6 – 8 kW/cm^2	[10]
Kim et al.	waveguide device fabricated with the blend	150-220 nm thick film	20 nJ/cm^2/pulse	[11]
Vezenov et al.	liquid-liquid micro-fluidic waveguide laser	5-20 nm long 100nm thick channel	22 μJ pulse energy	[12]
Harada et al.	dye-doped polymer-dispersed liquid crystals	10 μm thick, 4 μm diameter droplets	14 mJ/cm^2 for a 5mm^2 pump area	[13]
This work	dye-doped micro-capillary amplifiers	530-25 μm diameter 25 mm long	0.42-0.22 mJ/cm^2	

Table 4.2 Literature comparison of threshold values for gain media

From the selection of literature threshold values presented in Table 4.2, for the scale of amplifier in question, the ASE pump power threshold values hold well with those reported.

4.3.3 Comparison of unsaturated and saturated models

The gain coefficient is calculated by fitting the VSL data to the one-dimensional amplifier theory model, described in section 4.1.1. As ASE has been observed in the Rhodamine 590 filled capillary tubing, the data can then be fitted and values for the gain coefficients can be extracted.

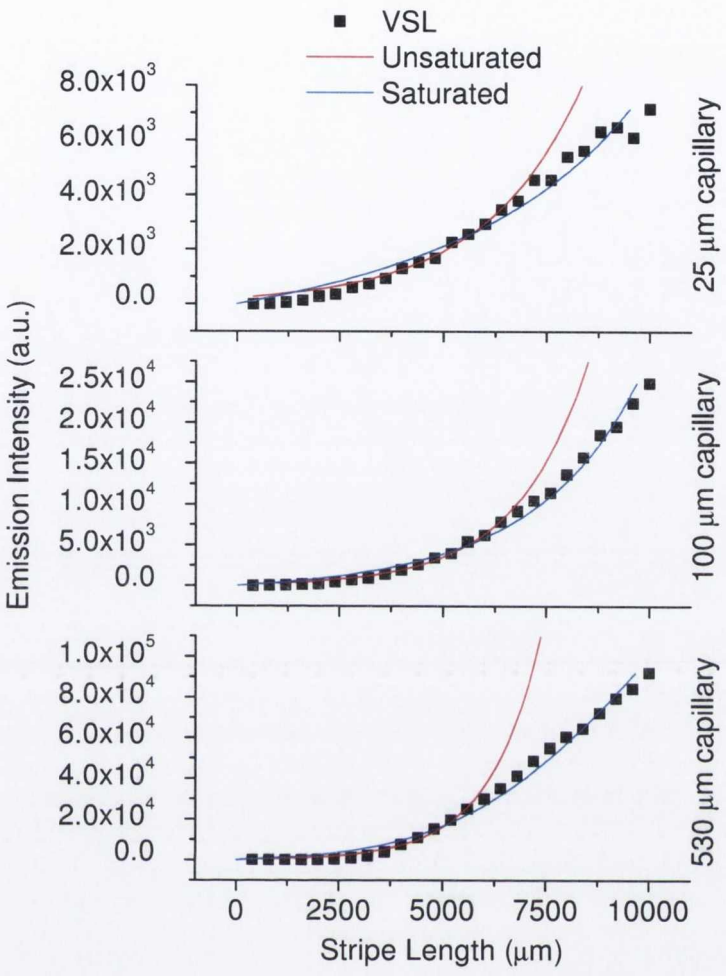

Figure 4.9 An example of a typical fitted unsaturated and saturated gain model of VSL as a function of emitted intensity for a 530, 100 and 25 µm amplifier respectively at 3mW pump power

Figure 4.9 illustrates the theoretical fittings using the unsaturated and saturated model, in which the fitted gain coefficients are 8.11 cm^{-1} and 6.08 cm^{-1}, respectively for the 530 µm capillary. The saturated model fits the whole data set for the stripe length, unlike the unsaturated model, whereby only the initial exponential increase in the intensity values is fitted. All five capillary diameters were fitted in this way, the results of which are tabulated below. Even for the narrowest 25 µm capillaries, values of approximately 5 cm^{-1} for the gain coefficient were observed. It should be noted that as the capillary diameter decreases, less saturation occurs and the two models become increasingly similar. The gain fitting model was only used at pump powers above 1mW. This was because of the fact that below the ASE pump power threshold, the data points were much more difficult to fit.

When saturation occurs, the gain coefficient decreases and the amplifier becomes less efficient. This is a consequence of the finite number of excited molecules being available in the amplifier for stimulated emission. As the ASE signal grows, it becomes strong enough to extract a large portion of the inversion energy into the directional beams by stimulated emission.

The unsaturated model is suitable for low pump powers, and low active molecule volumes. As the pump power increases, the tendency of the gain threshold to become saturated increases, so the fitted saturated model becomes increasingly more useful to get a more accurate depiction of the gain value. In this experimental setup, the pump powers are relatively low, so the gain saturation is not an extremely important factor.

4.3.4 Gain Results – Unsaturated Model

A summary of the unsaturated gain coefficients are plotted below in Table 4.3 for the five different diameters of capillary tubing.

pump power (mW)	530 μm gain (cm^{-1})	320 μm gain (cm^{-1})	100 μm gain (cm^{-1})	50 μm gain (cm^{-1})	25 μm gain (cm^{-1})
1	6.8 ± 0.2	6.8 ± 0.2	5.4 ± 0.2	5.2 ± 0.3	4.0 ± 0.3
3	7.3 ± 0.5	7.5 ± 0.2	5.8 ± 0.2	5.5 ± 0.2	4.2 ± 0.4
6	8.1 ± 0.5	7.4 ± 0.4	6.4 ± 0.3	5.9 ± 0.2	5.3 ± 0.2

Table 4.3 Unsaturated gain coefficients for the different diameters of capillary tubing and pump powers

As the pump power increases, so does the gain coefficient. Similarly, as the capillary diameter decreases, the gain decreases. This is due to the fact that there is a smaller volume of active molecules as the tube diameter is reduced. At the maximum pump power of 6 mW, the gain coefficient decreases from 8.1 cm^{-1} for the 530 μm capillary to 5.3 cm^{-1} for the 25 μm tube. It is interesting to note that although the tube diameter has decreased 20-fold, there is still a comparative and measurable gain value. The error limits listed are the standard error values from the fitting procedure. Comparatively, the error for the smallest capillary is highest. This is primarily due to the inherent experimental errors

when dealing with such small volumes of the active medium, and the fact that use of the neutral density filter only allows a fraction of the small emission intensity to be measured. The values for the gain are plotted below in Fig. 4.10, where the variation with capillary diameter is more evident.

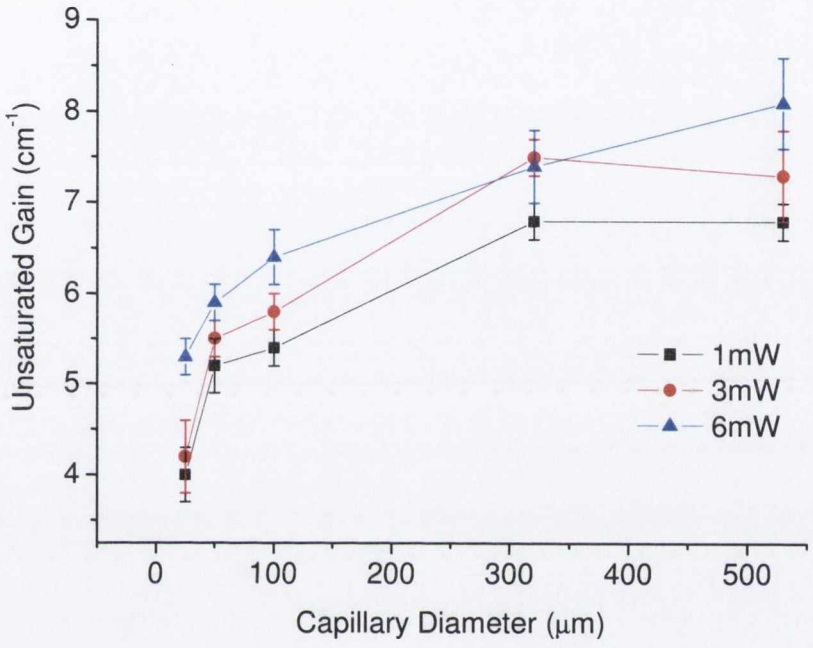

Figure 4.10 Variation of unsaturated gain with capillary diameter

From the derivation in section 4.1.1, there is a link between the input-output emission slope properties and the small signal approximation. This can be roughly summarised by following from the Beer-like equation

$$I_{out} = I_{in} \exp(gl) \qquad (4.11)$$

In other words, there is a correlation between the emission and amplification properties of a material. As the slope of input-output emission increases, so will the amplification of the material. Therefore, by subtly changing the conditions of the micro-capillaries, such as diameter or pump intensity, the output characteristics can be varied.

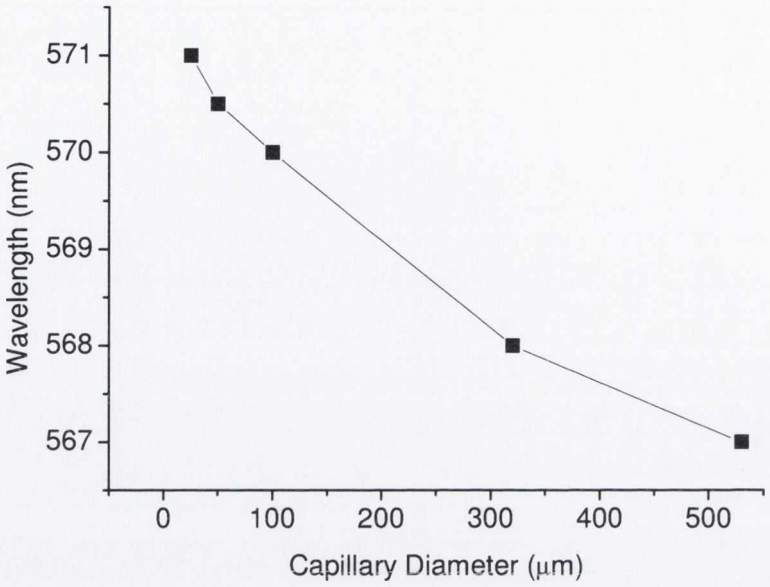

Figure 4.11 Shift in the peak wavelength with capillary diameter

With the change in gain, there is also a shift in peak emission wavelength. For the 530 μm capillary, the peak wavelength is 567 nm: when the diameter is reduced down to 100 μm the peak is at 570 nm, and at the smallest diameter, 25 μm the peak is at 571 nm. As the tube diameter decreases, the pumping efficiency of the dye molecules increases due to the enhanced confinement of the light, which results in the reabsorption of the emitted photons causing the red-shift of the peak wavelength, as discussed in section 4.3.2. The red-shift of the emission peak for Rhodamine 590 doped polymer optical fibres has been reported, experimentally, by Rajesh et al., as the length of excited fibre increases [14]. Karthaus et al. also found the wavelength dependence on the diameter of their cyanine dye-doped flakes: as their diameter decreased from 10 to 3 μm, the peak red-shifted by 3 nm [15].

4.3.5 Gain Results - Saturated Model

For comparison, the values for γ (i.e. AP_0), the fraction of spontaneous emission that travels along the amplifier axis, are presented in Table 4.4. As previously discussed, the pump beam passes through the two cylindrical lenses, forming a narrow stripe. This stripe is approximately 40 mm in length and 300 μm in width. From this it is possible to convert

the average power (in mW) to the peak power (in mJ/cm^2). So, for the gain fittings, γ was calculated and plotted below:

Average Pump Power (mW)	Peak Power ($mJ\ cm^{-2}$)	530 μm γ (a.u.)	320 μm γ (a.u.)	100 μm γ (a.u.)	50 μm γ (a.u.)	25 μm γ (a.u.)
1	0.5	31 ± 3	40 ± 2	35 ± 2	27 ± 2	10 ± 3
3	1.5	2.7 (± 0.9) x 10^3	2.5 (± 0.1) x 10^3	2.7 (± 0.1) x 10^3	4.1 (± 0.4) x 10^2	3.4 (± 0.5) x 10^2
6	3	1.8 (± 0.4) x 10^4	1.2 (± 0.2) x 10^4	9.1 (± 0.9) x 10^3	1.2 (± 0.2) x 10^3	1.1 (± 0.5) x 10^3

Table 4.4 Comparison of the γ values for the gain coefficient fittings

The table shows the strong dependence of the amount of spontaneous emission, along the amplifier, on the pump power and the capillary diameter (in other words the volume of active molecules). The errors listed are the standard deviation values. From these values, and the saturated model in Eq. 4.10, the VSL data can be fitted to obtain values for the saturated gain coefficients, the average values of which are plotted in Table 4.5. The effects of the capillary diameter on the values for the saturated gain coefficient are plotted in Fig. 4.12.

Pump power (mW)	530 μm gain (cm^{-1})	320 μm gain (cm^{-1})	100 μm gain (cm^{-1})	50 μm gain (cm^{-1})	25 μm gain (cm^{-1})
1	4.6 ±0.4	4.7 ± 0.3	3.1 ± 0.4	3.8 ± 0.6	3.1 ± 0.5
3	4.8 ± 0.4	5.2 ± 0.4	3.3 ± 0.4	4.4 ± 0.5	3.6 ± 0.5
6	6.1 ± 0.6	5.1 ± 0.4	4.1 ± 0.4	4.7 ± 0.5	3.9 ± 0.5

Table 4.5 Summary of saturated gain model values for increasing capillary diameter and pump power

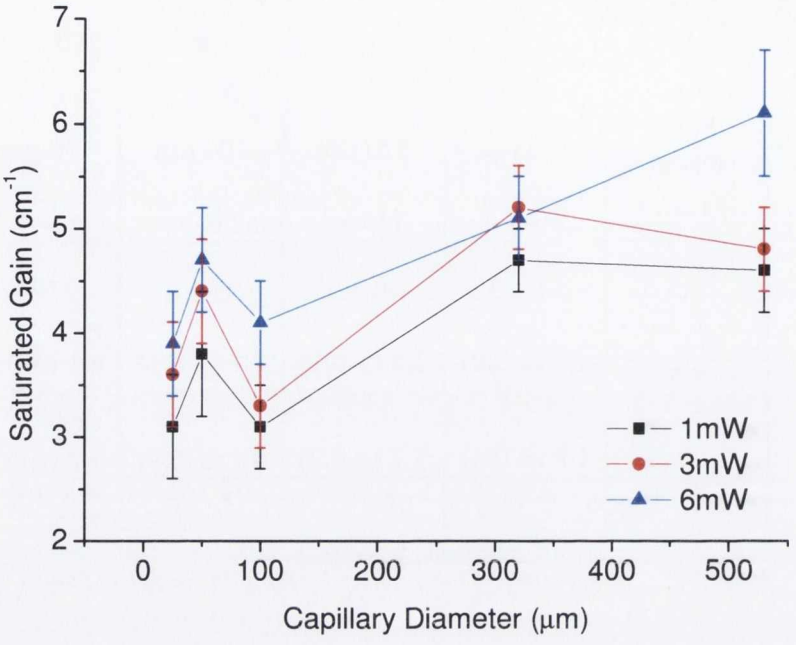

Figure 4.12 Dependence of the saturated gain on the capillary diameter

As shown in Fig. 4.9, the fitting range of the unsaturated gain only covers the small pumping power region. In contrast, the saturated gain fits all regions of the data. Under the unsaturated gain, i.e., small signal gain approximation, the inverted population is assumed to be infinite, while the saturated gain considers the finite population inversion. Thus it is seen that the values for the saturated gain are smaller than their unsaturated counterparts.

The effects of gain saturation can be most easily seen in Fig. 4.9, whereby the difference in plotting the unsaturated and saturated models can be clearly seen. For large pump power intensities, as the ground-state population is depleted, fewer molecules are available for pump absorption, the excited state population saturates and hence the gain coefficient decreases. Therefore, it can be concluded that the saturated model fits well for the larger capillaries, however, when the smaller diameters are used, i.e. smaller volumes of the gain medium, the attempts to fit the saturated model are much more difficult and the experimental error increases significantly, as mentioned in Section 4.3.3. This issue has been examined in detail by Costela et al. and McGehee et al. [3, 18], whereby they determined that the gain saturation is found to occur when $gl \approx 4$. That is to say, when the spontaneous emission is amplified by such a factor it is generally intense enough to

significantly depopulate the excitation density. As the unsaturated gain coefficient, for the 25 μm capillary in particular, is close to 4 cm^{-1}, this signifies why it is so difficult to fit the saturated model for the smaller tube diameters, as $l \approx 1$ cm.

4.3.6 Review of Gain Media

Author	Material	Pump Power	Gain Value	Ref.
In solid state				
Slooff et el.	polymer waveguide based on Er complexes	at 930 mW	1.7 dB	[16]
Cerdán et al.	planar waveguide doped with pyrromethene 597 dye	at 25 μJ/pulse	59 cm^{-1}	[17]
Djiango et al.	solid state waveguide LDS821 dye	at 1.5 mJ/cm^2	37.2 cm^{-1}	[6]
McGehee et al.	planar polymer waveguides	at 1.2kW/cm^2	18 cm^{-1}	[18]
Oton et al.	Nile blue dye doped porous silicon planar waveguides	at 27 mJ/cm^2	8.7 cm^{-1}	[19]
Calzado et al.	perylenedimide derivatives in polystyrene films	at 74 kW/cm^2	10 cm^{-1}	[20]
Tagaya et al.	selection of organic dye doped polymer optical fibres	at 620 W	30 dB	[21]
Rajesh et al.	Rhodamine 6G doped optical polymer fibre	at 6 mJ	18 dB	[22]
Karimi et al.	Rhodamine B doped polymer optical fibre	at 10 kW	30 dB	[23]
In solution				
Periasamy et al.	2cm long fibre immersed in a Rhodamine 6G solution	at 200 kW	3 cm^{-1}	[24]
Mohan et al.	Rhodamine B	at 0.67 MW	7.6 dB/cm	[25]
Mazurczyk et al.	Erbium-doped fibre amplifier	at 14 mW	19 dB	[26]
This work	(unsaturated gain coefficient)			
	530μm Rhodamine 590 amplifier	at 1-6mW	6.8-8.1 cm^{-1}	
	320μm Rhodamine 590 amplifier		6.8-7.4 cm^{-1}	
	100μm Rhodamine 590 amplifier		5.4-6.4 cm^{-1}	
	50μm Rhodamine 590 amplifier		5.2-5.9 cm^{-1}	
	25μm Rhodamine 590 amplifier		4.0-5.3 cm^{-1}	

Table 4.6 Summary of literature results for the measurement of gain media

It is difficult to directly compare these findings with those in literature as the parameters and materials vary significantly. In particular the volumes and pump powers used in this work at much lower than much of the work reported.

The values reported in this work are for the net gain (or gain coefficient), whose units are cm^{-1}. Some literature report on the small-signal gain (in dB), which can easily be obtained by using the method described by Kobayashi et al. [27] (or adapted from Eq. 4.11, as from the definition, the small-signal gain equates to the ratio of power in to power out). The small-signal gain, G, can be described as follows

$$G = \exp[gL_{us}] \qquad (4.12)$$

where g is the net gain and L_{us} is the unsaturated gain length. From this, the values for the small-signal gain at the maximum pump power, of 6 mW (or 3 mJ cm^{-2}), are

530 μm	320 μm	100 μm	50 μm	25 μm
21.1 dB	19.3 dB	16.7 dB	15.4 dB	13.8 dB

for an approximate 6 μm long unsaturated gain length, estimated from Fig. 4.9. For comparative pump powers, Mazurczyk et al., for example, measured gains of 19 dB for erbium doped optical fibres at 14 mW [26]. To compare solid state waveguides, at similar powers, Rajesh et al. measured gains of 18 dB in Rhodamine 590 doped polymer optical fibres [22]. Djiango et al. obtained very high gain values, 37.2 cm^{-1}, for planar waveguide structures [6]. They, however, used a different dye, LDS821, which may be a more efficient gain medium than the dye used for this thesis.

The ease at which these devices were realised is another important feature, when compared to similar literature findings. For example, more complicated fabrication processes can involve the polymerisation of the monomer to form solid-state optical rods [14] or the formation of micro-fluidic channels through micro-machining, lithography [28] and by chemical vapour deposition [29]. In comparison to these processes, the devices described in this work are much more easily achieved.

Another point to note is that much of the literature listed does not take into account the saturated model for gain fitting. However, Costela et al. do, whereby Pyrromethene 567

doped polymer waveguides measured net gain coefficients of 20.6 ± 2.7 cm^{-1} at a pump intensity of 3.4 MW/cm^2 [3]. However, overall, the values measured for our dye-doped capillary tubes obtained compare well with those reported in the literature, especially for their relative size and volume of active molecules required.

4.4 Summary

In summary, evidence of stimulated emission from the Rhodamine 590 filled capillary tubes has been observed, even in diameters as small as 25 μm. Line-narrowing of the emission peak was established and subsequently the ASE pump power threshold was calculated. Using the VSL method, the gain coefficients for each tube were successfully measured. A trend was observed for the gain values: as the pump intensity increases, so does the value of the gain coefficient. Hence, the amplification properties of these dye-filled micro-capillaries were obtained, when photoexcited with the laser pump beam. The largest gain value reported was 8.1 cm^{-1} for the largest 530 μm diameter doped amplifier, at 6mW pump power. When the capillary diameter was decreased to 25 μm, the smallest diameter available, the gain was measured to be 5.3 cm^{-1}. These values compare favourably to those in the literature, with Periasamy et al., for example, reporting a value of 3 cm^{-1} for Rhodamine 590 doped fibres [24], at much higher pump powers than possible in this setup. For the relative size, volume of gain medium used and powers used in this work, these dye doped micro-capillaries are very promising for use as amplifying devices.

The saturated gain values were also fitted for the dye doped micro-capillaries. However, the unsaturated model is deemed more suitable for fitting due to the inherent difficulties in fitting the saturated model to the lower volumes of the active molecules in the smaller doped capillary tubes. The conclusions drawn by Costela et al. and McGehee et al. [3, 30] were verified, in that the saturated model can only be fitted for values of gl that are greater than 4.

4.5 References

1. Shaklee, K.L. and R.F. Leheny, *Applied Physics Letters*, 1971. **18**(11): p. 475-&.
2. Mohs, G., T. Aoki, R. Shimano, M. Kuwata-Gonokami, and S. Nakamura, *Solid State Communications*, 1998. **108**(2): p. 105-109.
3. Costela, A., O. Garcia, L. Cerdan, I. Garcia-Moreno, and R. Sastre, *Optics Express*, 2008. **16**(10): p. 7023-7036.
4. Simon, P. and N. Juhasz, *Journal of Physics E-Scientific Instruments*, 1985. **18**(10): p. 829-830.
5. Roth, M., A. Hardy, and S. Ruschin, *IEEE Journal of Quantum Electronics*, 2001. **37**(2): p. 189-198.
6. Djiango, M., T. Kobayashi, W.J. Blau, B. Cai, K. Komatsu, and T. Kaino, *Applied Physics Letters*, 2008. **92**(8).
7. Schäfer, F.P. and K.H. Drexhage, *Dye lasers*. 2nd rev. ed. ed. Topics in applied physics ; vol.1. 1977, Berlin ; New York: Springer.
8. Kruhlak, R.J. and M.G. Kuzyk, *Journal of the Optical Society of America B-Optical Physics*, 1999. **16**(10): p. 1749-1755.
9. Kruhlak, R.J. and M.G. Kuzyk, *Journal of the Optical Society of America B-Optical Physics*, 1999. **16**(10): p. 1756-1767.
10. Lahoz, F., C.J. Oton, N. Capuj, M. Ferrer-Gonzalez, S. Cheylan, and D. Navarro-Urrios, *Optics Express*, 2009. **17**(19): p. 16766-16775.
11. Kim, Y.C., T.W. Lee, O.O. Park, C.Y. Kim, and H.N. Cho, *Advanced Materials*, 2001. **13**(9): p. 646-649.
12. Vezenov, D.V., B.T. Mayers, R.S. Conroy, G.M. Whitesides, P.T. Snee, Y. Chan, D.G. Nocera, and M.G. Bawendi, *Journal of the American Chemical Society*, 2005. **127**(25): p. 8952-8953.
13. Harada, H., M. Nakatsu, and H. Naito, *Japanese Journal of Applied Physics Part 2-Letters & Express Letters*, 2005. **44**(28-32): p. L915-L917.
14. Rajesh, M., K. Geetha, M. Sheeba, C.P.G. Vallabhan, P. Radhakrishnan, and V.P.N. Nampoori, *Optical Engineering*, 2006. **45**(7).
15. Karthaus, O. and Y. Kawatani, *Japanese Journal of Applied Physics Part 1-Regular Papers Short Notes & Review Papers*, 2003. **42**(1): p. 127-131.
16. Slooff, L.H., A. Polman, M.P.O. Wolbers, F.C.J.M. van Veggel, D.N. Reinhoudt, and J.W. Hofstraat, *Journal of Applied Physics*, 1998. **83**(1): p. 497-503.
17. Cerdan, L., A. Costela, I. Garcia-Moreno, O. Garcia, and R. Sastre, *Applied Physics B-Lasers and Optics*, 2009. **97**(1): p. 73-83.
18. McGehee, M.D., R. Gupta, E.K. Miller, and A.J. Heeger, *Synthetic Metals*, 1999. **102**(1-3): p. 1030-1033.
19. Oton, C.J., D. Navarro-Urrios, N.E. Capuj, M. Ghulinyan, L. Pavesi, S. Gonzalez-Perez, F. Lahoz, and I.R. Martin, *Applied Physics Letters*, 2006. **89**(1).
20. Calzado, E.M., J.M. Villalvilla, P.G. Boj, J.A. Quintana, R. Gomez, J.L. Segura, and M.A.D. Garcia, *Applied Optics*, 2007. **46**(18): p. 3836-3842.
21. Tagaya, A., S. Teramoto, E. Nihei, K. Sasaki, and Y. Koike, *Applied Optics*, 1997. **36**(3): p. 572-578.
22. Rajesh, M., M. Sheeba, K. Geetha, C.P.G. Vallaban, P. Radhakrishnan, and V.P.N. Nampoori, *Applied Optics*, 2007. **46**(1): p. 106-112.
23. Karimi, M., N. Granpayeh, and M.K.M. Farshi, *Applied Physics B-Lasers and Optics*, 2004. **78**(3-4): p. 387-396.
24. Periasamy, N. and F.P. Schafer, *Applied Physics*, 1981. **24**(3): p. 201-203.
25. Mohan, D., L. Taneja, A. Gaur, A.K. Sharma, and R.D. Singh, *Journal of Luminescence*, 1991. **50**(2): p. 127-131.

26. Mazurczyk, V.J. and J.L. Zyskind, *IEEE Photonics Technology Letters*, 1994. **6**(5): p. 616-618.
27. Kobayashi, T., M. Flammich, G. Jordan, R. D'Arcy, M. Ruther, W.J. Blau, Y. Suzuki, and T. Kaino, *Applied Physics Letters*, 2006. **89**(13).
28. Monat, C., P. Domachuk, and B.J. Eggleton, *Nature Photonics*, 2007. **1**(2): p. 106-114.
29. Dumais, P., C.L. Callender, J.P. Noad, and C.J. Ledderhof, *IEEE Photonics Technology Letters*, 2005. **17**(2): p. 441-443.
30. McGehee, M.D., R. Gupta, S. Veenstra, E.K. Miller, M.A. Diaz-Garcia, and A.J. Heeger, *Physical Review B*, 1998. **58**(11): p. 7035-7039.

Chapter 5

Polarised Dye Micro-amplifiers

5.1 Introduction

In this chapter, the polarization properties of the dye lasing micro-amplifiers were examined. The effects of changing the polarisation conditions of the laser pump beam were investigated in order to ascertain the optimum conditions for emission from the dye-doped amplifiers. The gain of many laser systems depends strongly on the state of polarisation and the direction of propagation of the emitted signal [1]. The ability to modulate the emission properties of the gain media within the micro-amplifiers not only improves their efficiency but can also provide a way to easily modify the absorption and gain of the active molecules.

Light sources with a particular polarisation state are useful for a wide variety of applications. Versatile systems, whose properties can be varied by simply changing the polarisation state of the pump source, are highly desirable. For example, satellite communications use two orthogonal polarisations to double the capacity of the channel [2]; circularly-polarized light sources are necessary to detect certain biological molecules [3]; and laser sources with a variety of polarisation states have relevance for quantum cryptography [4].

5.2 Theory

The properties of an optical device can be described, in part, by its polarisation behaviour. By understanding the polarisation phenomenon, the properties can be enhanced or controlled. The polarisation properties of light waves are especially important for propagation within anisotropic media, in which the physical properties vary with direction. The state of polarisation of the input pump beam can be changed by means of employing either a half-wave plate or a quarter-wave plate and is sensitive to the optical properties of the medium. The most general state of polarisation of a plane wave is the elliptical polarisation state, of which the linear and circular states of polarisation may be regarded as special cases.

An optical wave propagates in an optical medium via its interaction with the elementary dipole oscillators that comprise the molecules. For molecules with asymmetry, there is likely to be a variation in the absorption or amplification of the wave with polarisation state. Therefore, there will be a dependence of the amplitude and the velocity of the wave on the polarisation state [5]. This will lead to a polarisation-dependent loss or gain [6]. In the case of dye molecules, the polarisation characteristics are related to the relative orientation of the transition moments for absorption and emission and the rotational diffusion-relaxation time [7]. For many applications it is advantageous for dye lasers to provide strongly polarised narrow-linewidth radiation [7].

5.2.1 Polarisation Ellipse

Polarised light can be described using Maxwell's equations, whereby light is described as an electromagnetic (EM) wave. The electric field strength defines the state of polarisation of light, and the electromagnetic wave specifies the magnitude and displacement of the wave. If we consider two perpendicular optical fields moving in the z-direction, given by [5]

$$E_x = e_x \cos(\omega t - kz + \delta_x) \tag{5.1}$$

$$E_y = e_y \cos(\omega t - kz + \delta_y) \tag{5.2}$$

where δ_x, δ_y, are arbitrary (but constant) phase angles. This solution can be described by means of two waves: one in which the electric field lies in the xz plane and the other in which it lies in the yz plane (Fig. 5.1). The electric field $\vec{E}$ propagating along the z direction as a function of time, t, can be expressed as

$$\vec{E} = \exp[i(\omega t - kz)](\vec{E}_{0x} \exp[i\delta_x] + \vec{E}_{0y} \exp[i\delta_y]) \tag{5.3}$$

where ω is the optical frequency, k the wave number, $\vec{E}_{0x}$ and $\vec{E}_{0y}$ the $\vec{E}$ are the components in the x and y directions respectively, and δ_x, δ_y the phase.

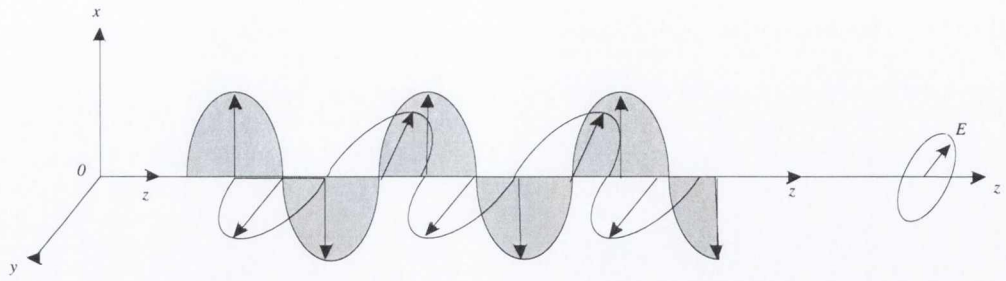

Figure 5.1 The electric field components for an elliptically polarized wave

From Maxwell's equations, if it is set that $(\omega t\text{-}kz) = 0$ and consider the real part of Eq. 5.3, we obtain the expression

$$\frac{E_x^2}{e_x^2}+\frac{E_y^2}{e_y^2}-\frac{2E_xE_y}{e_xe_y}\cos(\delta_y-\delta_x)=\sin^2(\delta_y-\delta_x) \qquad (5.4)$$

which is the equation of an ellipse (in the variables E_x, E_y) circumscribed by the tip of the resultant electric vector at any one point in space over one period of the combined wave. The ellipticity, e, of the ellipse is the ratio of the minor to the major axis and represents the amount of deviation of the ellipse from a circle. An ellipticity of 0 represents a linear polarisation and an ellipticity of 1 represents a circular polarisation. The sign of the ellipticity is defined as being negative for left-handed polarisation and positive for right-handed polarisation. The tip of the electric field vector describes an ellipse in the plane normal to z and the wave polarisation is characterised by the two parameters (ellipticity and orientation) of the polarisation ellipse.

A linear state is obtained with the components in Eq. 5.4 when either

$\left.\begin{matrix} e_x = 0 \\ e_y \neq 0 \end{matrix}\right\}$ linearly polarised in Oy direction

$\left.\begin{matrix} e_x \neq 0 \\ e_y = 0 \end{matrix}\right\}$ linearly polarised in Ox direction

Or

$\delta_y - \delta_x = m\pi$ where m is an integer.

A circular state is obtained when

$$e_x = e_y \text{ and } (\delta_y-\delta_x)=(2m-1)\pi/2 \qquad (5.5)$$

that is, in this case the two component waves have equal amplitudes and are $\pi/2$ out of phase. The waves will be right-hand circularly polarised when m is even and left-hand

circularly polarised when m is odd. The phase difference can be expressed as $\Delta\delta = \delta_y - \delta_x$, where the phase is related to the refractive index by

$$\delta_x = \frac{2\pi L n_x}{\lambda} \text{ (and the same for y)} \qquad (5.6)$$

where λ is the wavelength, L is the length of material traversed and n is the refractive index in the x or y direction.

Optical wave plates may be constructed from birefringent materials that introduce a phase difference between the fast and slow principal axis of the wave plate. The birefringent properties of the material create a difference in the refractive index between the two axes which, in turn, creates a difference in the velocity between the two orthogonal components. The fast principal axis of the wave plate has a lower refractive index resulting in faster wave velocity and vice versa. The actual phase shift created depends on the properties of the material, the thickness of the wave plate and the wavelength of the signal. When Eq. 5.6 is rearranged slightly, it can be described as:

$$\Delta\delta = \frac{2\pi d(n_1 - n_2)}{\lambda} \qquad (5.7)$$

where n_1 is the refractive index of the principal plane, n_2 is the refractive index of the orthogonal plane and d is the thickness of the wave plate.

5.3 Experimental Procedure

It is known that the polarisation of the emitted light from the dye-filled micro-capillary is dependent on the polarisation of the exciting laser beam, the relative orientation of the transition moments in the dye molecule for the pumping and laser transitions, and the rotational diffusion-relaxation time [7]. The latter is determined by solvent viscosity, temperature and molecular size.

The experimental layout is the same as seen in Chapter 4, except that a wave plate and two polarisers were inserted into the setup. The main polariser, denoted by s (also known as Transverse Electric (TE) i.e. when the electric field vector is perpendicular to the plane of incidence or along the x-axis) or p (also known as Transverse Magnetic (TM) i.e. when the electric field vector is parallel to the plane of incidence or along the y-axis), depending on the polarisation condition, and the waveplate were placed between the two

cylindrical lenses. The second polariser denoted s' and p' for the two orthogonal polarised components, was placed between the sample and the microscopic objective. The full experimental setup can be seen in Fig. 5.2.

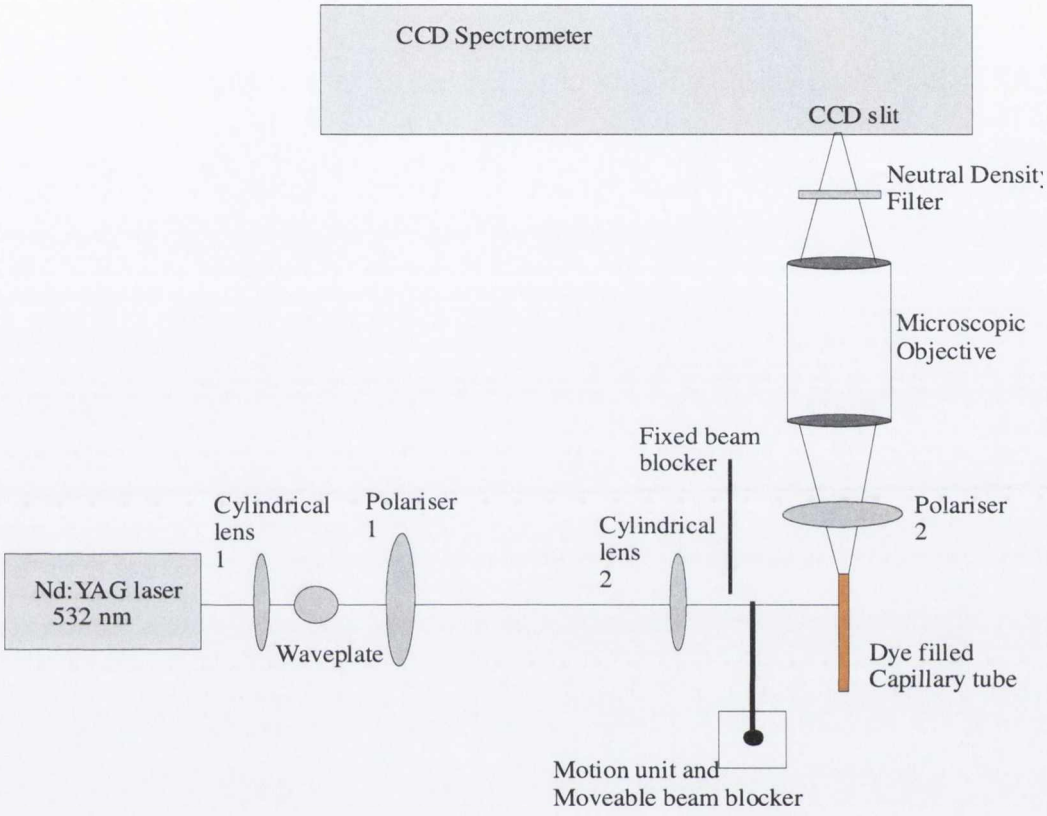

Figure 5.2 Schematic diagram of the experimental setup

When a linearly polarised beam is incident on a half-wave plate the beam will emerge as linearly polarised light but with a polarisation plane that is rotated with respect to the polarisation of the input beam. The rotation of the polarisation plane is such that the angle between the output polarisation and the wave plates optic axis is twice the angle between the input polarisation and the wave plates optic axis. In a similar manner, a quarter-wave plate is designed such that the phase shift created between the fast and slow axes is quarter of a wavelength ($\lambda/4$) or a multiple thereof. When a linearly polarised beam is aligned at 45° to the wave plate's principal plane, the output beam will be circularly polarised.

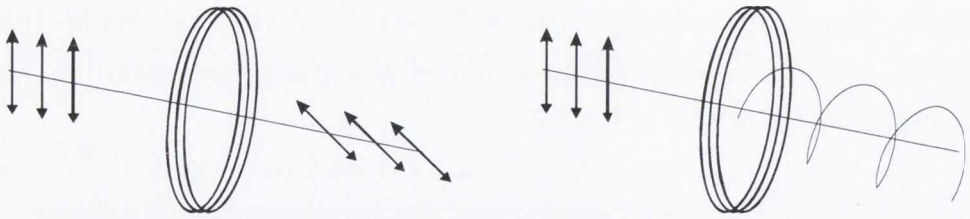

Figure 5.3 The effects of a (a) half-wave and (b) quarter-wave plate on an incident wave

In this chapter, three diameters of capillary were chosen for further investigation: 530, 100 and 25 μm (i.e. the largest, intermediate and smallest). This was done in order to give a good comparative image of the effects of changing the pump conditions on the wide variety of available capillaries. The capillary tubes were examined as separate entities, i.e. the same filter was not used on all of the tubes. This was because at low pump intensities, in particular for the smallest capillary tubes, the emission intensities were very noisy and potentially difficult to obtain information from. Hence, the NG 4 filter was removed for the 25 μm capillary diameter measurements.

The pump intensity was measured, not from where it exited the laser, but between the polariser (1) and the second cylindrical lens. This is due to the fact that, as the polarisation conditions of the pump beam were changed, so did the intensity of the laser beam. By measuring the power at the sample, it was ensured that the pump beam power was the same for all conditions. Hence, the maximum pump power obtainable under the variable polarisation conditions was 3 mW.

5.4 Results

5.4.1 Emission Intensity

The emission intensity of the capillary tubes varies as the polarisation conditions are changed. The s-polarised pumping position has the highest maximum peak intensity, followed by the circular- and, lastly, the p-polarisation condition. In each case the s' component is larger than the p'. The difference between these two components is greatest for the s-polarisation and follows the same downward trend as that of the maximum intensity values. In fact, for the p-polarisation, the difference between the s' and p' components is minimal, the two are almost equal. In Fig. 5.4, the variation in emission intensity can be observed for the 530 μm capillary, as an example.

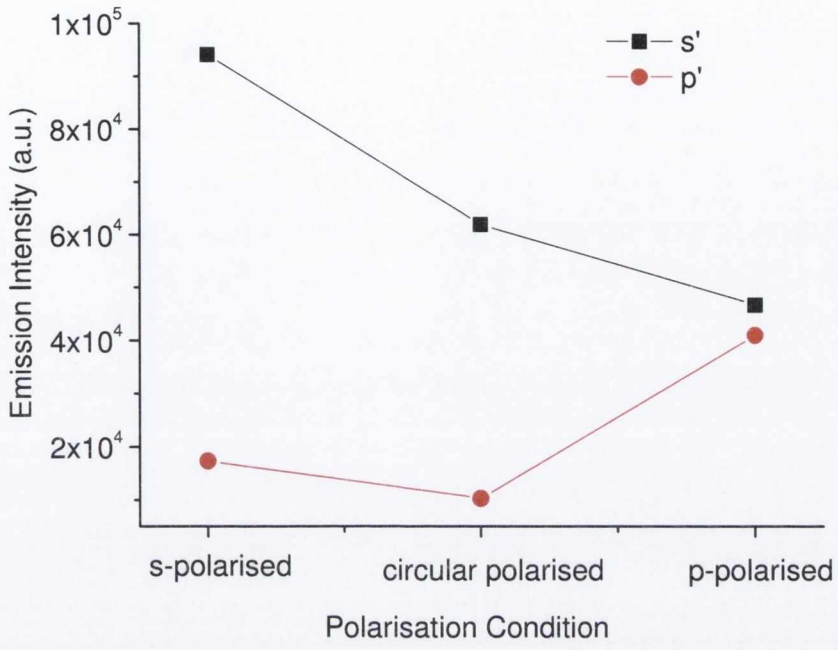

Figure 5.4 Emission intensity against polarisation at 3mW for the two different polarisation components, s' and p', for 530 μm capillary tube

The two smaller capillary tubes show similar deviations in the emission intensities as the pump conditions are changed and the pump power decreased. For all cases, the difference between the s'- and p'-components for the p-polarisation condition is minimal. The largest difference in the emission intensity values for the two positions is observed for the s- and circular-polarisation conditions. No obvious shift in the emission peak wavelength was observed for the changing polarised pump beam.

Figures 5.5 and 5.6 show the full-width half maximum values (FWHM) and input-output emission spectra for the 530 μm capillary tube, respectively, as an example of how changing the polarisation conditions affects the emission properties. The 530 μm capillary data is only shown as a representative example.

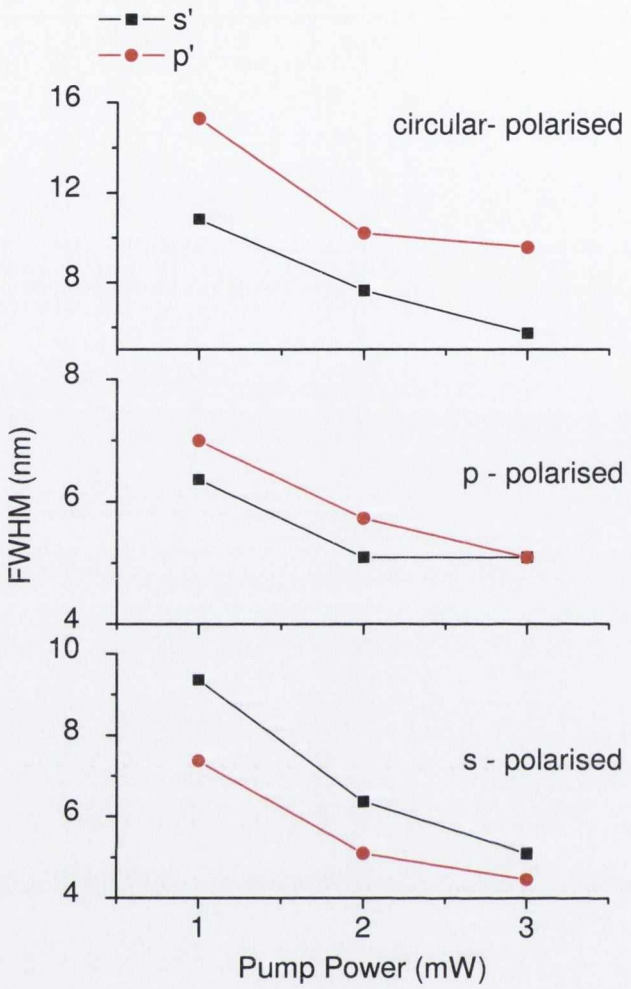

Figure 5.5 FWHM for the different pump polarisation powers for the 530 μm capillary

A distinct difference for the FWHM and emission properties of the 530 μm capillary tube was seen as the polarisation conditions are changed. A narrowing of the emission peak was observed for all polarisation conditions, although the extent of the line narrowing varies dramatically. It should be noted that the polarisation measurements were only taken for pump powers above the threshold for ASE, i.e. beginning at 1 mW. Hence, the line-narrowing is not as obvious as observed in the previous chapter, in which initial measurements started at 0.25 mW.

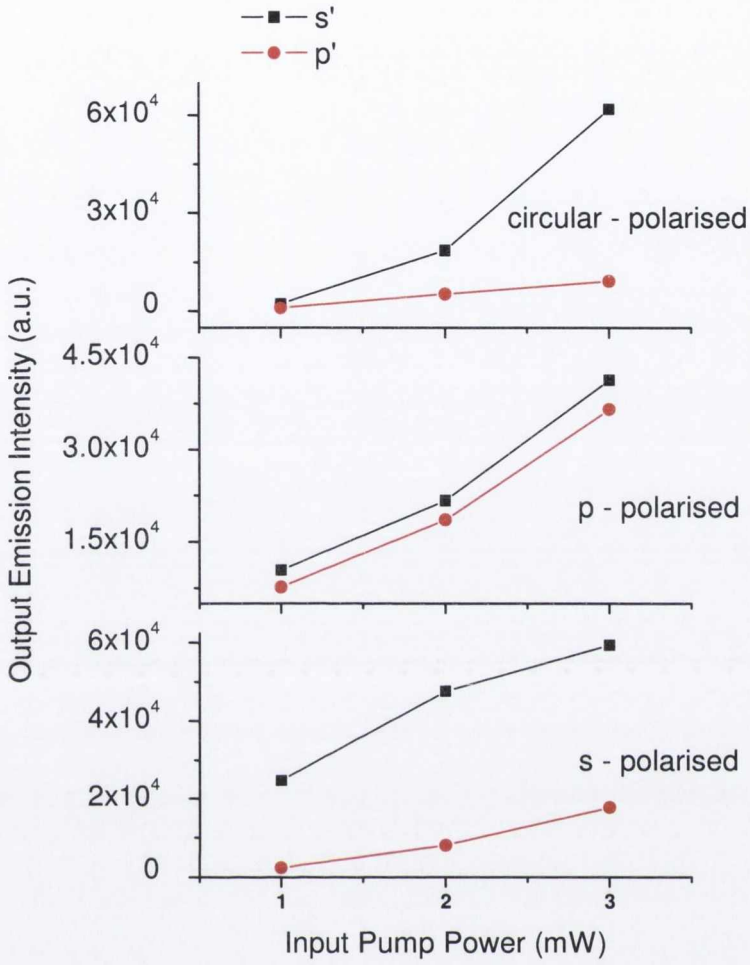

Figure 5.6 Input-output emission intensity for different pump conditions for the 530 μm capillary

The input–output emission properties also show the effects that the polarisation condition has on the emission output behaviour of the 530 μm capillary tube. For each condition, the s'-component has a higher intensity increase than the p-component, indicating the higher efficiency of the former.

5.4.2 Degree of Polarisation

Another way of presenting the polarisation emission characteristics of the pump beam is through calculation of the degree of polarisation (DOP), defined as [8]

$$P = \frac{I_{s'} - I_{p'}}{I_{s'} + I_{p'}} \qquad (5.8)$$

By inputting the intensity of the emission for each polarised beam component into the above equation, the degree of polarisation can be estimated and the results presented below.

Pump Power	Capillary (μm)	s-polarised	circular-polarised	p-polarised
3mW	530	0.69	0.72	0.07
	100	0.55	0.44	0.04
	25	0.46	0.58	0.05
2mW	530	0.72	0.55	0.06
	100	0.62	0.43	0.04
	25	0.59	0.65	0.09
1mW	530	0.82	0.41	0.17
	100	0.40	0.51	0.02
	25	0.62	0.37	0.15

Table 5.1 Summary of the degree of polarisation for the three capillary diameters

When the DOP is equal to zero, the light is said to be unpolarised, whereas when it equals a value of one it is said to be completely polarised. Due to inherent experimental error, it would not be expected that the laser light would be completely polarised and that the DOP would equal 1.

It is observed that, for the s- and circular-polarisation positions, the DOP is strong and the p-polarisation is almost completely unpolarised. Similar findings were obtained by Wang et al. [9] and Lahoz et al. [10], where the p-polarised state exhibited little or poor output intensity. In general, for each pump power, the 530 μm capillary exhibits the strongest DOP, whereas the 25 μm shows the weakest. This could be due to the fact that the state of polarisation depends on the orientation of the dye molecule. As the dye is in solution, the orientation of the molecules is not fixed. Therefore, the random molecular orientation can affect to what extent the dye emission is polarised. For the smaller capillary diameters, the level of confinement within the device is increased, which could lessen the degree to which the molecules are polarised.

5.4.3 Gain Measurement

The gain coefficients for the pump polarisation conditions were measured using the VSL method for the 530, 100 and 25 μm capillary diameters.

5.4.3.1 530 μm capillary

		3mW	2mW	1mW
s-polarised	s'	6.6 ± 0.4	5.0 ± 0.3	3.7 ± 0.3
	p'	4.0 ± 0.4	4.3 ± 0.4	2.8 ± 0.3
p-polarised	s'	5.4 ± 0.4	4.8 ± 0.5	3.4 ± 0.4
	p'	4.3 ± 0.4	4.0 ± 0.3	2.8 ± 0.4
circular-polarised	s'	5.4 ± 0.3	5.2 ± 0.4	5.7 ± 0.3
	p'	4.1 ± 0.3	4.8 ± 0.3	5.4 ± 0.3

Table 5.2 Polarised unsaturated gain values (cm^{-1}), from the VSL method, for the 530 μm capillary

The data in Table 5.2 shows the variation of the gain values as both the pump intensity and the polarisation condition of the pump beam are changed. The decreasing pump power appears to have less of an effect on the gain values for the circular-polarisation state, than for the other states. In other words, the s- and p-polarisation states show a decrease in the gain coefficient with decreasing pump power. The circular-polarised state however, exhibits little change. This could be attributed to the poor emission quality as the pump power decreases. Hence it becomes more difficult to fit the data to the one-dimensional amplifier theory. Another way of looking at the results from the VSL method is presented in Fig. 5.7. The fitted unsaturated and saturated gain model results are plotted for the 3 mW pump intensity.

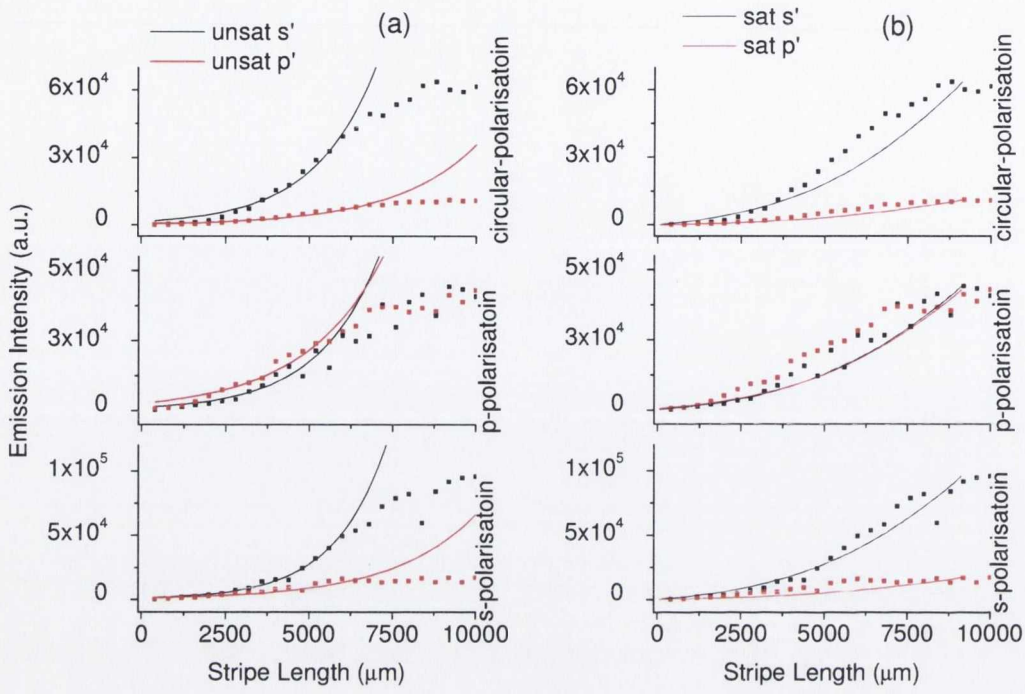

Figure 5.7 Fitted data of the (a) unsaturated and (b) saturated gain models for the different polarisation conditions of the 530 μm capillary tube (NG4) at 3 mW

From this graph, a difference in the gain can be more easily observed for the changing polarisation conditions. The lines represent the fitting model and the dots the VSL data points. The fitting models are plotted with the VSL data points for the three different polarisation pump beam conditions; s-, p- and circular-polarised. For example, for unsaturated gain 3 mW data set, the s-polarised s'-component has the highest gain value, followed by the circular-polarisation s'-component. By plotting the fitted data points from the VSL results, the optimum pump beam polarisation emission condition can be determined.

		3mW	2mW	1mW
s-polarised	s'	4.1 ± 0.9	2.6 ± 1.0	1.0 ± 0.5
	p'	1.9 ± 0.7	1.6 ± 0.6	0.4 ± 0.2
p-polarised	s'	2.5 ± 0.7	2.0 ± 0.9	2.4 ± 0.3
	p'	2.8 ± 0.9	1.1 ± 0.5	3.6 ± 0.9
circular-polarised	s'	3.4 ± 1.1	3.2 ± 0.9	3.4 ± 0.8
	p'	2.2 ± 1.0	3.0 ± 1.2	3.5 ± 0.7

Table 5.3 Polarised saturated gain values (cm^{-1}) for the 530 μm capillary

As discussed in Chapter 4, the data for the saturated gain values proved to be more difficult to fit, especially for the smaller pump intensities and smaller capillary diameters. This is primarily due to the fact that the unsaturated gain coefficient values are close to 4 cm^{-1}. It has been shown that at $gl \approx 4$ is when gain saturation occurs [11]. Below this, the unsaturated gain model is sufficient, as, in this case, $l \approx 1$ cm. In other words, for the 530 μm capillary diameters, the saturated model can be used. However, for the smaller diameters, 100 and 25 μm, the saturated gain values less than approximately 4 cm^{-1}.

5.4.3.2 100 μm capillary

For the 100 μm capillary tube diameters, with the NG 4 filter in place, the emission intensity once again follows the same pattern as with the larger diameter tubing. For each pump power, the s-polarised condition exhibited the highest emission intensity, followed by the circular-polarised. In each case, the intensity of the s'-component was higher than that of the p'-component; the difference between the two was greatest for the s-condition. The p-polarisation condition had the lowest intensity, where the s'- and p'-components were of similar amplitudes.

		3mW	2mW	1mW
s-polarised	s'	4.8 ± 0.2	4.9 ± 0.4	3.9 ± 0.4
	p'	3.7 ± 0.3	4.0 ± 0.4	3.4 ± 0.5
p-polarised	s'	3.3 ± 0.3	3.4 ± 0.4	3.3 ± 0.4
	p'	3.6 ± 0.4	3.2 ± 0.4	3.3 ± 0.3
circular-polarised	s'	4.8 ± 0.3	4.0 ± 0.4	4.0 ± 0.4
	p'	4.3 ± 0.2	3.8 ± 0.5	3.4 ± 0.4

Table 5.4 Polarised unsaturated gain values (cm^{-1}) for the 100 μm capillary tubes

The summary for the 100 μm capillary tubes in Table 5.4 again shows the variation of the gain coefficients as the pump conditions are changed. As with the previous section, the fitted data points from the VSL method can be plotted to more easily ascertain the difference in the amplification as the pump beam polarisation is changed. An example is shown below in Fig. 5.8 at the maximum 3 mW pump power.

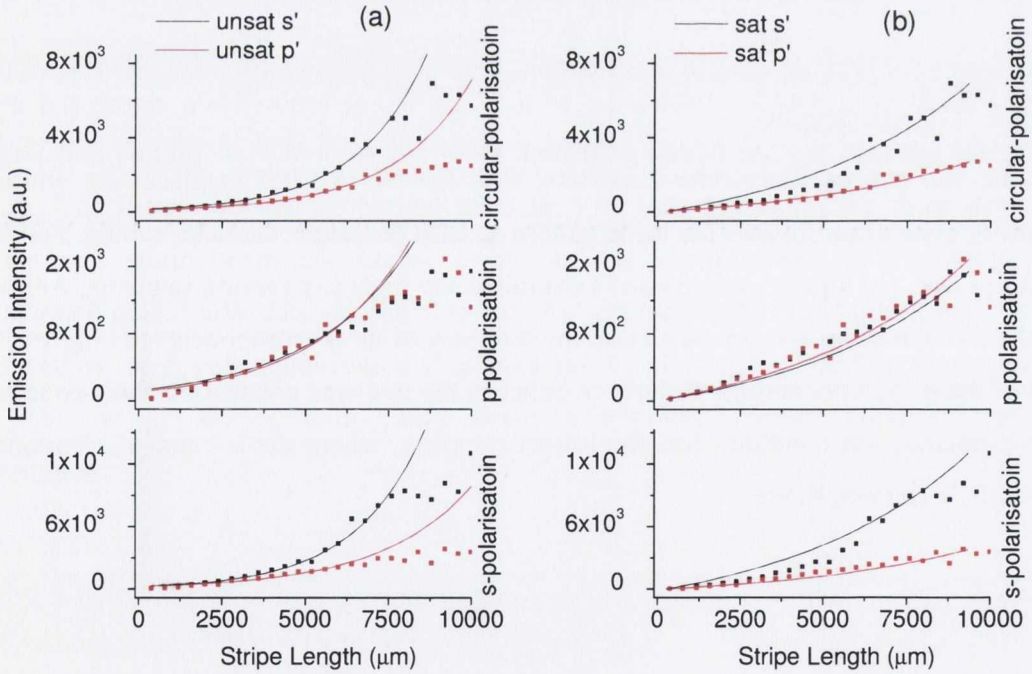

Figure 5.8 Fitted data of the (a) unsaturated and (b) gain modes for the different polarisation conditions of the 100 μm capillary tube (NG4) at 3 mW

For the 3mW pump intensity with the filled 100 μm capillary tube diameter, the s-polarised s'-component has the highest output intensity, followed closely by the circular-

polarisation s'-component. Again, we observe that the p-polarisation has the smallest gain value, i.e. the lowest amplification of the input intensity, and the two components, s' and p', are virtually indistinguishable from each other. The saturated gain values, in Table 5.5, have much lower gain and higher error values than the unsaturated model equivalent. In general, however, the same polarisation is observed in both models.

		3mW	2mW	1mW
s-polarised	s'	2.3 ± 0.3	1.9 ± 0.2	0.8 ± 0.2
	p'	0.9 ± 0.3	0.7 ± 0.3	0.4 ± 0.3
p-polarised	s'	0.4 ± 0.1	0.3 ± 0.1	0.2 ± 0.1
	p'	0.6 ± 0.2	0.3 ± 0.1	0.1 ± 0.1
circular-polarised	s'	2.1 ± 0.3	1.3 ± 0.2	1.3 ± 0.1
	p'	1.7 ± 0.3	0.8 ± 0.1	0.6 ± 0.1

Table 5.5 Polarised saturated gain values (cm^{-1}) for the 100 μm capillary tubes

5.4.3.3 25 μm capillary

The 25 μm capillary tube measurements were taken with no NG filter in place; due to the fact that the intensities are much lower as a result of the smaller volume of active molecules. Hence the emission spectra tend to be of a much lower intensity and of poorer quality when a filter was used. Without the NG filter, the emission intensities are high enough so that the 'noise' is not as great an issue.

The emission intensity for these, the smallest of capillary tube diameters, follows a slightly different pattern. As the pump powers decrease, the intensity of the circular-polarisation condition is highest, marginally higher than the s-polarisation, and shows the biggest difference between the s'- and p'-components. In other words, it follows the same model shown for the 530 μm capillary tube in Fig. 5.4, except that the s- and circular-polarisation intensities have reversed.

		3mW	2mW	1mW
s-polarised	s'	4.7 ± 0.7	7.1 ± 0.8	4.9 ± 0.6
	p'	5.7 ± 0.7	4.2 ± 0.6	7.5 ± 0.7
p-polarised	s'	5.5 ± 0.8	5.2 ± 0.6	5.8 ± 0.8
	p'	5.1 ± 0.5	5.8 ± 0.8	4.9 ± 0.4
circular-polarised	s'	4.0 ± 0.7	4.5 ± 0.5	5.6 ± 0.9
	p'	3.2 ± 0.5	6.1 ± 0.4	5.1 ± 0.4

Table 5.6 Polarised unsaturated gain values (cm^{-1}) for the 25 μm capillary tubes

		3mW	2mW	1mW
s-polarised	s'	1.0 ± 0.8	2.6 ± 0.9	1.2 ± 0.9
	p'	2.9 ± 0.9	2.2 ± 0.9	4.1 ± 0.9
p-polarised	s'	0.7 ± 0.4	1.0 ± 0.4	3.2 ± 0.9
	p'	2.9 ± 0.9	6.5 ± 0.9	3.8 ± 0.9
circular-polarised	s'	0.1 ± 0.1	4.5 ± 0.5	5.6 ± 0.9
	p'	1.1 ± 0.7	3.5 ± 0.9	2.0 ± 0.

Table 5.7 Polarised saturated gain values (cm^{-1}) for the 25 μm capillary tubes

The saturated gain values show very low gain values, with very high error limits. However, the unsaturated model proves to be more promising for the narrowest capillary diameter. There is more variation of the fitted (unsaturated) gain values for the 25 μm than what was measured for the larger capillary diameters. This could be attributed to the fact that with the smaller volumes in question, there is a greater difficulty in fitting the model to the VSL data points. A change was observed in the intensity of the emitted beam from the capillary tubes as the polarisation conditions of the pump beam are adjusted. The highest intensity is for the s-polarised condition, followed by the circularly-polarised beam and lastly the p-polarised beam. This pattern also corresponds to the fitted gain values. A strong dependence of the intensity of the light emitted from the filled micro-capillaries on the polarisation conditions was observed, once again, primarily for s-polarised and circular-polarised pumping.

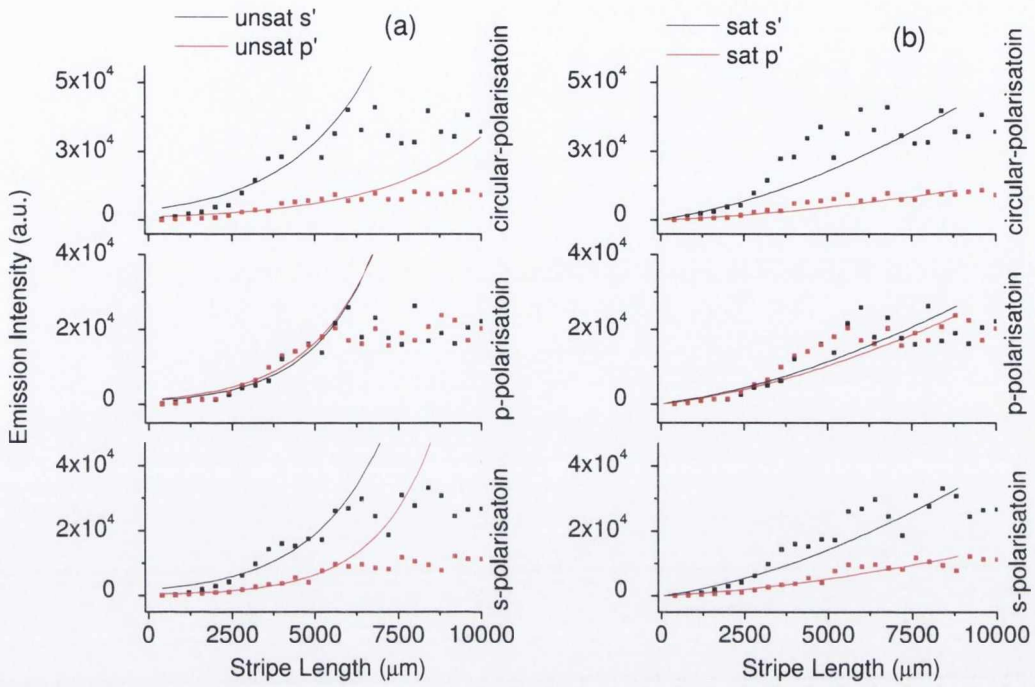

Figure 5.9 Fitted data of the (a) unsaturated and (b) saturated gain modes for the different polarisation conditions of the 25 μm capillary tube (no NG) at 3 mW

The effect of the changing state of polarisation on the fitted unsaturated gain model is plotted in Fig. 5.9 for the 3 mW pump power. The difference between the s' and p' components is clearly visible as the polarisation of the pump beam is changed.

5.5 Discussion

Much has been reported on the theoretical effects of changing the state of polarisation of the pump beam, however little can be found about the effects of this change on the emission properties of the organic dyes.

Fang et al. discussed the important role that polarisation plays on the threshold of ASE and the gain with organic crystal molecules [12]. They showed the strong dependence of the PL emission on the polarisation state of the incident light. Yamao et al. [13] and He et al. [14] reported the fact that solid state organic crystals demonstrated a strong dependence of their optical characteristics on the polarisation of the exciting light. This is caused by the anisotropic packing of the molecules in organic crystals, resulting in an orientation-dependent optical absorption or emission in the materials. Thus, they

concluded that the probability of optical transitions strongly depends on the crystal orientation with respect to polarization of the excitation light. In the work presented in this thesis, the organic molecules in solution have completely random molecular orientations. Therefore the probability of optical transitions occurring is also randomised. Similarly, Reyzer et al. discussed the effects of the orientation of the absorption and emission dipoles of the excited Rhodamine 590 photopumped molecules [8]. They also indicated the ability to modulate the gain or emission from a minimum to maximum, as the pumping alignment is changed from the y to x axis. Experimentally, Marshall et al. found that when the state of polarisation was parallel to the optical axis, the gain was highest, for cerium-doped crystals [15]. The applications of such processes in devices include electro-optical switches and remote-sensing.

5.5.1 Frozen-dipole Approximation

A semi-classical amplifier theory, developed by Reyzer and Casperson [1, 8] uses the *frozen-dipole approximation* to look at the effects of the reorientation of the dye molecule, which can be treated as a dipole, as shown in Fig. 5.10. As discussed in detail by Wang et al. the orientation of the dipole moments μ is represented by the Euler angles (θ, ϕ), which is expressed in Cartesian coordinates by [9]

$$\mu = (\hat{x}\cos\theta + \hat{y}\sin\theta\cos\phi + \hat{z}\sin\theta\sin\phi)|\mu| \quad (5.9)$$

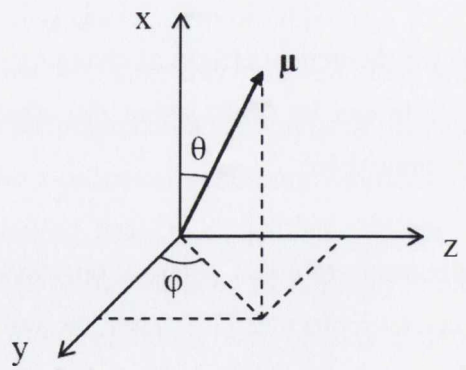

Figure 5.10 Polarisaton theory – can be considered as a dipole

Under the frozen-dipole approximation, the gain coefficients for the two orthogonal polarisations along the propagation direction are defined by [8]

$$g_x = \sigma_s \int_0^{2\pi} \int_0^{\pi} n(\theta,\phi) D \cos^2\theta \sin\theta d\theta d\phi \qquad (5.10)$$

$$g_y = \sigma_s \int_0^{2\pi} \int_0^{\pi} n(\theta,\phi) D \sin^2\theta \cos\theta d\theta d\phi \qquad (5.11)$$

where σ_s is the stimulated emission cross section, $n(\theta, \phi)$ is the number density along the (θ, ϕ) direction. For an isotropic distribution of the dipole moment orientations, we have

$$n(\theta,\phi) = N / 4\pi \qquad (5.12)$$

where N is the number density of the gain medium. D is the population difference between the two energy states where the stimulated transition takes place. Assuming no pump saturation, D is linearly dependent on the pump intensity, and is given by

$$D = \frac{\tau\sigma_p}{h\nu_p} \frac{\varepsilon c}{2n_0} \left| \boldsymbol{E}_p \cdot \boldsymbol{\mu} \right|^2 \qquad (5.13)$$

where τ is the fluorescence decay time, σ_p is the absorption cross-section, $h\nu_p$ is the photon energy of the pump light, $\boldsymbol{E_p}$ is the complex amplitude of the pump field and the term $\varepsilon c/2n_0$ relates the electric field with the light intensity.

Substituting Eq.s 5.12 and 5.13 into 5.10 and 5.11, we can express the gain coefficients for the two orthogonal polarisations

$$g_x = C_1 \int_0^{2\pi} \int_0^{\pi} \left| \boldsymbol{E}_p \cdot \boldsymbol{\mu} \right|^2 \cos^2\theta \sin\theta d\theta d\phi \qquad (5.14)$$

$$g_y = C_1 \int_0^{2\pi} \int_0^{\pi} \left| \boldsymbol{E}_p \cdot \boldsymbol{\mu} \right|^2 \sin^2\theta \cos^2\phi d\theta d\phi \qquad (5.15)$$

where

$$C_1 = \frac{N}{4\pi} \frac{\tau\sigma_s\sigma_p}{h\nu_p} \frac{\varepsilon c}{2n_0} \qquad (5.16)$$

For s-polarised pumping along the y-axis, the exciting field $\boldsymbol{E_p}$ can be written as

$$\boldsymbol{E_p} = \hat{x} E_p e^{-ikr} \qquad (5.17)$$

Substituting Eq.s 5.9 and 5.16 into 5.14 and 5.15, we obtain

$$g_x^s = C_2$$
$$g_y^s = \frac{1}{3} C_2 \qquad (5.18)$$

g_x and g_y are the gain coefficients for the s' and p' polarisation components, where

$$C_2 = \frac{4\pi}{5} C_1 E_p^2 = \frac{N\tau\sigma_s\sigma_p}{5h\nu_p} I_p \qquad (5.19)$$

where N is the number density, σ_s is the stimulated emission cross section and I_p is the exciting intensity.

For p-polarised pumping along the y-axis, the exciting field $\boldsymbol{E_p}$ can be written as

$$E_p = \hat{z} E_p e^{-ikr} \qquad (5.20)$$

Substituting Eq.s 5.9 and 5.19 into 5.14 and 5.15, we obtain

$$\begin{aligned} g_x^p &= \frac{1}{3} C_2 \\ g_y^p &= \frac{1}{3} C_2 \end{aligned} \qquad (5.21)$$

For circularly-polarised pumping along the y-axis, the exciting field $\boldsymbol{E_p}$ can be written as

$$\boldsymbol{E_p} = (i\hat{x} + \hat{z}) \frac{\sqrt{2}}{2} E_p e^{-ikr} \qquad (5.22)$$

Substituting Eq.s 5.9 and 5.22 into 5.14 and 5.15, we obtain

$$\begin{aligned} g_x^c &= \frac{2}{3} C_2 \\ g_y^c &= \frac{1}{3} C_2 \end{aligned} \qquad (5.23)$$

Hence, this model describes the experimentally observed difference in gain values for the horizontal and vertical components of the linear and circularly polarised light. Note, however, that this model does not take into consideration the saturation effect.

As stated, it is known that, theoretically, there should be a dependence of the amplification properties of a material on polarisation state [5]. From this model we can deduce that a difference in the gain coefficients should be observed for each different polarisation condition; s, p and circular. Further evidence that our results follow this model can be seen from the gain values, where the p-polarised pumping exhibited the lowest emission intensities and amplification values. Looking at Eq.s 5.18, 5.21 and 5.23

from the above approximation, the gain values for the p-polarised condition is theorised to have the smallest values.

By solving Eq. 5.19, the theoretical gain values can be calculated for each polarisation condition, knowing that σ_p is 3.8 x 10^{-16} cm^2, and σ_s is 1.2 x 10^{-16} cm^2 [6], the exciting intensity, I_p, is approximately 70 W cm^{-1} and $h\upsilon_p$ is 3.72 x 10^{-19} J. The theoretical estimates for the polarisation-dependent gain values are presented below in Table 5.6.

	g_x (cm^{-1})	g_y (cm^{-1})
s-polarised	10.8	3.6
p-polarised	3.6	3.6
circular-polarised	7.2	3.6

Table 5.8 Summary of the theoretical polarised gain values for the doped capillary tubes

This model holds well for the largest, 530 μm, capillary tube: the s-polarised g_x (or s' component) was the strongest measured, at 6.6 cm^{-1} for example at 3 mW pump power, when compared to the 10.8 cm^{-1} for the theoretical model. However, when the capillary diameter decreases, the model deviates slightly from the measured results. It should be remembered that the theoretical values presented are purely an estimate. The inherent error in calculating the exciting energy, which is the ratio of peak power to pump area, in particular is difficult to estimate. Due to the high level of scattering and the relative size of the pump beam and the capillary diameter, not all of the power emitted from the laser is absorbed. However, the model does indicate the effect that the polarisation state has on the amplification of the device, namely that the s- and circular-polarised beams generally have the higher gain values. The p-polarisation state, for the s' and p' components (g_x and g_y), remain similar in value.

5.6 Summary

The polarised emission of the laser beam is very important in fundamental science and real-life applications. In this work, the polarised stimulated emission was generated by adjusting the polarisation state of the pump beam. The polarisation direction within the

pump beam profile is orientated by way of a waveplate, whereby the direction of the oscillating electric field is altered. A strong dependence of the intensity of the light emitted from the filled micro-capillaries on the polarisation conditions was observed, primarily for s-polarised and positively circular-polarised pumping. The polarised components, i.e. the s' and p' components can be controlled very well by the pump polarisation status. The effect of these changes in the polarisation condition on the optical gain was measured.

As discussed in section 5.1, it has been theorised that the absorption and emission properties of a material usually depend greatly on the polarisation properties of the beam profile. This chapter has shown the dependence of the Rhodamine 590 dye molecule on the polarisation conditions, including the emission characteristics and the gain coefficients. By altering the polarisation of the beam, the emission and amplification properties of these dye filled micro-capillaries can be adjusted and optimised for the requirements of its application.

5.7 References

1. Reyzer, K.C. and L.W. Casperson, *Journal of Applied Physics*, 1980. **51**(12): p. 6083-6090.
2. Brachat, P. and J.M. Baracco, *IEEE Transactions on Antennas and Propagation*, 1995. **43**(7): p. 738-742.
3. Backman, V., R. Gurjar, K. Badizadegan, L. Itzkan, R.R. Dasari, L.T. Perelman, and M.S. Feld, *IEEE Journal of Selected Topics in Quantum Electronics*, 1999. **5**(4): p. 1019-1026.
4. Kurtsiefer, C., P. Zarda, M. Halder, H. Weinfurter, P.M. Gorman, P.R. Tapster, and J.G. Rarity, *Nature*, 2002. **419**(6906): p. 450-450.
5. Rodgers, A., *Polarization in Optical Fibers*. 2008, London: Artech House.
6. Duarte, F.J. and L.W. Hillman, *Dye laser principles : with applications*. Quantum electronics. principles and applications. 1990, Boston ; London Academic Press.
7. Schäfer, F.P. and K.H. Drexhage, *Dye lasers*. 2nd rev. ed. ed. Topics in applied physics ; vol.1. 1977, Berlin ; New York: Springer.
8. Reyzer, K.C. and L.W. Casperson, *Journal of Applied Physics*, 1980. **51**(12): p. 6075-6082.
9. Wang, J. and K.Y. Wong, *Applied Physics B-Lasers and Optics*, 2007. **87**(4): p. 685-691.
10. Lahoz, F., C.J. Oton, N. Capuj, M. Ferrer-Gonzalez, S. Cheylan, and D. Navarro-Urrios, *Optics Express*, 2009. **17**(19): p. 16766-16775.
11. McGehee, M.D., R. Gupta, S. Veenstra, E.K. Miller, M.A. Diaz-Garcia, and A.J. Heeger, *Physical Review B*, 1998. **58**(11): p. 7035-7039.
12. Fang, H.H., J. Yang, R. Ding, Qi-Dai, C. Lei, W.H. Xia, J. Feng, Y.G. Ma, and H.B. Sun, *Applied Physics Letters*, 2010. **97**(101101).
13. Yamao, T., T. Ohira, S. Ota, and S. Hotta, *Journal of Applied Physics*, 2007. **101**(8).
14. He, G.S., L.S. Tan, Q. Zheng, and P.N. Prasad, *Chemical Reviews*, 2008. **108**(4): p. 1245-1330.
15. Marshall, C.D., J.A. Speth, S.A. Payne, W.F. Krupke, G.J. Quarles, V. Castillo, and B.H.T. Chai, *Journal of the Optical Society of America B-Optical Physics*, 1994. **11**(10): p. 2054-2065.

Chapter 6

Dye Micro-Amplifiers Incorporating Micro-Scatterers

6.1 Introduction

In this chapter, a series of micro-scatter incorporated dye micro-amplifiers were developed. To effectively disperse the micro-scatters, polyvinylpyrrolidone (PVP) was chosen to be combined with the Rhodamine 590 solutions. The role of the polymer is to prevent possible aggregation and to change the refractive index of the active medium within the micro-capillaries without affecting the dye molecules. As discussed in Chapter 3, for solid state dye devices, a polymer is often added to the active medium in order to act as a host to the dye molecules, protecting the active media from aggregation and photodegradation effects as the material is pumped with a laser. Subsequently polystyrene micro-spheres were added to the Rhodamine 590 solutions. As will be discussed later in further detail, it has been theorised that the addition of micro-scatterers to the gain medium can have a beneficial scattering effect [1]. Lastly, the effects of changing the polarisation conditions of the pump beam were also investigated.

6.2 Theory

6.2.1 Scattering Incorporated Lasing Behaviour

The behaviour of light waves in disordered structures is highly complex, yet disordered materials are familiar to us all, i.e. substances that look white, such as white paint, fog, milk, etc., all contain scattering media.

Light scattering had been considered detrimental to laser devices because it alters the direction and the spatial coherence of photons [2]. However, the possibility of generating amplified light by a random scattering medium with gain was first suggested theoretically in the 1960's by Letokhov [1]. He predicted that the combination of multiple scattering of light that takes place in a disordered material does not really provide a feedback mechanism, but causes the path length of the emission to increase significantly for the amplification to become efficient. This multiple scattering is completely random, hence

the term 'random laser' is used. Further theoretical work by Ambartsumyan et al. indicated that the radiative properties of atomic or molecular systems may be altered significantly in the presence of a coherent optical scattering [3, 4]. In 1993 N. M. Lawandy [5] and N. B. Lawandy [6] observed strong emission from pumped organic dyes in colloidal solutions of suspended titania micro-particles.

While any scattering of light by particles is detrimental to the operation of regular laser systems, in the case of random lasers it is the condition which provides the possibility of gain [3]. Multiple elastic scattering of fluorescence from micro-particle ensembles have been shown to provide an efficient way of increasing the optical path length, which, if the gain exceeds losses, leads to light amplification within the excited volume [7-9]. The effect observed, described by the term 'random laser', points to the randomness of the scattering particles distribution within the system and the fact that, on pumping, the emitted radiation exhibits certain characteristics of laser action, such as spectral narrowing and threshold gain behaviour. In some cases direct lasing modes in the emission spectra have been observed [8-10].

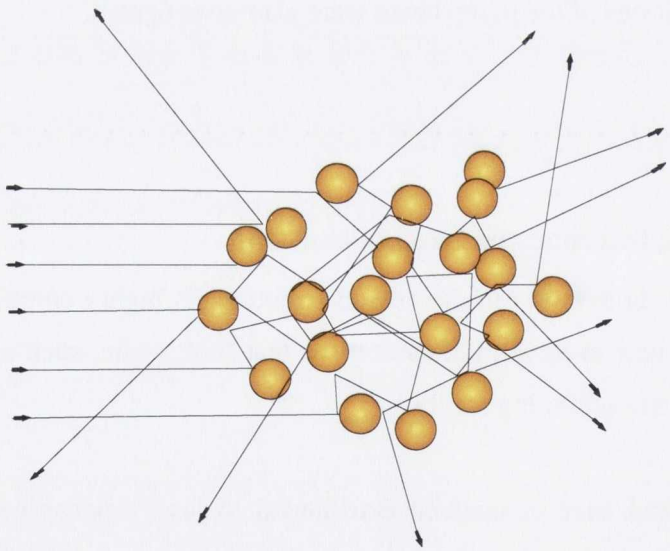

Figure 6.1 Schematic of the scattering effects of micro-spheres on the pump beam

It should be noted that research by Ahmed et al. has shown that there are no interactions between the dye molecules and the scatterers in random lasing media [10]. This is

important as it is the effects of the micro-scatterers on the emission properties of the system, and not any possible molecular interaction, which is of interest.

6.2.2 Mie Scattering

The theoretical analysis of scattering from spherical particles of any size was first published by Gustave Mie in 1908. It is a solution of Maxwell's equations for the scattering of electromagnetic radiation by spherical particles. Mie scattering can be used when dealing with both absorbing and non-absorbing particles, has no size limitations and can describe non-spherical particles. Rayleigh scattering is the small-size limiting case of Mie Scattering.

The light scattering cross-section of an individual dielectric sphere, σ_s, suspended in a homogeneous medium can be expressed as [3, 11-13]

$$\sigma_{sc} = \frac{\lambda_1^2}{2\pi}\sum_{n=1}^{\infty}(2n+1)(|a_n|^2 + |b_n|^2) \qquad (6.1)$$

where n is a positive integer and a_n and b_n are two complex coefficients defined by

$$a_n = (-1)^{n+1/2}\frac{S_n(\alpha)S_n'(\beta) - mS_n(\beta)S_n'(\alpha)}{S_n'(\beta)\phi_n(\alpha) - mS_n(\beta)\phi_n'(\alpha)}$$

$$b_n = (-1)^{n+3/2}\frac{mS_n(\alpha)S_n'(\beta) - S_n(\beta)S_n'(\alpha)}{mS_n'(\beta)\phi_n(\alpha) - S_n(\beta)\phi_n'(\alpha)} \qquad (6.2)$$

The term $m=n_2/n_1$, where n_1 and n_2 are the refractive indices of the surrounding medium and the sphere, respectively. The function, S_n and ϕ_n, can be described as

$$S_n = \left(\frac{\pi z}{2}\right)^{1/2} J_{n+1/2}(z)$$

$$S_n'(z) = \frac{\partial S_n(z)}{\partial z}$$

$$\phi_n = S_n(z) + i\left[(-1)^n\left(\frac{\pi z}{2}\right)^{1/2} J_{-n-1/2}\right](z) \qquad (6.3)$$

$$\phi_n'(z) = \frac{\partial \phi_n(z)}{\partial z}$$

where $J_{n+1/2}(z)$ and $J_{-n-1/2}(z)$ are Bessel functions of half-integral order, r is the radius of the sphere, $\lambda_1=\lambda_0/n_1$ is the wavelength of the incident beam in the surrounding medium and λ_0 is the wavelength of the incident beam in a vacuum. The z-component can be divided into α and β terms, whereby

$$\alpha = \frac{2\pi r}{\lambda_1} \ , \ \beta = m\alpha \qquad (6.4)$$

Based on Eq.s 6.1 to 6.4, it can be seen that the scattering cross section is a function of the wavelength, micro-scatterer radius and respective refractive indices of the scatterers and the surrounding system.

He et al. continue on from this theory, in order to describe the angular distribution of scattering light intensity that is dependent on the polarisation of the incident light beam [11]. The scattering angle θ is defined by the angle between the direction of propagation of the incident beam and the direction of the observed scattering beam. For simplicity, it is assumed that the incident beam is a linearly polarised light with the electric field vector perpendicular to the observation plane. The angular distribution of the scattering intensity from a sphere is described as

$$i_1 = \left| \sum_{n=1}^{\infty} \frac{2n+1}{n(n+1)} (a_n \pi_n + b_n \tau_n) \right|^2 \qquad (6.5)$$

where a_n and b_n are two complex coefficients. While

$$\pi_n = \frac{dP_n}{dx} \ , \ \pi_n' = \frac{d^2 P_n}{dx^2}, \qquad \tau_n = \pi_n x - (1-x^2)\pi_n' \qquad (6.6)$$

where P_n is the Legendre polynomial of degree n and $x=cos(\pi-\theta)$. If the electric field vector of the incident linearly polarised beam is parallel to the observation plane, the angular distribution can be described as

$$i_2 = \left| \sum_{n=1}^{\infty} \frac{2n+1}{n(n+1)} (a_n \tau_n + b_n \pi_n) \right|^2 \qquad (6.7)$$

In other words, it is expected that the state of polarisation of the scattering beam affects the scattered emission intensity.

6.2.3 Diffusion Theory

The distance traversed by the photon in a random medium can be approximated by the diffusion theory, as theorised by Letokhov [1]. For a disordered gain medium, the path length of light is vastly increased as a result of multiple scattering, and a large amplification is achieved. In essence, this is light diffusion with gain. This results in a drastic change in the emission properties of the gain medium.

A cloud of scattering particles submerged in an amplifying medium can be described as a type of a laser with non-resonant feedback. Other such media include; scattering surfaces and mirrors and dielectric rods containing active material. If the scattering mean free path of a photon is larger than the wavelength, the propagation of light can be described as a diffusion process [16, 17]. In other words, the amplification, which is stronger than the loss, is enhanced by the induced stimulated emission. This can be shown by taking a selection of identical dielectric particles with an average number per unit volume N_0. The free path of a photon, Λ_s, due to scattering is described by [4]

$$\Lambda_s = \frac{1}{\sigma_{sc} N_0} \qquad (6.8)$$

where σ_{sc} is the scattering cross-section. The amplification increases exponentially with the total distance travelled by the lasing photon in the gain medium [12]. This distance is determined by the photon transport mean free path, which is inversely proportional to the scatterer density. The amplification is also determined by the spatial distribution and the population inversion of the dye in the medium. This spatial gain distribution is determined by the transport mean free path and the absorption length of the excitation photon in the medium and by the saturation absorption of the dye. The results estimated for the system used in this work indicate that mean free path is larger than the wavelength and are presented in Appendix I.

6.2.4 Applications

In a recent paper by Yang et al., the potential of using microsphere-doped cavities as optical sensors for concentration-based detection in chemical or biomolecular systems is described [13]. Beckering et al. found that the introduction of scatterers into neat dye solutions leads to a significant change in the observed emission spectra [2]. They reported that the specific wavelength of operation, depending on the shape and size, makes the

miniature random laser suitable for the encoded marking of documents or materials (but invisible to the human eye).

The so-called 'random lasers' have several interesting features that cannot be achieved with common bulk or fibre lasers, such as simultaneous emission of several different wavelengths at the same time and emission at new extremely low gain lines [14]. They also permit miniaturization and very low cost. They are said to be likely to replace conventional lasers where coherence and linewidth are not important, i.e. where it is merely necessary to have a high intensity light source. The disadvantage of these systems at present is that they need a pump laser to excite the emission.

6.2.5 Review of Micro-Scattering Media

In 1994, N. M. Lawandy et al. observed an increase in the emission linewidths with the addition of TiO_2 colloid micro-scatterers to their samples [5]. This was attributed primarily to scattering enhanced self-absorption by the dye which results in re-emission at a different wavelength. They found that the colloid did not exhibit the strong saturation behaviour that was observed in the pure dye. They also determined a dependence of the peak emission on the pump energy for various nanoparticle densities.

In 1998 Cao et al. reported that the requirements for random laser action were strong scatterers and a gain medium [8]. Many reports, such as this work, involve the scattering clusters acting as both the gain medium and the scattering centres. Cao et al. also found that increasing the ZnO nanoparticle concentration results in a slight but noticeable decrease in the lasing threshold energy density. This is consistent with the increased elastic scattering of light, which is anticipated in more concentrated systems. The threshold for stimulated emission within a random medium is established as a trade-off between optical gain, which is proportional to the excitation volume, and the optical loss.

Kuwatagonokami et al. studied the laser emission of dye-doped polystyrene microspheres and observed laser oscillation only in rather large solid spheres of several millimetres in diameter [15-17]. An enhancement of stimulated emission has also been demonstrated in air-sol microspheres containing luminescent dye molecules [18], based on Purcell's theoretical work [19]. Cerqueira et al. have also presented work discussing the development of random laser based high-power fibre lasers and amplifiers [14, 18, 19].

In 2000, Cao et al. [20] reported on the amplification properties of cuvette-based Rhodamine 640 perchlorate dye and ZnO particles, 100 nm in diameter, in methanol. They showed an amplification of the emitted intensity as the concentration of scatterers was introduced, up to a critical particle density above which the emission decreased. They concluded that, at optimum particle concentrations, due to the fact that the optical scattering increases the path length of the emitted photon inside the gain region, the travelling photon may induce the stimulated emission of a second photon. Later that year they also reported on the fabrication of micro-lasers with disordered semiconductor nanoparticles [21, 22]. Individual ZnO particles, or clusters, of approximately 1.7 μm in diameter, were incorporated into 30 μm thick films and pumped produced an emission that had a FWHM narrowing of 12 to 0.2 nm.

Ling et al. presented a study of random lasers with resonant feedback, using PMMA thin films doped with Rhodamine 640 perchlorate and TiO_2 particles, 400 nm in diameter [21]. They found a lasing threshold dependence on the transport mean free path, pump area and sample size, for such systems. Gross et al. also measured the emission from other dye molecules, such as DCM dye molecules in porous quartz substrates [22]. More recently, in 2006 Psaltis et al. [23] reported on the addition of particles to a fluid, which were significantly smaller in size than the wavelength, can be used to change the refractive index or absorption coefficient of the medium as a whole [3]. They suggested that particles that are significantly larger than the wavelength can be treated as a spherical focusing lens in the medium [24, 25].

6.3 Experimental Procedure

6.3.1 Materials

6.3.1.1 Polyvinyl pyrrolidone (PVP)

In the case of solid-state dye-doped devices, where photodegradation tends to be prevalent, polymers are often added as a 'host' material to prevent this destruction. The polymers provide additional channels to disperse the excess energy, in other words thermal heat, which acts as the destructive force [26]. Hence, the photostability of the device is increased. It is thought that the addition of such a polymer to the dye-doped micro-capillaries could aid in the improvement of the emission properties.

According to Mie theory, the amplitude of the scattered light is related, amongst others, to the refractive index and the size parameter $x = 2\pi r/\lambda$, where r is the radius and λ is the wavelength [27]. This is a further reason to investigate the effects of altering the refractive index values.

The molecular structure of the polymer chosen, PVP $(C_6H_9NO)_n$, can be seen in Fig. 6.2. This polymer is commonly used in many medical, pharmaceutical, commercial applications. However, it was primarily chosen for this work because it dissolves readily in ethanol, up to high concentrations. The addition of PVP allows the Rhodamine 590 solutions in ethanol to remain transparent.

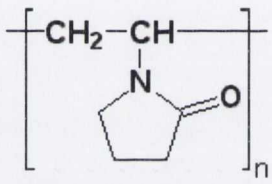

Figure 6.2 Molecular structure of PVP

6.3.1.2 Micro-spheres

Monodisperse polystyrene micro-spheres (MS) were purchased from Polybead in a 2.5 % weight per volume aqueous suspension, with diameters of 0.2 and 0.35 μm. Solutions containing these micro-spheres and the Rhodamine dye solutions were easily prepared. A 10:1 volume ratio of ethanol to micro-spheres was the chosen concentration. When the solution was drop-cast onto a substrate, it is this concentration which yields an 'ideal' close-packed monolayer, as seen in the SEM image below in Fig. 6.3. This indicates that there is a high concentration of micro-spheres within the solution. Therefore, the micro-spheres should be uniformly dispersed in solution. A small amount of a surfactant (400:1 ratio), Triton X, was added to the samples in order to suspend the micro-spheres in solution.

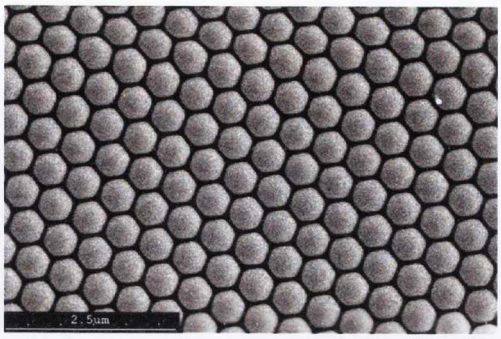

Figure 6.3 SEM image of a drop-cast micro-sphere monolayer (by N. McEvoy)

6.3.2 Device Fabrication

Care was taken to ensure that the concentration of active Rhodamine 590 molecules should remain as constant as possible, for all solutions. Hence, any changes in the properties observed should not be due to the concentration, but the scattering effects due to the PVP or micro-sphere additions. A 20:1 ratio, of dye solution to micro-sphere, was also investigated, but the emission intensities were shown to be much lower than that from the higher concentration. Therefore the 10:1 ratio was the only concentration used for this work.

The addition of the PVP had no effect on the transparency of the Rhodamine 590 solution. However, as would be expected, due to the scattering nature of the particles the addition of the micro-spheres causes the solution to become cloudy.

As with the previous chapter, different filters were used for the three capillary diameters and the pump power was measured at a position just before the sample. The capillary tubes were filled in the same way, as described in Chapter 3.

6.4 Results

6.4.1 Refractive Index Measurements

A refractometer was used to measure the refractive index, n, of the six solutions at 20°C. Should the polymer or micro-sphere addition increase the refractive index, it could aid in the prevention of emission loss, by improving the potential waveguiding effects within the capillary tube.

Solution	Refractive Index
Ethanol	1.36
Rhodamine 590	1.36
+ 50 g/l PVP	1.37
+ 100 g/l PVP	1.38
+ 200 g/l PVP	1.39
0.3 μm MS	1.36
0.3 μm MS + 100g/l PVP	1.38
0.2 μm MS	1.37
0.2 μm MS + 100 g/l PVP	1.38

Table 6.1 Refractive index values for the six Rhodamine 590 – doped solutions

The addition of Rhodamine 590 to ethanol makes no relative difference to the refractive index, which remains at 1.36. The polymer, PVP, which dissolves easily in ethanol, shows a slight increase to 1.38.

According to Polymicro Ltd., the refractive index of the fused silica capillary tubes is wavelength dependent. At 550 nm the refractive index is reported as being 1.46. Ideally, in order for the capillary tubes to sufficiently 'guide' the emission light along the length of the tube, the refractive index for the dye-doped solutions should have a higher value. However, due to the solvent of choice, there are limitations as to what polymers can be dissolved. Hence, these capillaries are said to guide the light in a 'leaky' manner. By adjusting the dye, solvent and polymer used, this 'leaking' issue could be overcome in order to increase the efficiency of the device. However, these measurements are preliminary, and as Rhodamine 590 is known to exhibit strong emission characteristics, it will be continued to be used in this work to further investigate the properties of the micro-capillaries.

6.4.2 PVP Concentration in Rhodamine and Micro-Scatterer Solutions

The concentration of the polymer, PVP, in the Rhodamine sample was investigated in the 530 μm capillary tube only. Three different concentrations: 50, 100 and 200 g/l solutions were measured in the Rhodamine 590 only solution and the 0.3 μm and the 0.2 μm micro-sphere solutions.

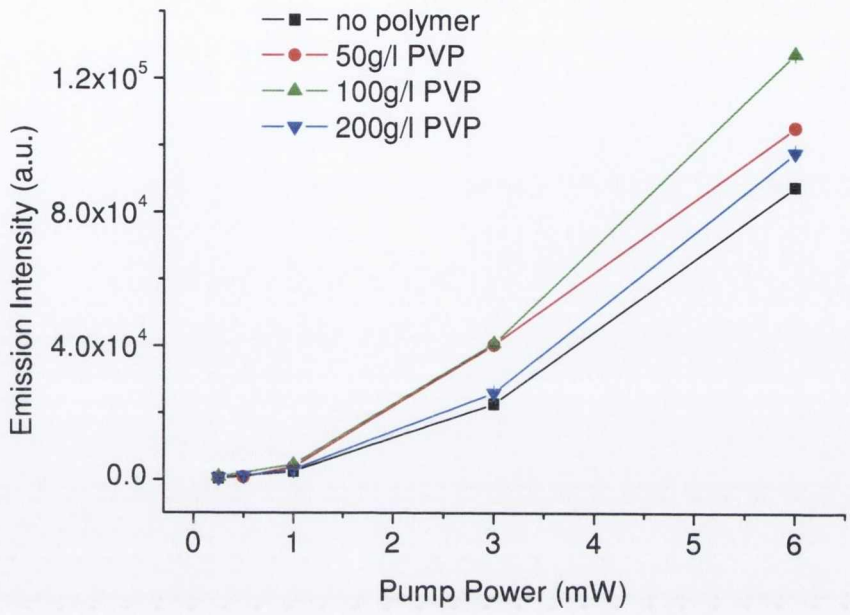

Figure 6.4 Input-output emission intensities of the PVP concentrations in a 530 μm capillary for the 0.3 μm micro-sphere solutions

The above graph is taken as an example of what occurs when different concentrations of PVP are added to the solutions in the capillary tubes. The three concentrations of PVP were added to the Rhodamine 590 and 0.3 μm micro-sphere solution, and placed in a 530 μm capillary tube. The emission intensity from the edge of the tube was measured, as the laser pump power was increased. From Fig. 6.4, it can be seen that there was a notable difference in the output emission properties of the solutions containing PVP. Although the three PVP concentrations have a similar slope, it is the 100 g/l PVP concentration solution that is seen to have improved the emission efficiency, in comparison with the 50g/l and 200 g/l solutions. These results are repeatable, within the standard deviation error bars plotted in Fig. 6.4. The standard deviation is calculated as the square root of the mean value. Potentially, the reason why the 100 g/l PVP solution exhibits superior emission efficiency could be due to the fact there is an optimum viscosity for the system, above which it causes the emission to be quenched.

This 100 g/l concentration of the PVP polymer was chosen for further investigation, as the same intensity-concentration dependence was also observed for the Rhodamine 590 solution and that containing the 0.2 μm microspheres.

6.4.3 Spectroscopic measurements

UV-Vis and PL spectra were taken for the new solutions containing PVP and the micro-scattering spheres and compared directly with the original Rhodamine 590 solution which contains neither.

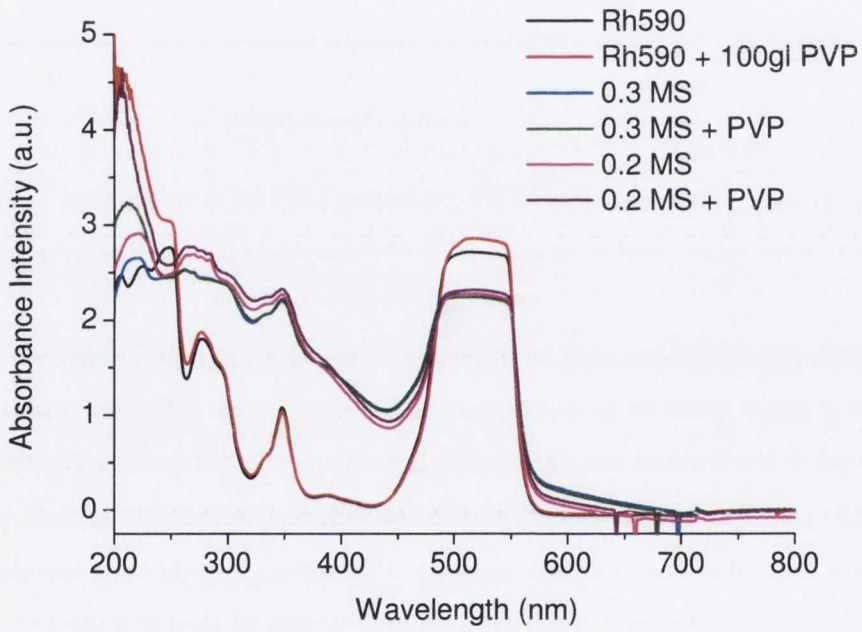

Figure 6.5 UV-Vis absorbance spectra of the six different solutions in a 1 mm glass cuvette

The UV-Vis absorbance spectra in Fig. 6.5 show that all of the six solutions have a strong and broad absorbance band between 490 and 550 nm. The maximum absorbance intensity for each solution is, once again, limited by the apparent saturation of the spectrometer's photodetector, as discussed in Chapter 3. The intensity of the absorbance peak appears to decrease slightly with the micro-sphere addition. However, due to the high concentration of the solutions, the effect that the polymer and micro-sphere additions have on the absorbance intensities cannot be verified.

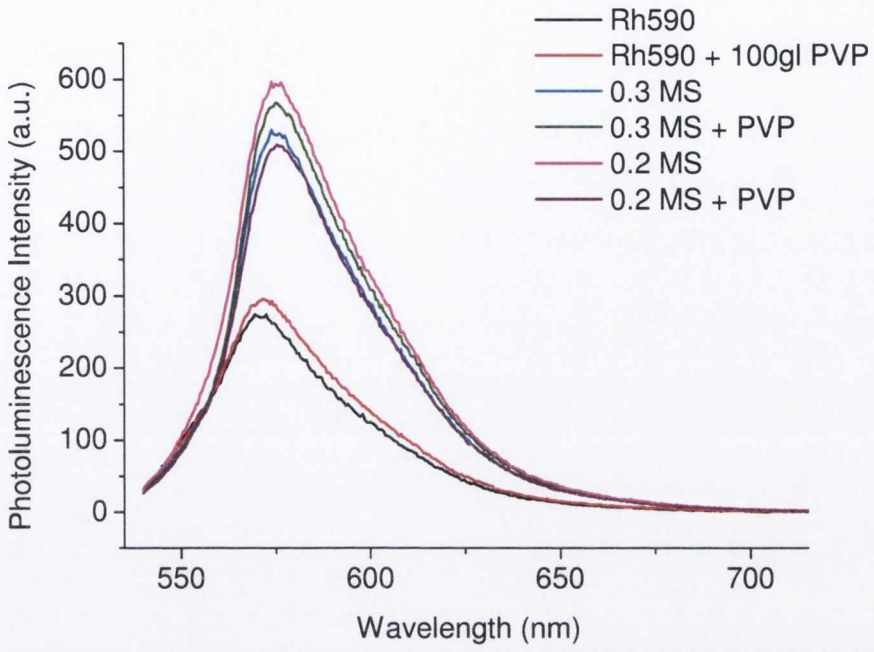

Figure 6.6 Photoluminescence (PL) emission spectra of the six solutions, in 1 mm glass cuvettes

The micro-spheres improve the PL emission intensity as seen in Fig. 6.6. The samples were excited at 532 nm in order to directly compare with the wavelength at which the Nd:YAG laser will emit. It should be noted that a neutral density filter, which allowed only 10 % transmission, was used in order to stop the saturation of the PL. It is seen that all micro-sphere incorporated solutions exhibit enhanced PL efficiency. The improvement of the PL emission can be attributed to the fact that the micro-spheres cause the excitation beam to be scattered, increasing the optical path length, thus enhancing the probability of more interactions occurring [28].

In this case the emission intensity for the Rhodamine sample, with and without PVP, was lower than when the micro-spheres were added. There is a slight shift of the peak wavelength, from 570 nm to 575 nm, with the micro-sphere addition. The 0.2 μm spheres have the highest emission intensity, with the emission intensity decreasing by approximately 90 a.u. with the addition of PVP. From the PL spectra, it is seen that the 0.2 μm micro-sphere solution has the highest efficiency due to its strong scattering and hence enhanced PL emission intensity, in comparison with the other solutions.

6.4.4 Fluorescence Lifetime Measurements

As discussed in Chapter 3, fluorescence lifetime measurements were carried out for each solution. This was done in order to see if the lifetime was affected by the PVP or micro-sphere addition. A slight variation in the lifetime values was observed for each solution. However, they all have an approximate value of 4 ns, which is expected for Rhodamine 590 solutions in ethanol [29].

Solution	Fl. Lifetime (ns)	Standard Error (ns)
Rhodamine 590	4.01	± 0.001
+ PVP	3.84	± 0.002
0.3 μm MS	3.98	± 0.001
0.3 μm MS + PVP	3.91	± 0.001
0.2 μm nm MS	3.97	± 0.001
0.2 μm MS + PVP	4.14	± 0.002

Table 6.2 Summary of fluorescence lifetime measurements for the six solutions

There is no distinct difference between the lifetime measurements of the solutions, as presented in Table 6.2. Any small variation could be attributed to the influence of a certain level of aggregation of the dye molecules, or indeed the different host or scatterer present in the solution. Habuchi et al. noted a decrease in fluorescence lifetime from 2 to 0.3 ns as the diameter of their suspension as micro-droplet diameter was decreased from 20 to 2 μm and as the concentration of Rhodamine 590 was increased [30]. This is a significant decrease in comparison to our results, although the diameters presented in their work are on a much larger scale. For scatterers of approximately the same size as those presented in this work, Schniepp et al. also observed a fluorescence lifetime dependence on the sphere diameter, the smallest of which were 100 nm in size [31]. In the work for this thesis, 8 μl of each solution was used in order to ensure continuity. It can therefore be concluded that the minimal decrease in the lifetime with micro-scatterer addition is due to the slight variations of the micro-scatterer induced environment in each solution.

6.4.5 Emission Properties

The emission properties of the micro-scatterer solutions were measured, when excited with the SHG of the Nd:YAG laser at 532 nm. This was done in order to compare the absorbance, fluorescence and stimulated emission properties of the materials.

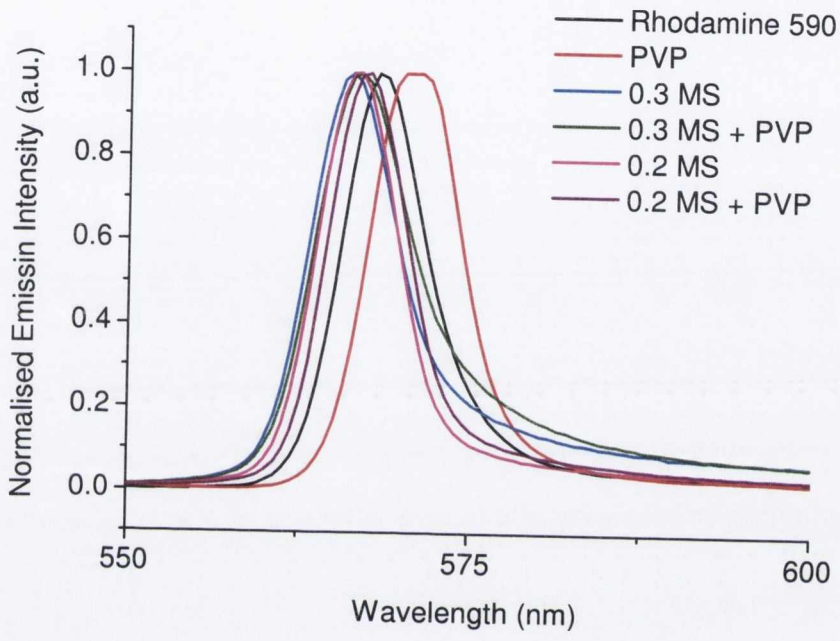

Figure 6.7 Emission intensity versus wavelength for the 530 μm capillary at 3mW

The emission intensity for each solution was normalised in Fig. 6.7 in order to directly compare the effect of the micro-scatterer addition. The emission peaks for the 530 μm capillary at 3mW, for example, exhibit a slight shift in the maximum wavelength with the addition of micro-scatterers to the dye doped solution. The Rhodamine 590 solution has its maximum peak at 567 nm; with the addition of PVP the peak red-shifts to 571.5 nm. The redshift can be qualitatively explained by an enhanced reabsorption of the emitted photons owing to longer paths caused by the scattering [2]. The addition of the scatterers confines light in restricted spatial regions and increases the interaction between light and materials. This increased path length within the gain medium then increases photon absorption and re-emission, causing the redshift [32]. For each micro-sphere solution, the maximum peak is observed to blueshift with respect to the Rhodamine 590 peak, to 566.4 nm. However with the addition of PVP the peak is seen to redshift slightly towards 567 nm. The 100 and 25 μm capillaries exhibit a similar shift with the PVP and micro-

scatterer addition, but with slightly higher wavelength values for the micro-sphere solutions, i.e. 568 nm in comparison to 566.4 nm.

It must be noted that the capillaries are not being directly compared, due to the omission of the neutral density filter for the smallest capillary tube. If a filter had been used for the smallest of diameters, the lowered intensity values would be very difficult to measure, so a good picture of the emission properties of these narrow capillaries could not be determined.

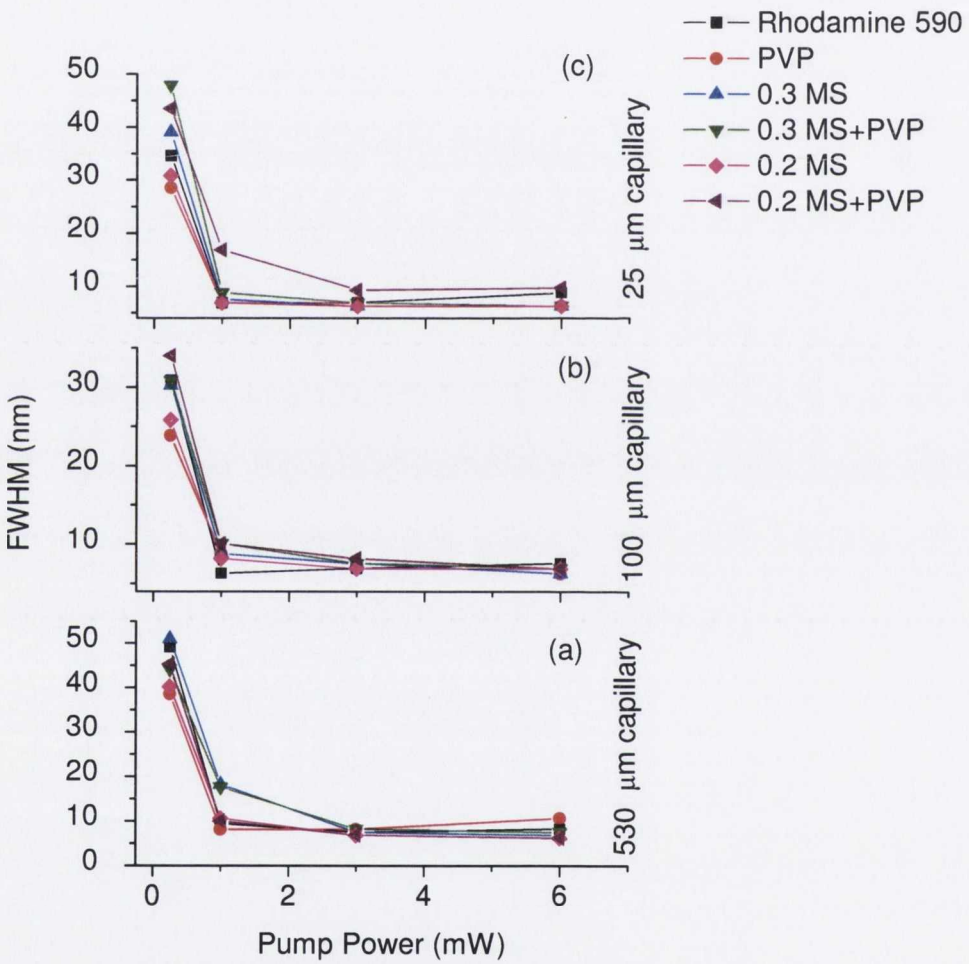

Figure 6.8 Variation in the FWHM with pump power for the 530, 100 and 25 µm capillary tubes

The FWHM data is shown in Fig. 6.8 (a) for the 530 µm capillary tube to see the effects the micro-scatterers have on the FWHM. Strong line narrowing is observed for each Rhodamine 590-based solution, but it is difficult to ascertain any difference between the solutions. Although the PVP solution does have a narrower initial peak at 0.25 mW pump

power, in general, little difference is observed in the narrowing of the emission peak when the micro-scatterers are added to the Rhodamine 590 solution. The strong exponential decrease in the FWHM is an indication of the significant amplifying nature of the dye cavity combination.

For the two smaller capillaries, seen in Fig. 6.8 (b) and (c), a similar pattern to the 530 μm capillary was observed. The 100 μm capillaries had FWHM beginning at 25 to 35 nm at 0.25 mW pump power, whereas the 25 μm capillary, which has no NG filter and hence high efficiency, had FWHM starting at 23 to 47 nm. For each case the PVP solution had the narrowest initial FWHM, and the 0.2 μm micro-sphere and PVP solution appears to have the broadest. Overall, the line-narrowing appears to be slightly improved with the addition of micro-scatterers, an effect which is observed more so in the smaller capillary diameters.

Beckering et al. found that the introduction of TiO_2 scatterers (320 nm diameter) into neat Rhodamine 640 dye solutions lead to a significant change on the observed emission spectra [2]. The intensity of the peak was a factor of 50 higher than for the neat solutions. A collapse of the linewidth from 35 to 3.5 nm at the same threshold was also observed. Similarly, Vishnubhatla et al. determined that the degree to which the FWHM narrowed, was improved with the addition of TiO_2 nanoparticle doped to the micro-fluidic channel [33].

The dye doped micro-scattering amplifiers in this work hold well with these reported results. The line-narrowing of the emission spectra are very similar to the literature findings. In 1999, Zacharakis et al. reported on the narrowing effects of scatterers on the spectral width of organic dyes in PMMA films. Polystyrene particles, 400 nm in diameter, were added to solutions containing Rhodamine 101, 6G and DCM dyes and made into thin films [34]. The films exhibited FWHM line narrowing to less than 10 nm and threshold values varied between 10 – 20 μJ. Comparatively speaking the narrowing of our dye-doped micro-amplifiers is strong, especially as the maximum power used was 6 mW (or 3 mJ/cm^2). Lawandy et al., for example, also reported on the dependence of the initial broad emission linewidth on the density of particles present in solution [35]. The initial peak broadened as the number of scatterers was increased. For all solutions, the linewidth narrowed to the same approximate width, independent of scatterer.

The main differences with the work in this thesis is that while the emission properties of micro-capillaries were investigated, the authors listed above used 10 mm thick glass cuvette cells. Therefore, the fact that our results hold well with those containing a much greater number of active molecules is encouraging. The ability to measure strong line-narrowing from the micro-scale capillary tubes is promising for potential future micro-fluidic applications.

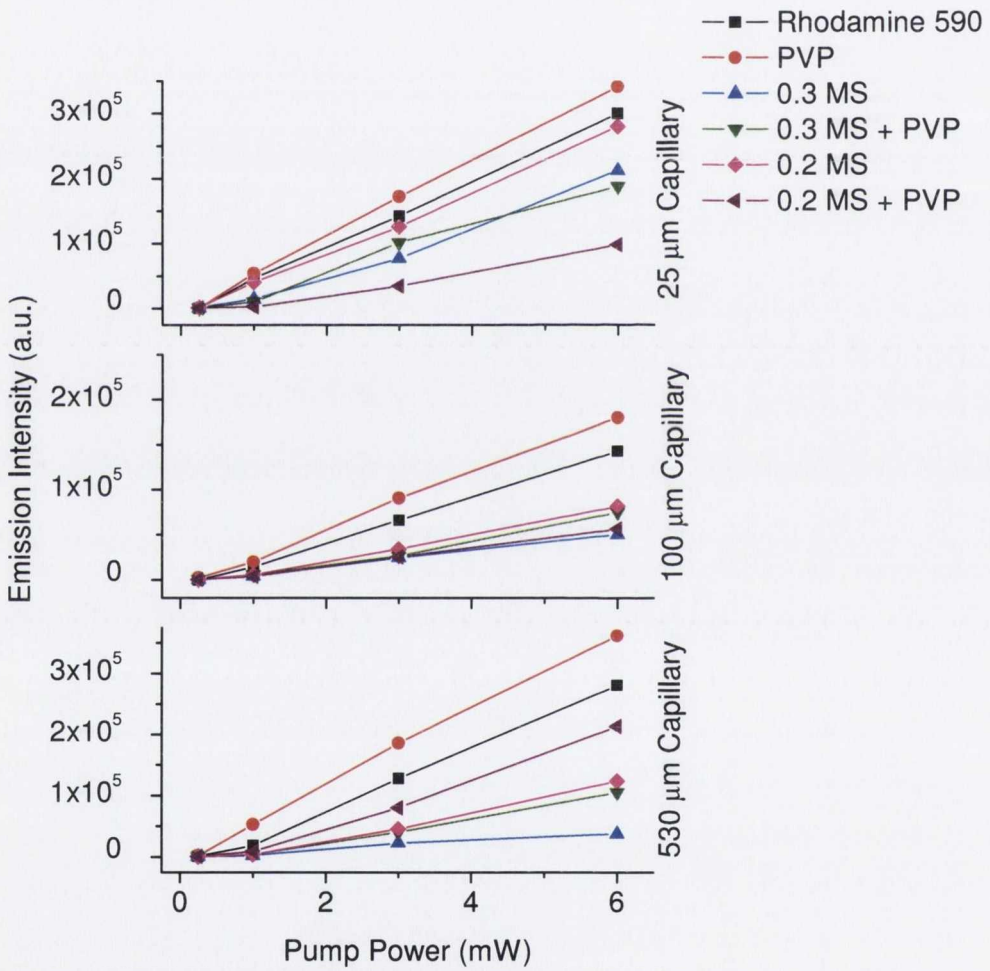

Figure 6.9 Input-output emission data of the different dye mixtures for the three capillary tubes

The output emission intensity graphs are quite similar for all three capillary diameters; however a slight difference in the maximum intensity values (or spread) does occur. This divergence in the emission as the pump power is increased is evident in Fig. 6.9. The intensity spread is broader for the 530 µm capillary, but decreases with the tube diameter.

In other words, as the volumes decrease, they tend towards having more similar output emission properties.

The emission intensity, in general for all three capillaries, is at a slightly higher maximum peak wavelength for the PVP addition, at 571 nm, compared to 568 nm for the other five solutions. This was first observed in Fig. 6.7. For the 100 μm capillary tubes, the peak shift with the PVP solution also observed, although this shift is less than what was seen with the 530 μm capillary tubes. The 25 μm amplifier, has no NG filter in place, so realistically, the 530 and 100 μm capillary emission data is 27 % higher in intensity than the smallest diameter. It once again shows that the PVP and Rhodamine 590 solutions have the highest slope efficiency. The two 0.2 μm micro-sphere solutions do appear to have a higher efficiency than in the previous capillaries. However, the 530 μm diameter capillary has the overall highest emission efficiency.

This observed improvement of emission intensity has been reported [35]. However, many reports find that a critical concentration of scatterers exists, after which the emission begins to decrease [8, 20]. If the concentration is too large, it will not only decrease the number density of dye molecule, but will also attenuate the emission intensity. Although the micro-sphere concentration has not been optimised in this work, it would be interesting to compare a solution containing a much lower concentration of scatterers.

In general, the PVP solution shows an improvement in the slope efficiency for the micro-amplifiers containing micro-spheres. However, the neat Rhodamine 590 solutions do exhibit the highest exponential increase in emission intensity. This could be due to the fact that the micro-spheres occupy too much space in the capillary, decreasing the number of dye molecules present, or the fact that the number density of the dye molecules within the capillaries has decreased. This could be the case in this work, as the larger 0.3 μm diameter micro-sphere solutions exhibit the smallest slope. For example, in the 530 μm capillary tube, the number of Rhodamine 590 molecules in a 25 mm length of tubing has approximately 1.59×10^{21} molecules. However, when the 0.3 μm micro-spheres are added, due to the extra volume they take up, the number of Rhodamine 590 molecules decreases by approximately 2×10^{18} active molecules (i.e. a decrease of 0.14 %). Similarly, for the 0.2 μm micro-spheres, the number of Rhodamine molecules is reduced to approximately 1.58×10^{21} molecules, which is a decrease of 0.6 %. This reduction, in

particular for the 0.3 μm spheres, could account for the decrease in the output emission properties. Similar decreases are observed for the two smaller capillary tubes: the 100 μm tubes have a 0.18 and 0.14 % decrease for the 0.3 and 0.2 μm microspheres, respectively; as with the 25 μm tubes which decrease by 0.37 and 0.17 %, respectively.

However, as discussed in Chapter 4, the number density of active dye molecules was shown to have little effect on the emission properties as the capillary diameter decreases when normalised with respect to the overlap of the area of the laser beam. In this chapter, the capillary diameters are treated as separate entities, due to the fact that a neutral density filter is used for the larger sizes.

6.4.6 ASE Pump Power Threshold

As described in Chapter 4, the ASE pump power threshold can be estimated for each solution containing PVP and micro-scatterers. The results are listed in the table below.

	Pump Power Threshold (mW)		
Solutions	530 μm capillary – NG 4 filter	100 μm capillary – NG 4 filter	25 μm capillary – no NG filter
Rhodamine 590	0.84	0.61	0.67
+100g/l PVP	0.63	0.48	0.57
+ 0.3 μm MS	0.99	0.65	0.72
+ 0.3 μm + PVP	0.96	0.67	0.79
+ 0.2 μm MS	0.79	0.52	0.61
+ 0.2 μm + PVP	0.81	0.71	0.78

Table 6.3 ASE pump power threshold values for the different solutions and capillary diameters

These calculations indicate that there is an increase in the threshold for ASE pump power as the micro-scatterers are added to the solutions. In general, as the capillary tube diameter decreases, so does the value for the ASE threshold. The 25 μm doped amplifiers have quite high threshold vales, compared to those of the larger diameter tubes. This is even though the error inherent in the narrow tubes, due to the quality of the emission intensity is much more of a factor (even with no NG filter in place). For the Rhodamine 590 solution, the threshold value decreased significantly when the PVP was added. In

general, the threshold for ASE is just below 1 mW, so the VSL method will be used to measure the gain coefficients above 1 mW pump power.

Due to the relatively low comparable threshold values, it can be concluded that amplification should be achievable, as above the threshold values, the stimulated emission should be strong enough to produce non-negligible amplification. Therefore, there is enough evidence to warrant further investigation into these micro-amplifiers which contain micro-spheres.

These values compare well with those in the literature, for example, Fujiwara et al. reported on a lasing threshold of 7 mW, for Rhodamine-doped PMMA micro-spheres 28 μm in diameter [36].

6.4.7 Gain Results

The variable stripe length method (VSL) was implemented in order to obtain the optical gain of dye-doped micro-capillaries with and without the addition of a polymer and micro-scatterers.

6.4.7.1 530 μm Capillary Tube

A summary of the gain coefficients is listed below, for pump powers ranging from 1 mW, which is just above the ASE pump power threshold, to 3 mW.

	1mW	3mW
Rhodamine 590	6.8 ± 0.2	7.3 ± 0.3
PVP only	5.8 ± 0.2	6.1 ± 0.3
0.3 μm MS	3.6 ± 0.2	4.1 ± 0.3
0.3 μm MS + PVP	2.9 ± 0.3	4.0 ± 0.4
0.2 μm MS	4.2 ± 0.3	4.3 ± 0.4
0.2 μm MS + PVP	3.8 ± 0.2	4.3 ± 0.4

Table 6.4 Unsaturated gain values (cm^{-1}) for 530 μm capillary tubes

The results in Table 6.4 show how the unsaturated gain coefficients vary as the properties of the solution are changed. The Rhodamine 590 amplifier has the highest gain value, 7.3 cm^{-1}, at 3 mW pump power. The PVP solution has a value which is a little lower, 6.1 cm^{-1}, while the micro-sphere solutions all have similar gain values, of approximately 4 cm^{-1}. This decrease in the gain values is more than likely due to the decrease in the number density of Rhodamine 590 molecules present, due to the micro-sphere volume, as previously discussed. Losses due to the increased scattering are likely to have also contributed to the decreased value. The degree of amplification is therefore variable, depending on whether or not the polymer or micro-scatterers are added into the device. However, even with the addition of the micro-scatterers, the gain coefficients are still the same order of magnitude as the Rhodamine 590 only solution. The standard error for the micro-sphere gain measurements are listed beside the gain values in Table 6.4.

	1mW	3mW
Rhodamine 590	4.6 ± 0.4	4.8 ± 0.5
PVP only	3.0 ± 0.4	3.5 ± 0.5
0.3 μm MS	1.1 ± 0.5	1.6 ± 0.8
0.3 μm MS + PVP	0.5 ± 0.5	1.8 ± 0.8
0.2 μm MS	1.7 ± 0.7	2.5 ± 1.0
0.2 μm MS + PVP	0.7 ± 0.4	2.2 ± 1.0

Table 6.5 Saturated gain values (cm^{-1}) for 530 μm capillary tubes

Table 6.5 lists the saturated model gain values for the 530 μm amplifier. For the Rhodamine 590 and PVP solutions, the VSL data is more easily fitted for the saturated gain values than for the micro-scatterer-doped solutions. The saturated gain values are very small, and do not give a good indication of the amplifying ability of these dyed-doped micro-amplifiers. The experimental error due to the increased scattering of the emission intensities and the fact that this model is only suitable for values of $gl > 4$ means that the saturated model is unsuitable for fitting such data sets.

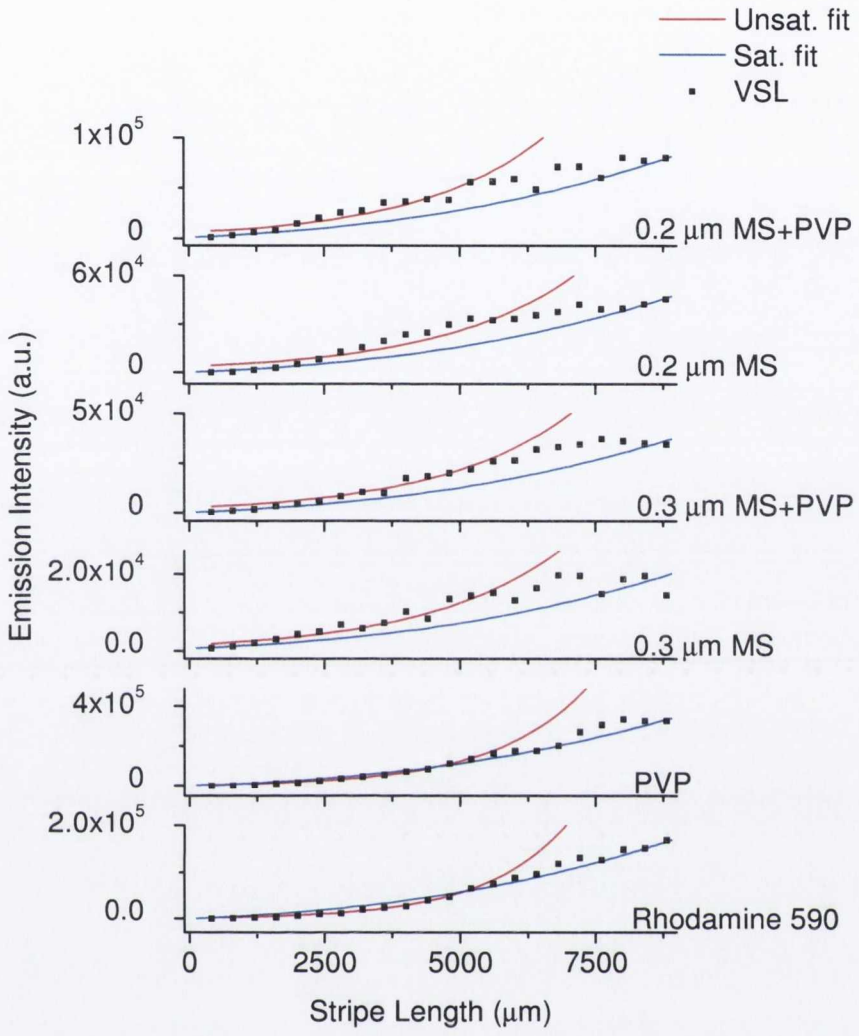

Figure 6.10 Fitted unsaturated and saturated gain models for the 530 μm capillary tube at 3 mW

As observed in Fig. 6.10, the saturated model does not fit easily to the VSL data for the solutions containing micro-scatterers, due to the fact that $gl \approx 4$ (c.f. Chapter 4) for these micro-sphere solution doped amplifiers.

6.4.7.2 100 μm Capillary Tube

In a similar manner as described in the previous section, the emission intensities for the 100 μm diameter capillary tubes follow the same pattern as before, whereby the PVP solution has the largest emission intensity and the micro-spheres only have the lowest intensity values.

	Unsaturated	Saturated
Rhodamine 590	5.8 ± 0.2	3.3 ± 0.8
PVP only	5.1 ± 0.3	2.5 ± 0.9
0.3 μm MS	4.4 ± 0.4	3.5 ± 1.0
0.3 μm MS + PVP	4.5 ± 0.4	3.7 ± 1.1
0.2 μm MS	4.0 ± 0.4	1.2 ± 0.7
0.2 μm MS + PVP	4.6 ± 0.4	3.9 ± 0.9

Table 6.6 Unsaturated and saturated gain values (cm^{-1}) for 100 μm capillary tube at 3 mW pump power

The unsaturated gain coefficients in Table 6.6 again have approximately the same values as for the 530 μm tubes. The Rhodamine 590 solution exhibits the strongest amplification, with an unsaturated gain value of 5.8 cm^{-1} at 3 mW pump power. The next most efficient amplifier is the PVP solution, with a gain of 5.1 cm^{-1}. Once again, the remaining four micro-sphere solution additions had the lowest unsaturated gain values of between 4.0 and 4.6 cm^{-1} at this particular pump intensity. As seen in the above table, relatively speaking, there is less of a difference between the intensity increases for these measurements. In each case, the addition of PVP to the micro-sphere solutions had a small increase in the gain values, of approximately 0.1 – 0.6 (± 0.2) cm^{-1}.

The gain values calculated using the saturated fitting model are also presented in Table 6.6 at 3 mW pump power. As previously determined, this model is more suitable for larger capillary diameters and higher pump powers. The saturated gain values calculated are very low, in comparison to the unsaturated model, and the error values are much higher.

6.4.7.3 25 μm Capillary Tube

The smallest 25 μm diameter capillary tube was also used to measure the effect of micro-sphere addition on the amplification properties.

	Unsaturated	Saturated
Rhodamine 590	4.0 ± 0.2	1.3 ± 0.5
PVP only	4.2 ± 0.3	1.0 ± 0.4
0.3 μm MS	4.5 ± 0.3	0.3 ± 0.6
0.3 μm MS + PVP	4.3 ± 0.3	1.0 ± 0.5
0.2 μm MS	3.8 ± 0.4	1.0 ± 0.3
0.2 μm MS + PVP	3.6 ± 0.4	0.2 ± 0.3

Table 6.7 Unsaturated and saturated gain values (cm^{-1}) for 25 μm capillary tube at 3 mW pump power

The unsaturated gain values for the small capillary diameter are smaller than those for the larger capillaries, primarily for the Rhodamine 590 and PVP solutions. However, unlike the larger capillaries, the gain values for the micro-sphere solutions are comparatively much stronger than previously measured. They exhibit a greater similarity to the first two solutions which, thus far, have shown a greater level of amplification. However, the addition of the PVP to the micro-spheres does not appear to have a positive effect on the gain coefficients, as was observed for the 100 μm diameter capillary. This increase could be attributed to the greater level of confinement within the narrowest capillary. When combined with the induced scattering caused by the micro-spheres, an enhancement of the amplification properties is observed.

6.4.7.4 Discussion - Gain

To summarise, the 100 g/l PVP solution showed the highest output emission intensity, yet the Rhodamine 590 solution still gave the highest gain value. The introduction of the polystyrene micro-spheres does affect the emission properties of the dye-filled micro-capillaries. For the two largest diameters the gain value decreases slightly when compared to the neat Rhodamine 590 solution filled capillaries. However, when the capillary diameter is significantly decreased to 25 μm, an improvement in the unsaturated gain values occurs. This indicates that these narrow capillaries enhance the amplification of light when micro-scatterers are added to them, due to the greater confinement.

In section 6.4.5, the issue of the decrease in the number of Rhodamine 590 molecules, due to the volume taken up by the micro-spheres, was discussed. The fact that gain is achieved, although considerably smaller when compared to those without any volume

loss due to the micro-scatterer addition, indicates that the doped capillary tubes exhibit strong amplification properties. For example, with the 0.3 μm micro-sphere solution in a 530 μm capillary, the number of active molecules decreased by 0.14 %, however the level of amplification decreased by approximately 54 % when compared directly with the Rhodamine 590–only solution. The decrease in the number of dye molecules cannot completely be attributed to this decrease in the amplification. Therefore, there must be other contributory factors, such as an increase in the loss due to the enhanced scattering caused by the presence of the micro-spheres. However, for the relative size and volume of Rhodamine 590 used, the actual observation of gain is encouraging. It should be noted that the results are repeatable, and those presented here are a representative of what occurs when the micro-capillary tubes are doped with PVP and micro-spheres.

Author	Material	Pump Power	Gain Results	Ref.
Kyhm et al.	CdSe in toluene	at 50 μJ/pulse	0.15 cm^{-1}	[37]
Al-shamiri et al.	Rhodamine B doped sol-gel rods (d = 8 mm)	at 5mJ	4.3 - 7.6 cm^{-1}	[38]
Cao et al.	ZnO polycrystalline films on fused silica substrates	at 2 $\mu J/cm^2$	over 100 cm^{-1}	[8]
Cao et al.	ZnO powder films (100 nm) on ITO glass	over 736 kW/cm^2	20 cm^{-1}	[9]
van Soest et al.	TiO_2 (d = 220 nm) in Sulforhodamine B	at 9 mJ	77 cm^{-1}	[39]
This work	Rhodamine 590, PVP and MS (0.2-0.3 μm) micro-capillary tubes	at 3 mW	3.8-7.3 cm^{-1}	

Table 6.8 Summary of literature gain results in similar scattering materials

Much of the reported literature, where lasing was observed from micro-spheres, deals with the spheres being doped during preparation with dye molecules [15], unlike the method presented in this work, in which the solution itself is doped. Table 6.8 lists some of the gain values reported in literature for micro-scattering systems. The most comparable results, as an example, are those of Al-shamiri et al. where Rhodamine B doped sol-gel rods, 8 mm in diameter, reported gain values of between 4.3 and 7.6 cm^{-1} for pump energies of approximately 5 mJ [38]. Although these results require higher pump energies and are in the solid-state, the micro-scattered doped amplifiers reported in this work compare well as less dye molecules are used at lower pump powers. To

compare with liquid-phase results directly: van Soest et al. measured strong amplification for micro-scatterer suspensions in 1 cm sample cells. They report very high gain values of 77 cm^{-1} but at higher pump energies than is achievable with our system [39]. In general, the micro-scatterer doped amplifiers presented in this thesis are comparable or an improvement on similar devices described in the literature.

6.4.8 Polarisation Results

In Chapter 5, the effects of changing the pump polarisation conditions were investigated, and it was concluded that the emission properties were dependent on the state of polarisation of the pump laser beam. The same experiment was carried out in order to see how the addition of the micro-scatterers to the Rhodamine 590 doped micro-amplifiers is affected. The effect of polarised scattering particles has been investigated, both theoretically by Holland et al. [40], and experimentally by Bridge et al. [41], as examples.

6.4.8.1 Emission Properties

The emission from each capillary tube diameter and each dye solution does vary as the polarisation pump conditions are changed. In general, the p-polarisation has the lowest intensity, followed by circular-polarised and the s-polarised condition.

The peak wavelength values do not vary as the polarisation conditions are changed, only when the solution in question is. This wavelength dependence on the conditions of the micro-sphere solution was discussed in section 6.4.5.

6.4.8.2 Degree of Polarisation

The degree of polarisation, as seen in Chapter 5, can be calculated from the s' and p' components of the polarised beam, inputted into Eq. 5.8. As such, the results are listed below in Table 6.9.

Sample	Capillary (μm)	s-polarised	circular-polarised	p-polarised
PVP	530	0.50	0.33	0.04
	100	0.87	0.59	0.13
	25	0.66	0.68	0.12
0.3 μm MS	530	0.48	0.41	0.04
	100	0.17	0.24	0.07
	25	0.50	0.31	0.14
0.3 μm MS + PVP	530	0.43	0.27	0.06
	100	0.10	0.06	0.03
	25	0.32	0.20	0.15
0.2 μm MS	530	0.32	0.35	0.06
	100	0.21	0.12	0.06
	25	0.40	0.32	0.01
0.2 μm MS + PVP	530	0.36	0.40	0.06
	100	0.14	0.20	0.02
	25	0.11	0.20	0.07

Table 6.9 Degree of polarisation for the six solutions at 3mW pump power

The Rhodamine 590 DOP results are listed in Chapter 5. As previously discussed, when the DOP is equal to zero, the light is said to be unpolarised, whereas when it equals a value of one it is said to be completely polarised. In general, the s-polarised condition has a greater degree of polarisation than the circularly-polarised. The outcome that the p-polarised condition has the lowest degree of polarisation, practically unpolarised, has not changed with the micro-scatterer addition. For each micro-amplifier however, the degree of polarisation is notably less than what was recorded for the Rhodamine 590 solution. The exception is the PVP solution, for the 100 and 25 μm amplifiers, which show an increase of approximately 70 % in the DOP. When the micro-spheres are added the degree of polarisation does decrease significantly in value.

6.4.8.3 Polarisation Gain Results

The unsaturated gain coefficients are measured using the VSL method and fitted using Eq. 4.6, for each capillary diameter.

		PVP (cm^{-1})	0.3 μm MS (cm^{-1})	0.3 μm MS+PVP (cm^{-1})	0.2 μm MS (cm^{-1})	0.2 μm MS+PVP (cm^{-1})
s-polarised	s'	5.4	5.2	4.6	4.3	4.6
	p'	5.2	4.4	3.3	3.5	4.2
p-polarised	s'	6.0	4.8	3.3	3.4	4.0
	p'	5.9	4.3	3.7	3.4	3.9
circular-polarised	s'	5.8	3.7	4.2	3.8	5.8
	p'	4.8	3.1	3.1	3.3	2.5

Table 6.10 Polarised unsaturated gain coefficient at 3mW for the 530 μm capillary tube (NG 4 filter)

Table 6.10 shows a variation in the gain coefficient, as both the contents of the amplifier and the polarisation state of the pump beam is changed. In general, and as observed in the previous sections, little difference in the gain values is measured for the micro-sphere solutions, which are lower than their Rhodamine 590 and PVP doped equivalents. The same conclusions can be drawn for the 100 μm doped amplifier, whose results are tabulated in Table 6.12.

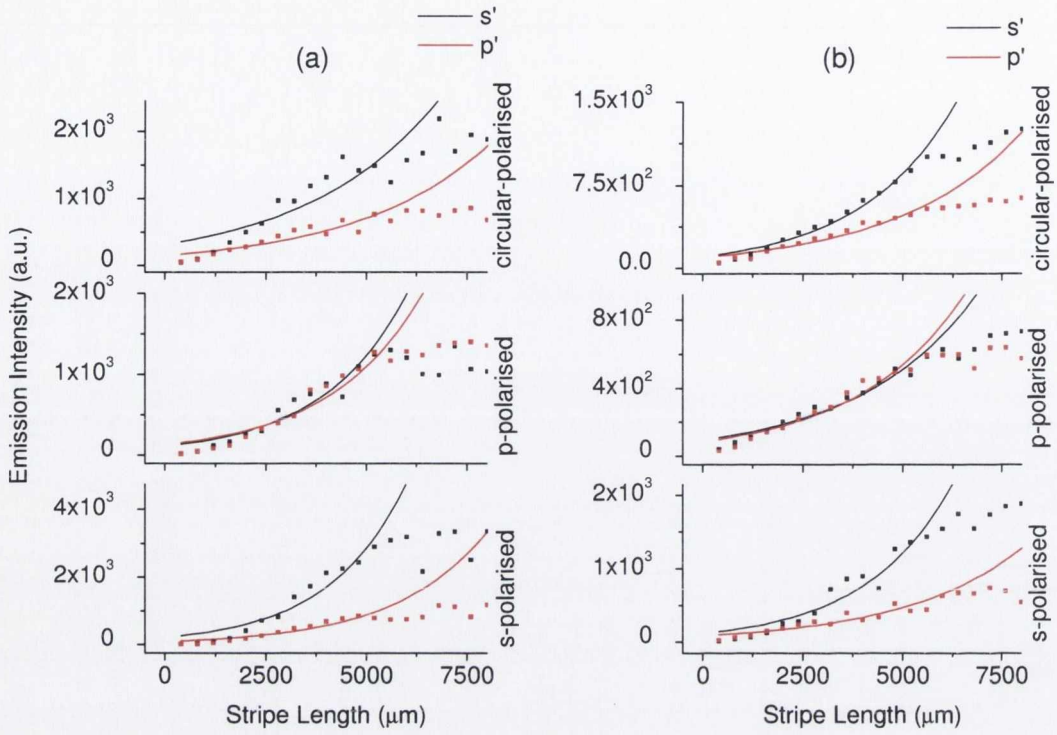

Figure 6.11 Unsaturated fit model for changing polarisation conditions of VSL data for (a) 0.3 μm micro-sphere and (b) 0.3 μm microsphere and PVP solution doped 530 μm capillary at 3mW

The unsaturated gain fitting model for each state of polarisation is plotted in Fig. 6.11, as an example of the variation in the amplification for each condition of the pump beam. The line signifies the unsaturated fitting and the point signifies the VSL data. The Rhodamine 590 gain values are presented in Chapter 5, therefore only the 0.3 μm micro-sphere solutions are presented here for the 3 mW pump power, as an example. The micro-spheres scatter the incident polarised light (i.e. the orientation of the electric field of the scattered radiation follows the dipole pattern), as described by Mie Theory, which results in a level of 'depolarisation' of the polarised light. As a result, the pump beam becomes less polarised and hence the ASE emission is less polarised in comparison to those capillaries containing no micro-scatterers. This accounts for the decrease in the DOP observed in Table 6.9.

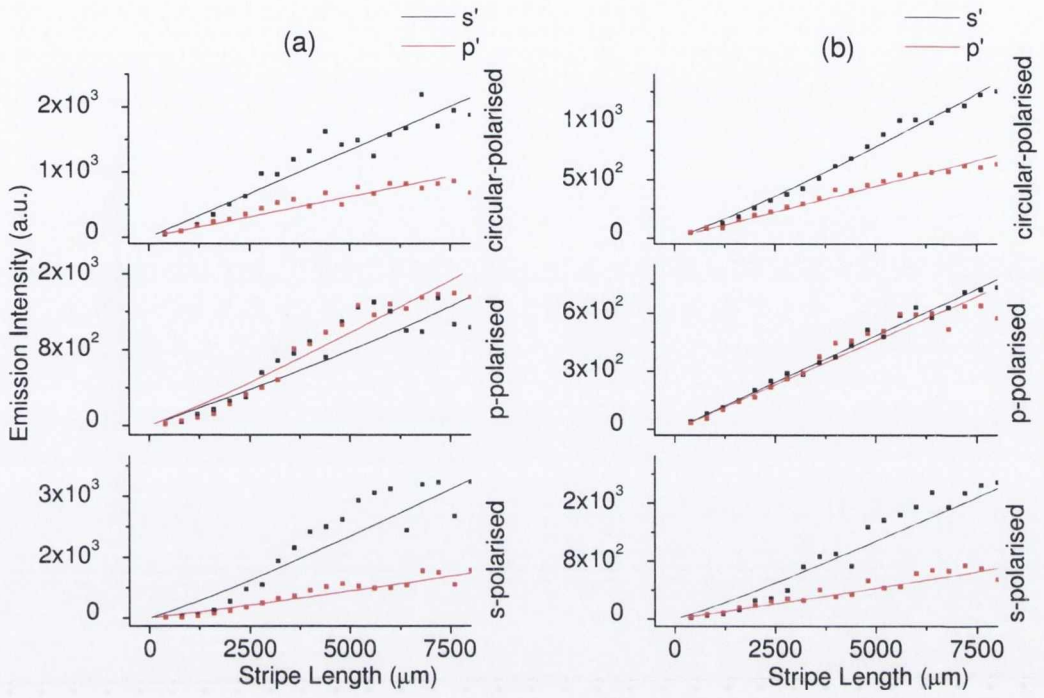

Figure 6.12 Saturated model for changing polarisation conditions of VSL data for (a) 0.3 μm micro-sphere and (b) 0.3 μm micro-sphere and PVP solution in a 530 μm capillary tube at 3 mW

		PVP (cm^{-1})	0.3 μm MS (cm^{-1})	0.3 μm MS+PVP (cm^{-1})	0.2 μm MS (cm^{-1})	0.2 μm MS+PVP (cm^{-1})
s-polarised	s'	2.6	2.8	2.5	2.0	1.3
	p'	2.6	2.1	1.9	1.3	0.9
p-polarised	s'	3.3	2.3	1.6	0.8	0.9
	p'	3.0	2.6	1.6	0.9	0.8
circular-polarised	s'	2.8	2.2	1.7	1.5	1.9
	p'	2.0	1.7	1.8	0.7	1.5

Table 6.11 Polarised saturated gain coefficient at 3mW for the 530 μm capillary tube (NG 4 filter)

In order to compare the polarised gain results, the saturated fitting model is presented in Fig. 6.12 and Table 6.11 for the 530 μm capillary tube at 3 mW pump power. The saturated model clearly does not fit the data points well, as seen in Fig. 6.12, especially when compared to the unsaturated model fitting in Fig. 6.11. The saturated gain values

are much lower than the unsaturated model equivalent values: the gain coefficient results are so low that they are almost at the limitation of the smallest gain values measurable using the VSL method. This further strengthens the argument previously discussed, that the saturated fitting model is suitable for gain coefficient values above approximately 4 cm^{-1}. The apparent saturation of the data points in Fig. 6.11 could be due to a number of factors, including increased errors due to the addition of the micro-scatterers, loss of solution within the capillary due to solvent evaporation or a level of photodegredation of the active dye molecules.

		PVP (cm^{-1})	0.3 μm MS (cm^{-1})	0.3 μm MS+PVP (cm^{-1})	0.2 μm MS (cm^{-1})	0.2 μm MS+PVP (cm^{-1})
s-polarised	s'	6.9	4.1	4.0	3.4	3.8
	p'	5.4	3.6	3.4	2.5	3.7
p-polarised	s'	4.2	3.5	3.5	3.2	3.7
	p'	6.0	3.6	3.9	3.0	3.5
circular-polarised	s'	7.1	3.9	3.6	3.2	4.2
	p'	3.7	3.3	3.5	3.6	4.7

Table 6.12 Polarised unsaturated gain values at 3mW for 100 μm capillary (NG 4 filter)

		PVP (cm^{-1})	0.3 μm MS (cm^{-1})	0.3 μm MS+PVP (cm^{-1})	0.2 μm MS (cm^{-1})	0.2 μm MS+PVP (cm^{-1})
s-polarised	s'	7.7	3.6	6.4	3.3	7.2
	p'	6.3	3.9	6.2	3.5	8.3
p-polarised	s'	9.4	3.6	6.1	4.1	5.9
	p'	8.6	4.3	5.9	3.6	7.9
circular-polarised	s'	11.3	3.5	5.6	3.6	5.8
	p'	7.7	5.7	5.4	4.0	5.3

Table 6.13 Polarised unsaturated gain values for 25 μm capillary tube at 3mW (no NG filter)

The polarisation study for the micro-scatterer doped 25 μm amplifier exhibits a greater spread in the measured amplification values. For the PVP solution, it appears to exhibit a

larger gain coefficient than the Rhodamine 590 equivalent, for all polarisation conditions. Although the inherent experimental errors are larger for the small capillaries, the greater level of confinement within the 25 μm tube could act favourably and cause the increase in the amplification of the pump beam. The 0.2 μm microsphere and PVP solution has the highest exponential increase in emission intensity as the stripe length was increased. This doped amplifier indicated the highest level of amplification, with a gain of 8.3 cm^{-1}, for s-polarised light.

Generally, a smaller variation is observed in the magnitude of the gain values when the state of polarisation is adjusted. The micro-sphere doped solutions do show an increase in the level of amplification, with the addition of PVP when compared to the solutions without any polymer.

6.4.8.4 Polarisation Summary

The effect of the polarisation of the pump beam appears to be dependent on the diameter of the amplifier. For the larger amplifiers, 530 and 100 μm, the s- and circular-polarised beams show stronger emission intensities and gain coefficients than the p-polarised beam, as discussed in Chapter 5. However, varying the polarisation conditions appears to have only a small effect on the gain values measured for the micro-scattering solutions. The scattering intensity, and angular distribution thereof, is dependent on the state of polarisation of the incident beam, as determined by He et al. [11]. The addition of the micro-spheres causes a level of 'depolarisation' due to Mie scattering. Solutions containing the micro-spheres have similar gain values, which are only slightly changed with the polarisation state.

However, for the 25 μm tubes, the changing of the pump conditions appears to increase the gain. The increase in the level of amplification is greatest for those solutions containing the PVP. As discussed, due to the greater degree of confinement within this narrow capillary, the small increase in the refractive index could have a bigger role to play and hence cause the higher gain value.

6.5 Summary

To summarise, with the addition of PVP and the 0.3 and 0.2 μm microspheres to the Rhodamine 590 solution, the refractive index of the solutions is slightly increased, and it is observed that the PL emission intensity is improved for the micro-sphere solutions.

The fluorescence lifetime and ASE pump power thresholds remain relatively unchanged with the micro-scatterer addition as the threshold for all solutions remains under 0.9 mW. The emission properties of the doped micro-amplifiers do, however, show a level of variation. For the two larger diameter devices, the PVP and Rhodamine 590 solutions have the highest emission efficiency. As the capillary diameter decreases to 25 μm, less of a difference in the efficiencies is observed. This could be due to the greater confinement which is not affected, to the same extent, by the scattering effects as the diameter is decreased. The same diameter dependence is observed in the values for the gain coefficient. Rhodamine 590 shows the strongest level of amplification, while the PVP is marginally less so. The micro-sphere solutions, for the 530 μm diameter, exhibit an approximate drop in amplification of 30 % when compared to the PVP doped equivalent. Overall, the addition of micro-spheres to the Rhodamine 590 doped micro-capillaries causes a slight decrease in the amplification performance of the micro-capillaries. However, when the diameter decreases, the gain values are virtually unaffected by the micro-scatterer addition. For example, with the 25 μm amplifier at 3 mW, those with and without micro-spheres or PVP all have a gain coefficient of approximately 4 cm^{-1}. Overall, the micro-scatterers do affect the emission properties of the dye-doped micro-amplifiers, in a similar manner to what has been reported in literature.

The polarisation study shows, as in Chapter 5, that the emission properties do depend on the polarisation condition of the pump beam. The s- and circular-polarised conditions have a higher efficiency, and greater degree of polarisation, than the p-polarisation equivalent. For the larger capillaries, 530 and 100 μm, the gain values are highest for the Rhodamine 590-only and PVP solutions. However, as the amplifier diameter is decreased to 25 μm, the polarisation conditions, as well as the micro-sphere or PVP dopants, have a greater effect on the amplification of the device.

References

1. Letokhov, V.S., *Soviet Physics Jetp-Ussr*, 1968. **26**(4): p. 835-840.
2. Beckering, G., S.J. Zilker, and D. Haarer, *Optics Letters*, 1997. **22**(18): p. 1427-1429.
3. Hulst, H.C.v.d., *Light Scattering by Small Particles*. 1981, New York : Dover ; London Constable.
4. Ambartsumyan, R.V., N.G. Basoc, D.G. kryukov, and V.S. Letokhov, *Non-Resonant feedback in lasers* ed. J.H. Sanders and K.W. Stevens. Vol. Quantum Electronics. 1970, Oxford: Pergamon.
5. Lawandy, N.M., R.M. Balachandran, A.S.L. Gomes, and E. Sauvain, *Nature*, 1994. **369**(6478): p. 340-340.
6. Lawandy, N.B., *Photonics Spectra*, 1994(July): p. 119-125.
7. Wiersma, D.S. and A. Lagendijk, *Physical Review E*, 1996. **54**(4): p. 4256-4265.
8. Cao, H., Y.G. Zhao, H.C. Ong, S.T. Ho, J.Y. Dai, J.Y. Wu, and R.P.H. Chang, *Applied Physics Letters*, 1998. **73**(25): p. 3656-3658.
9. Cao, H., Y.G. Zhao, S.T. Ho, E.W. Seelig, Q.H. Wang, and R.P.H. Chang, *Physical Review Letters*, 1999. **82**(11): p. 2278-2281.
10. Ahmed, S.A., Z.W. Zang, K.M. Yoo, M.A. Ali, and R.R. Alfano, *Applied Optics*, 1994. **33**(13): p. 2746-2750.
11. He, G.S., H.Y. Qin, and Q. Zheng, *Journal of Applied Physics*, 2009. **105**(2).
12. Zhang, W., N. Cue, and K.M. Yoo, *Optics Letters*, 1995. **20**(9): p. 1023-1025.
13. Yang, J. and L.J. Guo, *IEEE Journal of Selected Topics in Quantum Electronics*, 2006. **12**(1): p. 143-147.
14. de Matos, C.J.S., L.D.S. Menezes, A.M. Brito-Silva, M.A.M. Gamez, A.S.L. Gomes, and C.B. De Araujo, *Physical Review Letters*, 2007. **99**(15).
15. Kuwatagonokami, M., K. Takeda, H. Yasuda, and K. Ema, *Japanese Journal of Applied Physics Part 2-Letters*, 1992. **31**(2A): p. L99-L101.
16. Garrett, C.G., W. Kaiser, and W.L. Bond, *Physical Review*, 1961. **1**(6): p. 1807-&.
17. Baer, T., *Optics Letters*, 1987. **12**(6): p. 392-394.
18. Campillo, A.J., J.D. Eversole, and H.B. Lin, *Physical Review Letters*, 1991. **67**(4): p. 437-440.
19. Purcell, E.M., *Physical Review*, 1946. **69**(11-1): p. 681-681.
20. Cao, H., J.Y. Xu, S.H. Chang, and S.T. Ho, *Physical Review E*, 2000. **61**(2): p. 1985-1989.
21. Ling, Y., H. Cao, A.L. Burin, M.A. Ratner, C. Liu, and R.P.H. Chang, *Physical Review A*, 2001. **6406**(6).
22. Gross, E., D. Kovalev, N. Kunzner, J. Diener, F. Koch, and M. Fujii, *Physical Review Letters*, 2002. **89**(26).
23. Psaltis, D., S.R. Quake, and C.H. Yang, *Nature*, 2006. **442**(7101): p. 381-386.
24. Domachuk, P., M. Cronin-Golomb, B.J. Eggleton, S. Mutzenich, G. Rosengarten, and A. Mitchell, *Optics Express*, 2005. **13**(19): p. 7265-7275.
25. Brody, J.P. and S.R. Quake, *Applied Physics Letters*, 1999. **74**(1): p. 144-146.
26. Arbeloa, F.L., T.L. Arbeloa, I.L. Arbeloa, A. Costela, I. GarciaMoreno, J.M. Figuera, F. AmatGuerri, and R. Sastre, *Applied Physics B-Lasers and Optics*, 1997. **64**(6): p. 651-657.
27. Hulst, H.C.v.d., *Multiple Scattering: Tables, Formulas and Applications*. 1980, New York, London: Academic Press.
28. Bernards D. A., M.G.G., *Organic semiconductors in sensor applications*. 2008, Berlin Heidelberg New York: Springer.

29. Magde, D., R. Wong, and P.G. Seybold, *Photochemistry and Photobiology*, 2002. **75**(4): p. 327-334.
30. Habuchi, S., H.B. Kim, and N. Kitamura, *Journal of Photochemistry and Photobiology a-Chemistry*, 2000. **133**(3): p. 189-196.
31. Schniepp, H. and V. Sandoghdar, *Physical Review Letters*, 2002. **89**(25).
32. Totsuka, K., M.A.I. Talukder, M. Matsumoto, and M. Tomita, *Physical Review B*, 1999. **59**(1): p. 50-53.
33. Vishnubhatla, K.C., J. Clark, G. Lanzani, R. Ramponi, R. Osellame, and T. Virgili, *Applied Optics*, 2009. **48**(31): p. G114-G118.
34. Zacharakis, G., G. Heliotis, G. Filippidis, D. Anglos, and T.G. Papazoglou, *Applied Optics*, 1999. **38**(28): p. 6087-6092.
35. Lawandy, N.M., R.M. Balachandran, A.S.L. Gomes, and E. Sauvain, *Nature*, 1994. **368**(6470): p. 436-438.
36. Fujiwara, H. and K. Sasaki, *Japanese Journal of Applied Physics Part 1-Regular Papers Short Notes & Review Papers*, 1999. **38**(9A): p. 5101-5104.
37. Kyhm, K., S.M. Kim, J.H. Kim, B.J. Kim, H.H. Lim, K.S. Hong, M.S. Cha, and H.S. Yang, *Journal of Luminescence*, 2007. **122**: p. 808-811.
38. Al-Shamiri, H.A.S., I.M. Azzouz, M.S. Shafik, and Y.A. Badr, *Journal of Sol-Gel Science and Technology*, 2007. **41**(1): p. 65-69.
39. van Soest, G., M. Tomita, and A. Lagendijk, *Optics Letters*, 1999. **24**(5): p. 306-308.
40. Holland, A.C. and G. Gagne, *Applied Optics*, 1970. **9**(5): p. 1113-1121.
41. Bridge, N.J. and Buckingh.Ad, *Proceedings of the Royal Society of London Series a-Mathematical and Physical Sciences*, 1966. **295**(1442): p. 334-349.

Chapter 7

Photonic Crystal Fibre Amplifiers

7.1 Introduction

Dye doped micro-capillaries have been shown to exhibit good emission and gain coefficient values, the properties of which can be varied with the addition of micro-scatterers. In this chapter, the micro-capillary tubing used thus far was replaced with a hollow-core photonic crystal fibre (PCF). A series of gain media were employed for modifying the micro-amplifier performance, such as dye solutions containing polymers and micro-scatterers. The gain characteristics were measured using the VSL technique and the polarisation properties were also studied. These PCF micro-amplifiers provide new opportunities for the development of novel light source for fibre optical communications, biomarkers and "lab-on-a-chip" systems [1-3].

7.2 Theory

Conventional optical fibres guide light along their length by total internal reflection (TIR), which requires that the core have a higher refractive index than the cladding [4]. The only losses which occur are due to the intrinsic absorption and scattering losses within the materials themselves. Since no solid cladding material exists which has a refractive index lower than that of air, light cannot normally be guided along an air hole [5].

In 1991, Phillip Russell proposed that light could be trapped inside a hollow fibre core by creating a periodic wavelength-scale lattice of microscopic holes in the cladding glass [6]. It was known as a photonic crystal fibre (PCF). Photonic crystals were originally introduced in the context of controlling spontaneous emission of atoms [7]. PCFs are optical fibres which have a built-in microstructure, usually consisting of a periodic array of small air holes in glass. It is these small and closely spaced holes, which travel along the length of the fibre, which provide the waveguiding properties. They offer many degrees of freedom in their design in order to achieve a variety of properties, depending

on the different possible arrangements of the holes. This makes them interesting and flexible for a wide range of applications.

PCFs are generally divided into two main categories. The first are known as Index Guiding fibres that have a solid core (Fig. 7.1 (a)) which generally guide light by TIR. The second category comprises the Photonic Bandgap (PBG) fibres or air guiding fibres, which have periodic micro-structured elements and a core of low index material, e.g. a hollow core (Fig. 7.1 (b)). Typically, for this latter type of PCF, TIR is not possible due to the fact that the cladding refractive index (silica and air) is higher than the core index [8, 9]. In very basic terms, the fabrication technique involves the drawing-out of stacked fused capillary tubes, until the desired diameter is obtained [10].

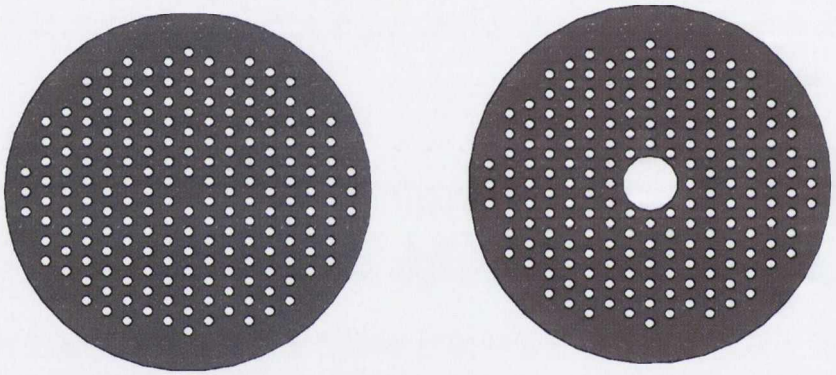

Figure 7.1 *The two different types of PCFs commercially available: (a) index guiding and (b) hollow-core photonic bandgap fibres*

PBG fibres were developed by Cregan et al. in 1999, whereby the light is guided, without leakage, in the hollow core [11]. The highly periodic structure of air holes in the cladding of the fibre creates a photonic bandgap. The theory behind this mechanism is that the light, in certain well-defined wavelength bands, is trapped in the air by the PBG of the cladding, instead of by TIR [12, 13]. In other words, by surrounding the air hole with a photonic crystal, frequency ranges corresponding to the band gap of the crystal would be confined within, and guided along the air core [12]. In contrast to index-guiding fibres, it is not required that the refractive index of the core region be larger than the index of the cladding. The fibre only guides in a limited and relatively narrow wavelength region, outside of which the fibre core is anti-guiding.

7.2.1 Photonic Bandgap Effect

In the photonic crystal material, the photonic bandgap structure is analogous to the electronic band structure of a real crystal of atoms, and shows the relation between the particle's energy, i.e. the photon's energy, and its momentum in a given direction [7, 13]. The periodicity and effective refractive index of photonic crystals gives them this optical bandgap, at which they are reflective [14, 15]. The effective index can be thought of as the average index in the fibre cladding which is dependent on the propagation of the light within the medium.

A straightforward way of describing the effect of a photonic bandgap is through Fermi's golden rule [16]. Consider spontaneous emission, whereby an electron drops from a filled upper level to an empty lower level with the emission of a photon. The downward transition rate ω between the filled and empty atomic level is given by

$$\omega = \frac{2\pi}{\hbar}|V|^2 \rho(E) \qquad (7.1)$$

where $|V|^2$ is the matrix element and $\rho(E)$ is the final density of states per unit energy. In spontaneous emission, the final density of states is the density of the optical modes available to the emitted photon. If there is no optical mode available, there will be no spontaneous emission.

PBG materials possess one or more photonic stop bands with respect to frequency [17]. Such a picture reveals bands of photon energies separated by gaps which can help predict the emission directions of the output laser beams. Wavelengths that lie within the band gap are forbidden from propagating through the material, allowing PBG structures to be employed in the application of filtering as well as confinement, such as planar waveguides and photonic crystal fibres. Through changing the structure of the PCF, the bandgap can be changed, hence creating a shift in transmission and reflectance [18].

The microscopic and atomic structure of the channel itself plays a much greater role in micro-fluidic flow than it does in the larger capillary-based micro-amplifiers. In this work, when fluid is introduced, a lot of the features of the spectrum are expected to become attenuated due to the lowered index contrast between the PBG material and the surrounding silica. As the fluid refractive index is altered, a change in the features is observed.

7.2.2 Review of Photonic Crystal Fibres

Since the development of PCFs, much has been reported in literature in recent years. As discussed, PCFs have confinement characteristics which are not possible in conventional optical fibres. Stimulated emission has been reported in hollow core fibres containing photo-pumped colloidal suspensions of TiO_2 nanoparticles and laser dyes and interpreted as either random lasing or ASE [19-25].

Porous opal photonic crystals, which have a periodic array structure filled with solutions of various laser dyes have also been studied, where the photonic bandgap formation was suppressed due to the face-centred cubic structure of the opal lattice [26]. It has been proven that spatially periodic dielectric structures have photonic stop bands, i.e. energy bands with a practically zero light transmission, in certain directions in the crystal lattice [27, 28]. More recently, Puzzo et al. demonstrated lasing from one-dimensional photonic crystals, consisting of films of alternating SiO_2 and TiO_2 nanoparticles [29].

The use of liquid PCFs, through the addition of liquid crystals and photonic crystals, was proposed by Busch and John in 1999 [30]. They have demonstrated that a tunable PBG material can be established by introducing optically birefringent aligned liquid crystal into the void regions of an inverse opal PBG material. Liquid PCFs, the concept of which was first introduced by Eggleton et al. in 2001 [31], were successfully fabricated by Larsen et al. in 2003 [32].

The prospect of using of PCFs as amplifiers has been recently reported in the literature. In 2006, Roy et al. described the possibility of using PCFs as lasers and amplifiers. They discussed that an attractive feature of the PCF is the likelihood to efficiently guide light in a low-index medium, such as ethanol, in order to realise waveguides with low-index-liquid cores [33]. In 2007 de Matos et al. investigated the lasing properties of Rhodamine 6G doped TiO_2 particles (250 nm) inserted into the hollow core of a PCF (10 μm diameter), which involved selective filling techniques, using a modified syringe [34]. They observed stronger FWHM narrowing with the addition of micro-scatterers to the solution. They reported that such behaviour indicates that the threshold is not only a result of spectral narrowing, but also of the existence of directionality in the emission

above threshold. They describe how a PCF is a confining waveguide, and because of this the random lasing action is more efficient than in similar bulk formats.

Vasdekis et al. demonstrated the possibility of compact fluidic fibre lasers based on capillary tubes (2 μm) and solid core photonic crystal fibres (3.68 μm) [35]. Toluene and Perylene Red dye were used to fill the two fibres, referred to as single and multi-channel fibres which were longitudinally pumped (i.e. 'end-on'). Line narrowing was observed, as was threshold behaviour from the input-output emission intensities, which was higher for the single-channel fibres. They suggested these devices can be used for optofluidic sensing and spectroscopy applications. However, in much of the work reported in the literature the fabrication of these micro-laser devices requires expensive state-of-the-art crystal growth and micro-fabrication facilities. In this thesis, we propose a straightforward filling and fabrication process.

7.2.3 Potential Applications and Advantages

PCFs can demonstrate superior guiding properties and have been touted as having the potential to outperform conventional fibres in many areas such as telecommunications [9]. The many advantages of PCFs, over other optical fibres, include selectivity of wavelength, effective modification of spontaneous emission and better directionality; therefore, an enhanced optical yield and hence low threshold are expected [28-31]. Photonic Crystal Fibres (PCF) can provide characteristics that ordinary optical fibres do not exhibit, such as single mode operation from the UV to IR with large mode-field diameters, highly nonlinear performances for super continuum generation, optimized dispersion properties, and air core guidance, amongst others. They have been fabricated using, for example, rare-earth doped rods as the core, as fibre lasers and amplifiers [9, 36, 37], as distributed feedback lasers [38, 39] and also as sensors [40, 41]. The air-guiding hollow-core fibres in particular exhibit substantially higher damage thresholds than conventional fibres, making them suitable for delivery of high-power beams for laser machining and welding [42]. It has been shown that hollow-core fibres filled with hydrogen can act as a cell for stimulating Raman scattering experiments [43]. Optical localisation due to light scattering in randomly scattering amplifying media has already been shown to result in optical gain enhancement [30-34]. They have been an attractive medium for the study of nonlinear optical phenomena in gas phase materials [43]. They provide an excellent platform for the infiltration of liquid phase materials and the

construction of micro-fluidic photonic devices such as tunable optical filters and switches [12, 39].

Overall, PCFs have many applications, including fibre-optic communications, fibre lasers, nonlinear devices, high-power transmission, highly sensitive gas sensors, etc. They can also be used in many areas, which include spectroscopy, metrology, biomedicine, imaging, telecommunications, industrial machining, military, etc. The air-guiding photonic bandgap fibres have applications which include high power delivery, particle guidance, nonlinear optics (such as with gas-filled cores), waveguiding in radiative environments and short pulse delivery.

7.3 Device Fabrication

The fibre used was pure silica F-AIR-6-800 Airguided PCF purchased from Newport. The coating, a single layer of acrylate was removed by boiling in a bath of concentrated sulphuric acid. The silica cladding was 122 ± 5 μm in diameter and the core was 6 ± 1 μm. While these fibres are traditionally used for the guiding of light, a comparison with the capillary tubes discussed earlier was considered to be of interest.

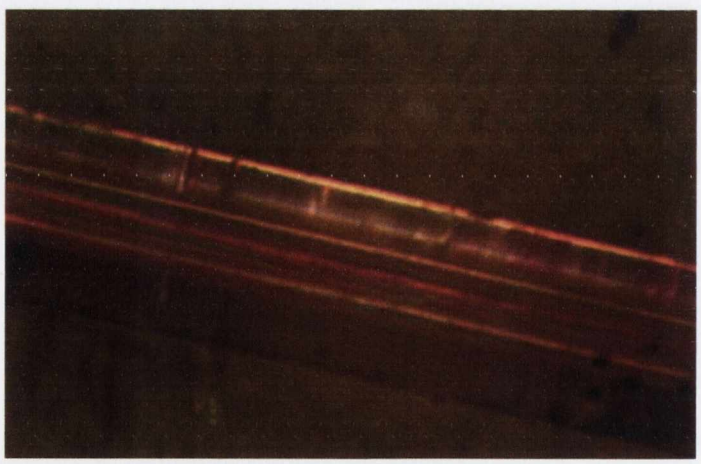

Figure 7.2 Side-on image from an optical microscope of a dye-doped PCF

As opposed to the manner in which the capillary tube was used in the previous works, a PCF was employed as the micro-cavity for the dye amplifiers. The fibre was cut into 25 mm lengths. As described in Chapter 3, the amount of liquid which fills the tube is related to the surface tension of the liquid, its diameter and the contact angle. As the diameter of the PCF is much narrower than that of the capillary (6 μm in comparison to

25 μm for the smallest capillary tube), there is increased difficulty in ensuring the length of fibre is sufficiently filled with the solution.

Another issue with these PCFs, which does not arise with the capillary tubes, is exactly which holes are filled with the solution. In a capillary tube the inner diameter is fully filled, whereas in a PCF the hollow core, the surrounding holes or both could be filled. An optical microscope with maximum resolution of 150x magnification was used to further investigate this issue.

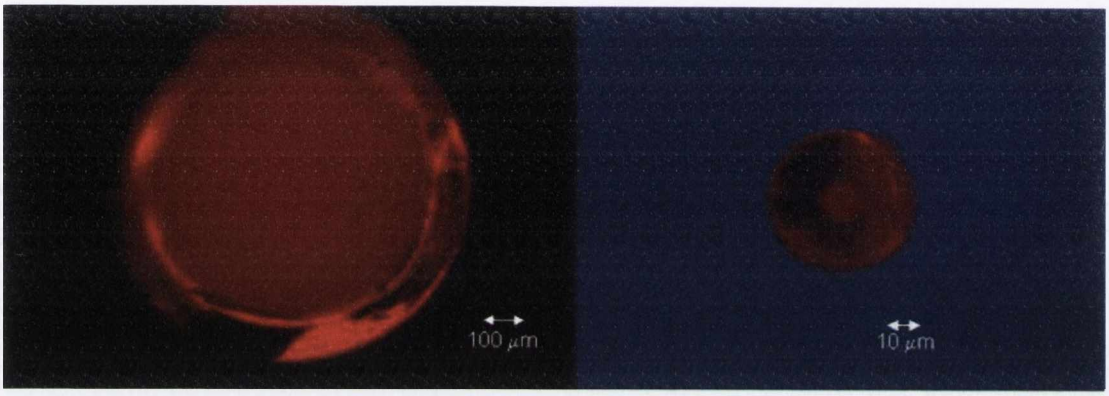

Figure 7.3 End-on image of Rhodamine 590 filled (a) 530 μm capillary and (b) PCF

Using an end-on approach, the open ends of a filled 530 μm capillary tube and a PCF fibre were imaged, respectively. Unfortunately, due to the small size of the PCF it is difficult to ascertain exactly how the dye fills the holes.

7.4 Experimental Procedure

The experiment is set up in an identical manner to that in section 4.2.4.

7.5 Results

7.5.1 PVP Concentration

In chapter 6, the concentration of PVP within the Rhodamine 590 solutions was investigated. This was repeated with the filled PCF to see if there was a polymer concentration dependence on the emission properties of the dye-doped solutions. Once again, the 100 g/l PVP concentration gave the highest efficiency for all three samples: Rhodamine 590, 0.3 μm micro-spheres and 0.2 μm micro-spheres. When the input-output

emission intensity data is compared to that of the neat Rhodamine solution without any PVP addition, a clear trend is observed.

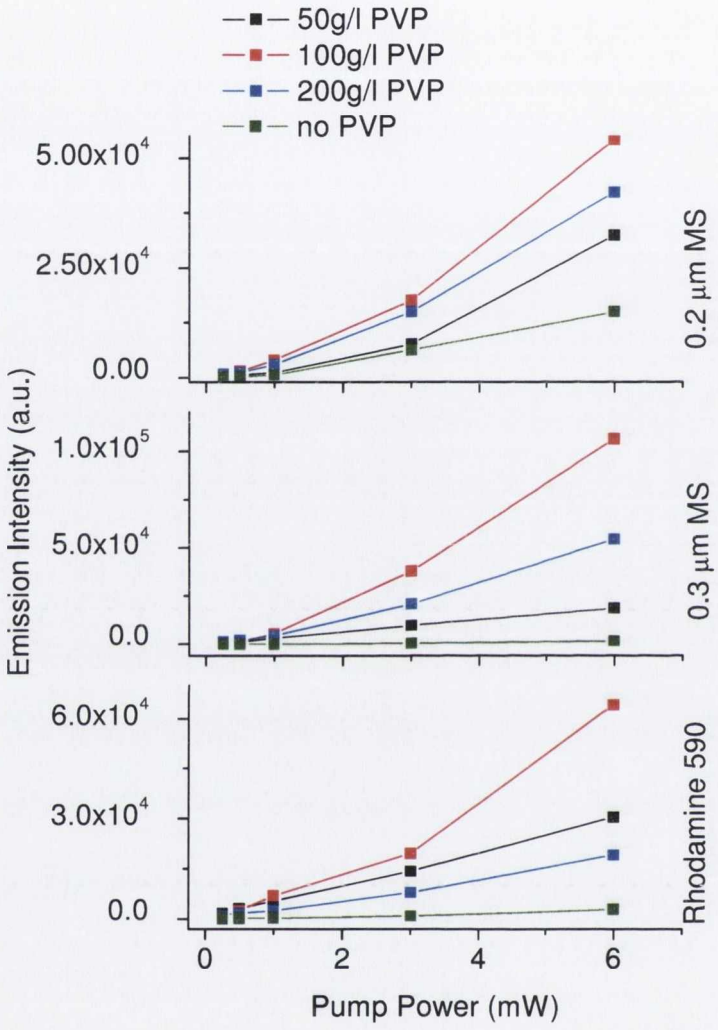

Figure 7.4 *Input-output intensity for the different concentrations of PVP in the Rhodamine 590 and 0.3 and 0.2 µm microsphere solutions*

Fig. 7.4 is an example of how the PVP concentration affects the output intensity from the dye-filled PCFs. For all three solutions, the 100 g/l solution shows the highest increase in the slope of emission intensity as the pump power is strengthened. When compared with the solution containing no polymer, the 200 g/l and 50 g/l solutions show slightly higher increases in slope intensity. The addition of PVP to the solutions has a positive effect on the emission intensity output from the doped PCFs. From these graphs it is deduced that the 100 g/l concentration of PVP was of most interest and needed to be examined further.

When the VSL method was applied to the PVP concentrations, the values for the gain coefficient were higher, and more easily fitted, for the 100 g/l PVP concentration.

7.5.2 Emission Characteristics

As in the previous chapters when dealing with the micro-scale doped capillaries, the emission properties of the solutions in the PCFs were measured, when excited with the SHG of the Nd:YAG laser. This was done in order to compare the emission and amplification properties of the materials in such a periodically order structure.

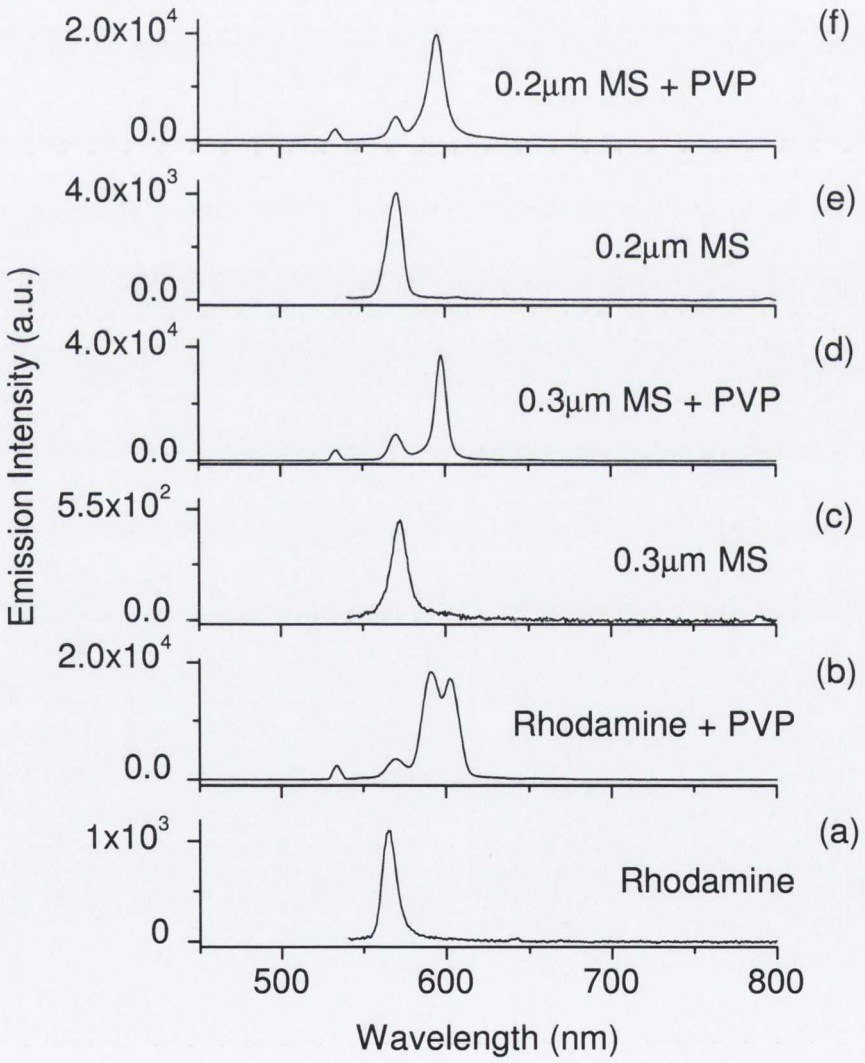

Figure 7.5 *Emission intensity against wavelength for the different solutions at 3 mW pump power*

For each solution containing no PVP, the emission exhibits a single peak at approximately 570 nm. When the PVP is added, a different picture emerges: the main maximum peak wavelength redshifts by approximately 20-30 nm. This variation in the emission properties can also be seen in the FWHM and input-output data. A smaller peak remains at the initial maximum wavelength, 570 nm, and, even smaller remnants of the SHG peak appear at 532 nm. This is not surprising, as the diameter of the PCF is so small, relative to the larger capillary tubes, that it was difficult to prevent any of the laser beam itself being guided directly into the narrow slit of the CCD. For the PCF-doped solutions containing no PVP, the SHG peak is larger, so it has been removed from the figures.

The emission intensity is notably higher, by an order of magnitude, for the solutions containing polymer, as seen in Fig. 7.5. The solutions containing both PVP and micro-spheres exhibit the highest intensity values. The 0.3 μm micro-sphere and PVP solution, in particular has a maximum peak intensity of approximately 4 x 10^4 a.u. The emission peaks for the Rhodamine solutions containing no polymer in the PCFs have a straight forward emission peak at approximately 565, 572 and 570 nm (Fig. 7.5 (a),(c),(e)), respectively. However, once the PVP is added to these solutions, a different picture emerges. With the Rhodamine 590 and PVP solution, an apparent doublet appears with features at 590 and 603 nm (Fig. 7.5 (b)). The 0.3 μm micro-sphere and PVP solution has a large peak at 597 nm and a much smaller one at 570 nm (Fig. 7.5 (d)). The 0.2 μm micro-sphere and PVP solution displays a similar spectrum, with the main peak at 595 nm (Fig. 7.5 (f)).

The observation of such a strong emission wavelength shift can be attributed to the greater confinement effect within the hollow-core of the PCF, as seen in the 25 μm capillary tubes. With the addition of the PVP and micro-scatterers to the Rhodamine 590, the refractive index is altered. This increase in the refractive index, although small, changes the resonance frequency enough to alter the periodic structure of the wavelength, i.e. the interference effect causes this change in the emission properties of the dye-doped PCF. In other words, the confinement within the periodic structure is strong enough to significantly alter the emission spectrum.

This shift in wavelength was visible to the human eye. When excited by the laser, ordinarily the Rhodamine 590 solution exhibited a strong yellow/orange coloured

emission. However, when the PCFs were filled with the micro-sphere doped PVP solutions, this emission colour shifted strongly to the red.

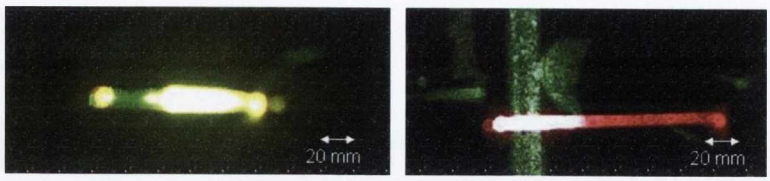

Figure 7.6 *Image of the colour change when photoexcited for the (a) Rhodamine 590 doped 25 μm capillary and (b) 0.3 μm MS and PVP doped PCF*

Further investigation into the emission properties of the dye-doped micro-sphere filled PCFs is needed. The full-width-half-maximum and input-output properties for each solution are plotted below.

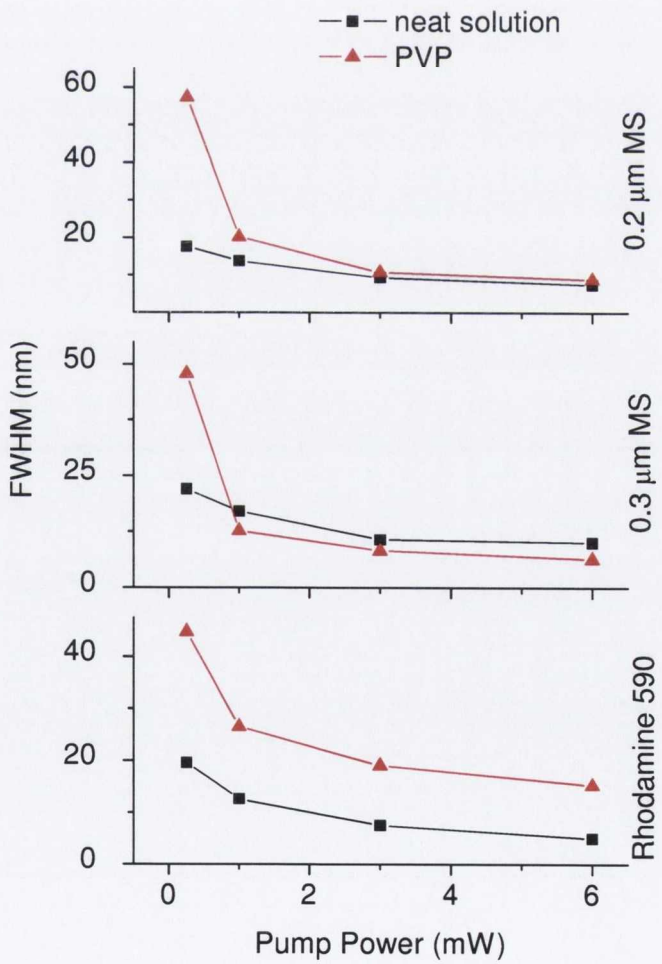

Figure 7.7 *FWHM properties for the six solution in a doped PCF*

There is a marked difference in the narrowing of the emission peak, for the solutions with and without the PVP. For those solutions without PVP, the FWHM was initially approximately 20 nm and decreases to 7 nm. This corresponds to the maximum peak intensity values observed in Fig. 7.5. Meanwhile, the three solutions containing PVP exhibited a much broader initial peak (for 0.25 mW pump power) of between 45 and 57 nm. The line narrowing was much more pronounced for these solutions, as the pump power is increased, to a width of 16 – 11 nm. In other words, for the dye-doped PCF, the addition of the polymer, PVP, appears to enhance the ASE. The addition of the micro-spheres and PVP together indicates an improvement in the line-narrowing properties of the gain medium within the PCF. This line-narrowing is stronger than the results reported by de Matos et al. for somewhat similar structures, consisting of a PCF filled with Rhodamine 6G doped TiO_2 particles. For pump powers up to 2.1 J/cm^2 they observed line narrowing from 22 to 18 nm, without, and 24 to 7 nm, with, the micro-particles [34].

These FWHM values were taken for the primary emission peaks, from Fig. 7.5, for the solutions containing PVP which exhibited either two distinct peaks or a doublet. This is mainly due to the fact that the initial broad peak (fluorescence), at 0.25 mW pump power, encompasses both peaks, which do not become distinct until the power is increased to 1 mW. By plotting the FWHM data for pump powers above 0.25 mW, a good comparative picture could not be obtained, as it would merely show the narrower linewidths achievable. A narrowing of the minor peak linewidths is observed, although it is less pronounced than that for the primary (i.e. major) emission peaks. For example, the normalised emission peaks wavelengths for the three solutions in question are plotted in Fig. 7.8 with increasing pump power.

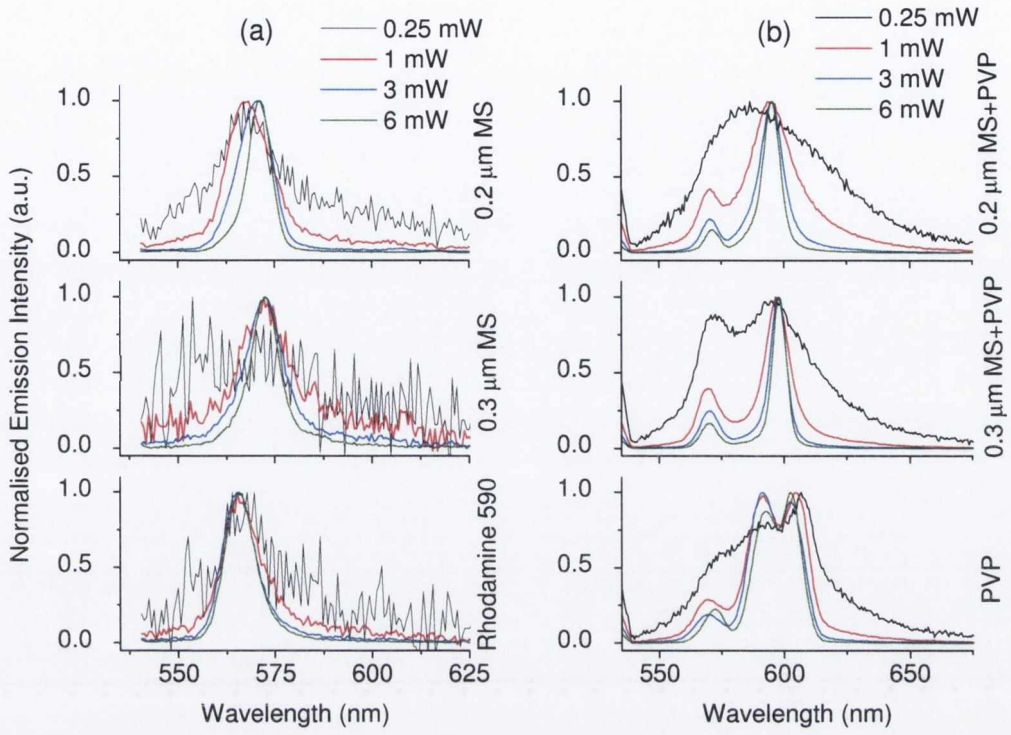

Figure 7.8 *Normalised emission intensity versus peak wavelength for PCF solutions (a) containing no polymer and (b) containing PVP*

The notable redshift in the peak wavelength is observed for the PVP doped PCFs in Fig. 7.8 (b), in particular for the fibres containing micro-spheres, as the pump power is increased. The narrowing of the emission peaks is also more evident in those fibres containing PVP, compared to those without. The SHG peak has been omitted from the graphs in order to concentrate on the emission peaks alone.

As with Chapter 4, if lasing modes do occur from the dye doped PCF devices, they are not able to be measured using this experimental setup due to the limitations of the CCD grating. The devices potentially have enough feedback to produce lasing.

To compare the linewidth values, as previously discussed, de Matos et al. in 2007 described a suspension of 250 nm TiO_2 particles in ethylene glycol which was inserted into the hollow core of a photonic crystal fibre [34]. This was reported to be the first random fibre laser. They increased their pump power from 9 to 144 MW/cm^2, which showed line width narrowing from 24 to 7 nm. This is said to be typical of the so-called random lasers. They also observed an improvement in the line-narrowing characteristics with the addition of the TiO_2 particles, when compared to filled PCFs without.

The evidence above strongly indicates that random lasing was achieved within a PCF. The line narrowing observed in this thesis is even more significant when the refractive index values are taken into account. The ethylene glycol used by de Matos et al. has a refractive index of 1.43, which is much higher than that of ethanol (1.36). This means that the emission would be expected to be more strongly guided in a PCF containing ethylene glycol. For similar solvents, in 1999 Frolov et al. reported on dye-infiltrated opal photonic crystals, i.e. crystallised SiO_2 particles [44]. When the crystals were doped with Rhodamine 6G, the FWHM decreased from 50 to 10 nm (over the threshold of 1.2 MW/cm^2).

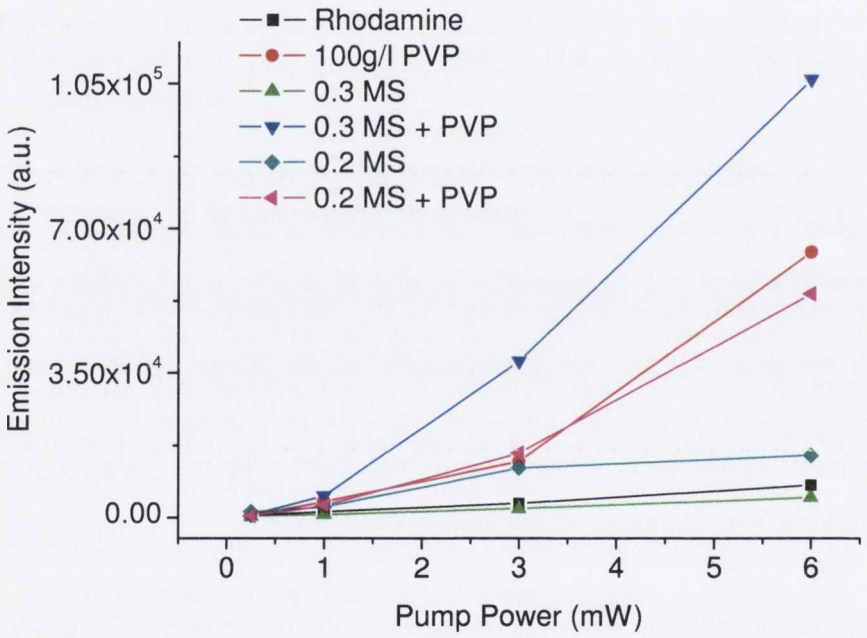

Figure 7.9 *Input-output emission properties for the six solutions in PCFs*

The input-output emission spectrum, in Fig. 7.9, shows exactly what the emission spectra illustrated in Fig. 7.5: the 0.3 μm micro-sphere doped PVP solution has the highest emission intensity, and strongest slope. The PVP appears to improve the output emission power of the Rhodamine 590 doped PCF. The solutions without any PVP addition have much lower emission intensities than their polymer-doped counterparts. The slight increase in the refractive index with the addition of the micro-scatterers and PVP indicate that they enhance the emission characteristics. The emission observed here is

considerably different to that of the capillary tubes in Fig. 6.7, indicating that the periodic structure of the PCF alters the output emission properties.

7.5.3 ASE Pump Power Threshold

The effect of the micro-scatterers on the ASE pump power threshold was investigated for each solution. It must be noted, however, that these values were more difficult to fit as, in some cases, doublets or two peaks were present (see Fig. 7.5 for reference). They therefore cannot be taken as a definitive answer for the threshold due to the larger inherent error.

Solution	ASE Pump Power Threshold (mW)
Rhodamine 590	0.26
100g/l PVP	1.24
0.3 μm MS	0.66
0.3 μm + PVP	0.87
0.2 μm MS	0.31
0.2 μm + PVP	1.18

Table 7.1 ASE pump power threshold values for the six solutions in the PCF, with and without the addition of PVP and micro-scatterers

As mentioned above, some of the values for the threshold are very high, when compared to the capillary equivalents in previous chapters. This could be due to the multiple peaks observed. It can also be attributed to the fact that, as seen with the smallest capillary diameter, the noise of the emission intensity does become a factor. For each solution containing no PVP, the power threshold is approximately 1 mW. The PVP solutions exhibit much higher threshold values than their polymer-free equivalents. This equates to the much higher emission intensity values observed in Fig. 7.5.

These values for the threshold hold well with the FWHM observed in Fig. 7.7 as, at approximately 1 mW pump power, a dramatic narrowing of the emission peak is observed. The same observations are made for the solutions containing no polymer.

7.5.4 Gain Results

In the same manner as with the dye-doped capillary tubes, the VSL method was used to measure the amplification, or gain coefficient, of the Rhodamine 590 filled PCF. The solutions containing micro-spheres and PVP were also investigated in order to see what effects, if any, the micro-scatterers had on the amplification properties. Below, in Table 7.2, is a full summary of the gain data for the solutions in the PCFs.

As discussed in more detail in Chapter 4, the saturated model cannot be used to fit the data for the majority of PCF doped solutions, due to the constraints inherent with the low gain values in question. The increased error limits created a numerical instability, causing fitting issues. For the solutions containing PVP, $gl > 4$, so the saturated model can be employed; however, to compare the gain results more readily, only the unsaturated model will be used for all PCF doped solutions.

	(a) PCF		(b) 25 μm capillary	
	1mW (cm^{-1})	3mW (cm^{-1})	1mW (cm^{-1})	3mW (cm^{-1})
Rhodamine	4.2 ± 0.5	4.6 ± 0.8	3.9 ± 0.2	4.0 ± 0.2
PVP	3.6 ± 0.4	5.7 ± 0.6	3.3 ± 0.2	4.2 ± 0.3
0.3 μm MS	2.2 ± 0.3	2.8 ± 0.8	3.5 ± 0.2	4.5 ± 0.3
0.3 μm MS + PVP	5.4 ± 0.6	6.3 ± 0.8	4.0 ± 0.2	4.3 ± 0.3
0.2 μm MS	2.6 ± 0.8	2.7 ± 0.3	3.6 ± 0.4	3.8 ± 0.4
0.2 μm MS + PVP	4.9 ± 0.6	6.2 ± 0.5	3.4 ± 0.4	3.6 ± 0.4

Table 7.2 Summary of the unsaturated gain results in (a) PCF and (b) 25 μm capillary

The values of the gain coefficient, for 1 and 3 mW, are listed in Table 7.2 (a). These values are repeatable; representative data is presented above. Comparing the 3 mW pump power gain coefficient values, as an example, indicates that the dye doped PCFs exhibit a stronger level of amplification, or higher gain value, when the solutions contain PVP. Those without the polymer addition have a lower gain coefficient, by comparison. Out of the three samples without any polymer present, the Rhodamine 590 itself has the highest gain. However, with the addition of the polymer, the 0.3 μm microsphere and PVP filled PCF has the highest gain value of 6.3 cm^{-1} at 3 mW pump power. The random scattering from the micro-sphere may further improve the interaction of the pump light with the gain

medium within the confined fibre. As noted in section 7.5.2, the periodic structure of the PCF and the increased value of the refractive index, due to the PVP and micro-sphere addition, combine to alter the emission output characteristics.

It is interesting to compare these values or trends with the results for the 25 μm capillary tubes, as they are the capillaries with the closest equivalent diameter. The PCF gain values, at 3 mW pump power, in general are higher than those for the 25 μm capillary as seen in Table 7.2. However, these capillary tubes also showed a small increase in the gain with the 0.3 μm micro-sphere addition, but the PVP doped solutions did not produce as pronounced an effect as for the PCFs. This is particularly impressive when the relative overlap of the pump beam is taken into account, as discussed in Chapter 4. For the PCFs used in this study, which have an inner diameter of 6 μm, approximately one fifth of the energy excites the dye molecules, in comparison to the nearest sized capillary tube. Therefore, it can be concluded that the periodic structure causes enhancement of the amplification, as described by de Matos et al. [34]. The micro-scatterers are shown to improve this effect.

7.5.5 Gain Summary

In order to compare the results obtained in this work with those reported in literature, a table of results is presented.

Author	Material	Pump Power	Results	Ref.
Ng et al.	solid state photonic crystal LED structures		two-fold increase of PL intensity	[45]
Sridharan et al.	Yb^{3+} doped polarising PCF (~ 40 μm diameter core)	8.6 W	69 dB	[46]
Hougaard et al.	Er-doped PCF amplifier (solid core)	0.7 mW	15 dB	[47]
Tagaya et al.	selection of organic dye doped guided index fibres	at 620 W	30 dB	[48]
This work	Rhodamine 590 and micro-scatterer doped PCF	3 mW	up to 13.8 dB	

Table 7.3 Summary of literature results for doped PCF devices

Groups such as de Matos et al. and Ng et al. determined that, where narrowing of the emission spectrum is observed, there is an increase in the output emission intensity [34, 45]. This was confirmed for the dye and micro-scatterer doped PCF in section 7.5.2.

By using the method discussed in section 4.3.6, the net gain measured can be converted into small-signal gain. At 3 mW pump power, the Rhodamine 590 doped PCF yielded a small-signal gain of 10 dB and the 0.3 μm micro-sphere and PVP solution yielded 13.8 dB. Thus, these results show an improvement from those reported in literature, when the size and magnitude of the pump power are taken into account. For example, Hougaard et al. reported on high gain values, 15 dB, at low pump powers using an erbium doped PCF amplifier [47]. Erbium is a well known and very strongly emitting rare earth ion, which emits in the infrared region. When comparing organic dye doped PCF devices, Tagaya et al. measured strong amplification (30 dB) from a selection of organic dyes, including Rhodamine 590, which were incorporated into solid-state graded index PC rods [48]. However, they used extremely high pump powers, of approximately 620 W from an Nd:YAG laser. Therefore, when comparing the results in this thesis, for much lower exciting powers, the amplification measured (up to 13.8 dB) is very high, considering that the dye is in solution and the pump powers used are low.

7.5.6 Polarisation Measurements

An overview of the effects of changing the polarisation conditions of the input pump beam on the emission properties from the PCF is presented. The results shown are those from the 3 mW pump power measurements, for illustration purposes only, as they are well above the pump power threshold estimates for all solutions.

7.5.7 Degree of Polarisation

The degree of polarisation (DOP) was measured by comparing the ratio of intensity values for each polarisation state, as in the previous chapters.

Sample	s-polarised	circular-polarised	p-polarised
Rhodamine 590	0.22	0.19	0.06
PVP	0.24	0.25	0.12
0.3 μm MS	0.20	0.17	0.04
0.3 μm MS + PVP	0.29	0.24	0.11
0.2 μm MS	0.21	0.22	0.03
0.2 μm MS + PVP	0.24	0.28	0.11

Table 7.4 Summary of the degree of polarisation for the Rhodamine 590 doped PCF

The DOP values are much smaller for the PCF than the capillary tubes. This is primarily due to the lower intensity levels and increased amount of experimental error involved in both taking the measurements and even filling the fibres. However, in general, the same conclusions can be drawn for the capillary-based micro-amplifiers. The s- and circular-polarised states have a higher degree of polarisation than the p-polarised counterpart.

As discussed in Chapter 6, the micro-spheres scatter the incident polarised light, resulting in a certain amount of "depolarisation" of the pump polarized light, which can be explained through Mie scattering (Chapter 6). As a result, the polarised pump beam becomes slightly less polarised, and hence the emission ASE becomes less polarized in comparison with the micro-sphere-free solutions. The greater confinement caused by the small area within the PCF may cause this effect to be enhanced.

7.5.8 Polarised Gain Results

The emission intensity for the changing polarisation conditions in the PCFs followed the same trend as for the emission intensities in Fig. 7.5, whereby the solutions containing PVP had higher intensity values than their polymer-free counterparts. Recall that, in comparison to the capillaries, the dye-doped PCFs showed a higher gain value for the PVP-doped solutions over those containing no polymer. The s- and circular-polarisation positions again showed the higher degree of amplification, however for the 0.2 μm PVP solutions, the p-polarisation state has slightly larger gain values than the s-polarised. In general, the circular-polarisation positions showed marginally higher emission intensities than the s-polarised.

		Rh590 (cm^{-1})	Rh590 +PVP (cm^{-1})	0.3 μm MS (cm^{-1})	0.3 μm MS+PVP (cm^{-1})	0.2 μm MS (cm^{-1})	0.2 μm MS+PVP (cm^{-1})
s-polarised	s'	4.5	5.3	2.7	5.7	2.3	5.6
	p'	3.9	4.5	2.8	5.4	2.5	5.1
p-polarised	s'	4.4	3.4	1.9	5.2	2.8	6.2
	p'	3.9	3.6	2.0	5.0	2.4	6.0
circular-polarised	s'	4.6	4.4	3.0	7.3	3.3	6.5
	p'	4.1	4.3	3.0	7.0	2.9	5.9

Table 7.5 Polarised unsaturated gain values for the PCF at 3mW pump power

When the polarisation condition of the pump beam is changed, the peak only shifts approximately 2 nm. No dependence of the peak wavelength shift is attributed to the change in polarisation of the pump beam.

The gain values follow on from the emission intensities observed. In comparison to the large capillary tubes in the earlier chapters, the gain values remain relatively similar, no matter what the polarisation state of the pump beam is, particularly for solutions containing no polymer. The addition of PVP and the micro-spheres to the PCF produces a wider spread in gain values for the different polarised states, i.e. for p-polarisation the gain is approximately 5 cm^{-1}, while for the circular-polarised beam the gain increases to approximately 7 cm^{-1}. In general, the main contributing factor continues to be the properties of the solution itself, and not the condition of the incident beam. The s'- and p'-components are very close in value; this could be due to the 'depolarisation' effect, as previously described.

7.6 Summary

The gain coefficients for the dye-doped photonic crystal fibre, in general, exhibited a strong dependence on the micro-scatterers which were added to the solution. Although it is difficult to ascertain exactly how the solutions fill the fibre, a definite difference in the emission properties is observed for each solution. The intensity and wavelength of the emission peak varies with the addition of micro-sphere and polymer. This ability to shift the wavelength and vary the intensity could have applications when it comes to fine-tuning these parameters for the applications requirements.

In comparison to the 25 μm capillary tube, which has the closest diameter, the PCF has a higher gain coefficient, and more efficient amplification. The PCF, which has a core diameter of 6 μm, also requires less solution, which is more cost effective for its potential applications. However, with this smaller size comes a greater difficulty in handling, and in filling, the fibres sufficiently.

When compared to the emission properties of similar structures reported in literature (section 7.5.5), these Rhodamine 590 doped micro-scattering PCFs hold well. In particular, when the exciting pump powers are taken into account, these PCFs have comparably high gain values. Specifically, the addition of micro-spheres and PVP sufficiently alters the emission properties of the PCF to improve the amplification of the device.

The effects of changing the polarisation conditions were also investigated. Although modifying the polarisation states has little effect on the peak wavelength, the choice of micro-scatterer in the dye doped solution does affect the amplification. Once again, the amplification of the device was found to depend strongly on the polarisation state of the exciting pump beam. Therefore, by making these slight changes, the emission properties at a desired wavelength can be fine-tuned. This possibility for tuning greatly enhances the practicality of the devices.

Overall, it is the combination of the periodic surrounding structure, the increased refractive index and the micro-scattering spheres which favourably modify and enhance the emission properties. Due to the confining periodic structure, the PCF shows greater efficiency than its capillary-based counterpart.

7.7 References

1. Buswell, S.C., V.A. Wright, J.M. Buriak, V. Van, and S. Evoy, *Optics Express*, 2008. **16**(20): p. 15949-15957.
2. Psaltis, D., S.R. Quake, and C.H. Yang, *Nature*, 2006. **442**(7101): p. 381-386.
3. Li, Z.Y. and D. Psaltis, *Microfluidics and Nanofluidics*, 2008. **4**(1-2): p. 145-158.
4. Snyder, A.W. and J.D. Love, *Optical waveguide theory*. 1983, London ; New York Chapman and Hall.
5. Knight, J.C. and P.S. Russell, *Science*, 2002. **296**(5566): p. 276-277.
6. Russell, P.S.J., in *Unpublished results*. 1991.
7. Yablonovitch, E., *Physical Review Letters*, 1987. **58**(20): p. 2059-2062.
8. Yeh, P., A. Yariv, and E. Marom, *Journal of the Optical Society of America*, 1978. **68**(9): p. 1196-1201.
9. Knight, J.C., *Nature*, 2003. **424**(6950): p. 847-851.
10. Russell, P., *Science*, 2003. **299**(5605): p. 358-362.
11. Cregan, R.F., B.J. Mangan, J.C. Knight, T.A. Birks, P.S. Russell, P.J. Roberts, and D.C. Allan, *Science*, 1999. **285**(5433): p. 1537-1539.
12. Joannopoulos, J.D., P.R. Villeneuve, and S.H. Fan, *Nature*, 1997. **386**(6621): p. 143-149.
13. John, S., *Physical Review Letters*, 1987. **58**(23): p. 2486-2489.
14. Birks, T.A., J.C. Knight, and P.S. Russell, *Optics Letters*, 1997. **22**(13): p. 961-963.
15. Clark, J. and G. Lanzani, *Nature Photonics*, 2010. **4**(7): p. 438-446.
16. Yablonovitch, E., *Journal of the Optical Society of America B-Optical Physics*, 1993. **10**(2): p. 283-295.
17. Domachuk, P., H.C. Nguyen, B.J. Eggleton, M. Straub, and M. Gu, *Applied Physics Letters*, 2004. **84**(11): p. 1838-1840.
18. Hu, X.Y., Y.H. Liu, J. Tian, B.Y. Cheng, and D.Z. Zhang, *Applied Physics Letters*, 2005. **86**(12).
19. Lawandy, N.M., R.M. Balachandran, A.S.L. Gomes, and E. Sauvain, *Nature*, 1994. **368**(6470): p. 436-438.
20. Sha, W.L., C.H. Liu, and R.R. Alfano, *Optics Letters*, 1994. **19**(23): p. 1922-1924.
21. Wiersma, D.S., M.P. Vanalbada, and A. Lagendijk, *Nature*, 1995. **373**(6511): p. 203-204.
22. Noginov, M.A., H.J. Caulfield, N.E. Noginova, and P. Venkateswarlu, *Optics Communications*, 1995. **118**(3-4): p. 430-437.
23. Balachandran, R.M., D.P. Pacheco, and N.M. Lawandy, *Applied Optics*, 1996. **35**(4): p. 640-643.
24. Siddique, M., R.R. Alfano, G.A. Berger, M. Kempe, and A.Z. Genack, *Optics Letters*, 1996. **21**(7): p. 450-452.
25. Hide, F., B.J. Schwartz, M.A. DiazGarcia, and A.J. Heeger, *Chemical Physics Letters*, 1996. **256**(4-5): p. 424-430.
26. Sanders, J.V., *Nature*, 1964. **204**(496): p. 1151-1153.
27. Kuai, S., S. Badilescu, G. Bader, R. Bruning, X.F. Hu, and V.V. Truong, *Advanced Materials*, 2003. **15**(1): p. 73-75.
28. Rybin, M.V., K.B. Samusev, and M.F. Limonov, *Photonics and Nanostructures-Fundamentals and Applications*, 2007. **5**(2-3): p. 119-124.
29. Puzzo, D.P., F. Scotognella, M. Zavelani-Rossi, M. Sebastian, A.J. Lough, I. Manners, G. Lanzani, R. Tubino, and G.A. Ozin, *Nano Letters*, 2009. **9**(12): p. 4273-4278.
30. Busch, K. and S. John, *Physical Review Letters*, 1999. **83**(5): p. 967-970.

31. Wolinski, T.R., S. Ertman, P. Lesiak, A.W. Domanski, A. Czapla, R. Dabrowski, E. Nowinowski-Kruszelnicki, and J. Wojcik, *Opto-Electronics Review*, 2006. **14**(4): p. 329-334.
32. Eggleton, B.J., C. Kerbage, P.S. Westbrook, R.S. Windeler, and A. Hale, *Optics Express*, 2001. **9**(13): p. 698-713.
33. Roy, P., P. Leproux, S. Fevrier, D. Pagnoux, J.L. Auguste, J.M. Blondy, S. Hilaire, L. Lavoute, R. Jamier, A. Desfarges-Berthelemot, V. Kermene, and C. Restoin, *Comptes Rendus Physique*, 2006. **7**(2): p. 224-232.
34. de Matos, C.J.S., L.D.S. Menezes, A.M. Brito-Silva, M.A.M. Gamez, A.S.L. Gomes, and C.B. De Araujo, *Physical Review Letters*, 2007. **99**(15).
35. Vasdekis, A.E., G.E. Town, G.A. Turnbull, and I.D.W. Samuel, *Optics Express*, 2007. **15**(7): p. 3962-3967.
36. Wadsworth, W.J., J.C. Knight, W.H. Reeves, P.S. Russell, and J. Arriaga, *Electronics Letters*, 2000. **36**(17): p. 1452-1454.
37. Price, J.H.V., K. Furusawa, T.M. Monro, L. Lefort, and D.J. Richardson, *Journal of the Optical Society of America B-Optical Physics*, 2002. **19**(6): p. 1286-1294.
38. Haus, H.A. and C.V. Shank, *IEEE Journal of Quantum Electronics*, 1976. **12**(9): p. 532-539.
39. McCall, S.L. and P.M. Platzman, *IEEE Journal of Quantum Electronics*, 1985. **QE-21**(12): p. 1899-1904.
40. MacPherson, W.N., M.J. Gander, R. McBride, J.D.C. Jones, P.M. Blanchard, J.G. Burnett, A.H. Greenaway, B. Mangan, T.A. Birks, J.C. Knight, and P.S. Russell, *Optics Communications*, 2001. **193**(1-6): p. 97-104.
41. Rindorf, L., P.E. Hoiby, J.B. Jensen, L.H. Pedersen, O. Bang, and O. Geschke, *Analytical and Bioanalytical Chemistry*, 2006. **385**(8): p. 1370-1375.
42. Temelkuran, B., S.D. Hart, G. Benoit, J.D. Joannopoulos, and Y. Fink, *Nature*, 2002. **420**(6916): p. 650-653.
43. Benabid, F., J.C. Knight, G. Antonopoulos, and P.S.J. Russell, *Science*, 2002. **298**(5592): p. 399-402.
44. Frolov, S.V., Z.V. Vardeny, A.A. Zakhidov, and R.H. Baughman, *Optics Communications*, 1999. **162**(4-6): p. 241-246.
45. Ng, W.N., C.H. Leung, P.T. Lai, and H.W. Choi, *Nanotechnology*, 2008. **19**(25): p. 1-5.
46. Sridharan, A.K., P. Pax, M.J. Messerly, and J.W. Dawson, *Optics Letters*, 2009. **34**(5): p. 608-610.
47. Hougaard, K.G., J. Broeng, and A. Bjarklev, *Electronics Letters*, 2003. **39**(7): p. 599-600.
48. Tagaya, A., S. Teramoto, E. Nihei, K. Sasaki, and Y. Koike, *Applied Optics*, 1997. **36**(3): p. 572-578.

Chapter 8

Conclusions and Future Work

The aim of this work was to investigate the possibility of incorporating organic dye doped solutions into micro-scale capillary tubes and, by demonstrating the amplifying properties of these devices, show the feasibility of incorporating them into optofluidic networks or lab-on-a-chip systems.

Rhodamine 590 was the chosen organic laser dye, as its spectroscopic properties are strong and its emission characteristics are well known. When the micro-capillaries, ranging in diameter from 530 to 25 μm, were filled with the laser dye, they exhibited strong amplification characteristics. The gain was measured using the variable stripe length (VSL) method, which was first developed by Shaklee and Leheny [1], for a range of pump intensities. The gain coefficients were found to range from 8.1 cm^{-1} for the largest capillary diameter to 5.3 cm^{-1} for the smallest, at 6 mW pump power. Taking into account the relative size, the overlap of the exciting pump beam area on the capillary and dye density of these devices, they compare well to the reported literature values.

As has previously been discussed, Rhodamine 590 has been comprehensively studied as a laser dye. Now that the experimental parameters have been optimised, the same methods can be used for other laser dyes. Therefore, these capillary-based laser amplifiers can be tuned for whatever wavelength, or excitation region, is required. The use of different solvent and polymers are also known to affect the orientation of the dye molecule, and hence the emission properties [2]. By looking at the different combinations of dye : solvent : polymer, these properties can be optimised. Another option is to replace the laser dye solutions with those containing quantum dots, as has been reported, for example, in polymer optical fibres by Yu et al. [3]. In the case of solid state waveguide amplifiers, the issue of quenching is a major disadvantage when dealing with quantum dots. By dealing with the quantum dots in solution, this issue can be overcome.

The micro-scatterer addition to the micro-amplifying devices was determined to affect the emission properties. Whereas the scatterer-involved micro-amplifiers exhibited similar amplification performance with the dye-doped micro-capillaries, the scatterers significantly improved the photoluminescence efficiency of the dye solutions, implying a

better emission of the devices. However, when the diameter was decreased, the gain values were generally unaffected by the micro-scatterer addition. For example, with the 25 μm amplifier at 3 mW pump power, those with and without micro-spheres or PVP all have a gain coefficient of approximately 4 cm^{-1}.

When the capillary parameters were altered by replacing them with hollow-core photonic crystal fibres (PCF), the micro-scatterers had an enhanced effect of the emission properties. The combination of PCF, the polymer PVP and the micro-spheres caused a sharp shift if the maximum peak wavelength from 570 to approximately 590 nm. An improvement in the amplification was measured, when compared to the 25 μm devices. The greater level of confinement within the structure of the PCF, and the increase in refractive index with the PVP, are thought to alter the periodic structure, and hence contribute to the interference causing this change in the emission properties.

In the case of the micro-sphere addition, it is known that at this concentration of micro-spheres, when deposited on a substrate they form a monolayer. Although solid state dye-doped waveguides do have issues with photodegredation, the emission properties of such periodic monolayers could be of interest. In particular, clusters or small areas of these dye-doped micro-spheres could be segregated for individual or cluster analysis. Kuwatagonokami et al. used optical tweezers to look at one Rhodamine B dye-doped micro-sphere and showed that it exhibited lasing emission [4]. Clusters of ZnO micro-particles have also been shown by Cao et al. to act as random lasers [5]. In the same paper, Kuwatagonokami et al. also noted that the emission behaviour depends strongly on the size of the particle. They found that particles less than 10 μm in diameter did not exhibit lasing. It would be interesting therefore, for the different diameters of capillary tubing to look at the effects of micro-spheres of this size (as, obviously, these large diameters would be too big for the PCF). The use of different microspheres, as opposed to polystyrene spheres, could also affect the properties observed. For example, other micro-sphere options are phthalocycanine, titanium oxide, etc. as they are either readily available to purchase commercially, or are easily fabricated [6, 7] for a variety of diameters. A further investigation into the effects of the micro-scatterer concentration would allow the emission properties to be further optimised.

The effects of changing the polarisation properties of the exciting pump beam were also investigated as the properties of many systems depend on the polarisation state of the

exciting beam. A strong dependence of the emission intensity on the polarisation was observed. Hence, it was proven that the s- and circular-polarised pump beam conditions were more efficient than the p-polarisation. With the micro-scatterer addition, the 'depolarisation' caused by the scattering affected the polarisation dependency. In fact, it was primarily the small-diameter structures, the 25 μm and PCF, that the changing polarisation state exhibited a greater improvement on the amplification properties of the devices.

The potential future applications of such devices are plentiful. A viable application of particular interest is in the field of polymer optical fibres (POF). Such fibres are currently widely researched and commercially implemented in areas such as short-haul data communications networks and in the automotive industry, amongst others [8]. POFs are used to replace conventional systems as they are versatile, efficient and more cost effective. The dye doped micro-capillaries in this work exhibited strong amplification of the input signal. Such organic devices have the potential, through further optimisation and characterisation, to be used in such applications, either in conjunction with POFs or as a replacement [9].

In conclusion, dye doped micro-amplifiers have been shown to exhibit promising and tunable amplification emission properties. The strong amplification, ease of fabrication and high level of versatility mean that they have good potential for use as micro-scale optical amplifiers for optofluidic applications. These are not stand-alone devices, due to the requirement of off-chip optical pumping; however they still have very strong potential for use as amplification devices for a range of applications, as highly tunable light sources.

8.1 References

1. Shaklee, K.L., R.F. Leheny, and R.E. Nahory, *Applied Physics Letters*, 1971. **19**(8): p. 302-305.
2. Schäfer, F.P. and K.H. Drexhage, *Dye lasers*. 2nd rev. ed. ed. Topics in applied physics ; vol.1. 1977, Berlin ; New York: Springer.
3. Yu, H.C.Y., A. Argyros, G. Barton, M.A. van Eijkelenborg, C. Barbe, K. Finnie, L. Kong, F. Ladouceur, and S. McNiven, *Optics Express*, 2007. **15**(16): p. 9989-9994.
4. Kuwatagonokami, M., K. Takeda, H. Yasuda, and K. Ema, *Japanese Journal of Applied Physics Part 2-Letters*, 1992. **31**(2A): p. L99-L101.
5. Cao, H., Y.G. Zhao, S.T. Ho, E.W. Seelig, Q.H. Wang, and R.P.H. Chang, *Physical Review Letters*, 1999. **82**(11): p. 2278-2281.
6. Nitschke, C., S.M. O'Flaherty, M. Kroll, and W.J. Blau, *Journal of Physical Chemistry B*, 2004. **108**(4): p. 1287-1295.
7. Nitschke, C., S.M. O'Flaherty, M. Kroll, J.J. Doyle, and W.J. Blau, *Chemical Physics Letters*, 2004. **383**(5-6): p. 555-560.
8. Clark, J. and G. Lanzani, *Nature Photonics*, 2010. **4**(7): p. 438-446.
9. Peng, G.D., P.L. Chu, Z. Xiong, T. Whitbread, and R.P. Chaplin, *Optics Communications*, 1996. **129**(5-6): p. 353-357.

Appendix I

Mean Free Path of a Photon

The mean free path of a photon was described in Chapter 6. The free path of a photon due to scattering is described by [1]

$$\Lambda_s = \frac{1}{\sigma_{sc} N_0}$$

where the scattering cross-section σ_{sc} is estimated from Eq. 6.1 to be 3.2 x 10^{-14} and 2.7 x 10^{-15} cm^2 for the 0.3 and 0.2 μm scattering spheres, respectively. The values are calculated by inputting the parameters into Eq. 6.1, using the Mathematica program. The value for N_0, the average number of molecules per unit volume, is specific to the manufacturer's guidelines; for the concentrations used, there are approximately 1.6 x 10^{15} and 5.7 x 10^{15} particles per volume. Therefore, the free path of a photon due to scattering is approximately in the order of 0.2 and 0.6 mm for the two sphere diameters, 0.3 and 0.2 μm. These estimated values are larger than the wavelength, therefore it can be concluded that the scattering is due to diffusion.

References

1. Ambartsumyan, R.V., N.G. Basoc, D.G. kryukov, and V.S. Letokhov, Non-Resonant feedback in lasers ed. J.H. Sanders and K.W. Stevens. Vol. Quantum Electronics. 1970, Oxford: Pergamon.

Appendix II
List of Publications

Major research achievements in this thesis have been published or will be submitted in international journals and proceedings. Hereinafter we give a publication list to highlight the results in this thesis:

1. Paula Russell-Hill, Jun Wang, Werner J. Blau, "Capillary-based dye laser micro-amplifiers", Japan-Europe Joint Workshop, The 9th International Symposium on Advanced Organic Photonics, ISAOP-9, 2009.

List of Presentations

1. ICSM 2006, Dublin, Ireland – 'Optical Gain and Lasing in Micro- and Nano-Structured Luminescent Polymers', poster presentation
2. MRS 2008, Boston, United States – 'Rare-Earth Doped Polymeric Gain Media for Visible Amplification', poster presentation
3. ISAOP 2009, Bunratty, Ireland – 'Capillary-Based Dye Laser Micro-amplifiers', poster presentation
4. School of Physics Seminar, 2009 – 'Optical Gain in Dye Filled Micro-Capillaries', presentation